1-1-1982

An analytical and experimental study of the bending stresses in the tie girder of a tied arch bridge.

Sainath B. Venkatachalam

AN ANALYTICAL AND EXPERIMENTAL STUDY

OF THE BENDING STRESSES IN THE TIE GIRDER

OF A TIED ARCH BRIDGE

by

Sainath B. Venkatachalam

A THESIS
Presented to the Graduate Committee
of Lehigh University
in Candidacy for the degree of
Master of Science
in
Civil Engineering

Lehigh University
Bethlehem, Pennsylvania

September 1982

CERTIFICATE OF APPROVAL

The thesis is accepted and approved in partial fulfillment of the requirements for the degree of Master of Science in Civil Engineering.

Sept 8, 1982

Date

Dr. John W. Fisher

Dr. David A. VanHorn

ACKNOWLEDGMENTS

The research reported herein was conducted at Fritz Engineering Laboratory, Lehigh University, Bethlehem, Pennsylvania. The Director of Fritz Engineering Laboratory is Dr. Lynn S. Beedle, and the Chairman of the Department of Civil Engineering is Dr. David A. VanHorn.

The help and guidance of Dr. J. W. Fisher, Thesis Supervisor is greatly appreciated. Thanks are due Mr. John Gera, who drafted the figures. A very special thanks to Mrs. Ruth Grimes, who typed the manuscript. The invaluable help and advice offered by Mr. Dennis Mertz through the various stages of this research is gratefully acknowledged.

TABLE OF CONTENTS

LIST OF TABLES

LIST OF FIGURES

ABSTRACT

An analytical and experimental study of the Unit II tied arch span of the I24 bridge over the Ohio River is presented herein.

A finite element study was carried out to determine the live load stress response of the tie girder at a spliced panel point. Stresses were studied at locations at various distances from the spliced panel point.

A comparison was made between the analytical study and field study results, to determine the validity of the analytical model. The comparison does not provide for all the differences in the response.

The study of stresses at various locations on tie girders showed that bending was a significant mode of response. Bending stresses made a predominant contribution to the stress cycles experienced by the tie girder flanges. The study also showed that the bending response was primarily a localized effect. The presence of bending in the tie girder cannot be ignored. A modification of current design philosophy is required to account for the bending of the tie girder.

Based on the stress history measurements in the field, an effective stress range was determined for the box corner weld detail. Fatigue life estimates were developed for various crack sizes.

1. INTRODUCTION

1.1 Background and Objectives

The arch may be defined as a structural unit which satisfies the following two criteria:

1. It must be sustained by supports all of which are capable of developing lateral as well as normal reaction components.
2. It must be of such shape that the lateral reaction components are, in fact, developed under load, and these must, in general, constitute inward thrusts or inward pulls.

In a tied arch, the horizontal reactions to the arch rib are supplied by a tie girder at deck level. In any practical arch, non-zero bending moments result, and these may be provided for by designing the arch rib for a combination of moment and thrust. The tie girder is designed either as a tension member or a bending member. Those structures designed with tension members to balance the thrust and small moment developed at rigid connections between the arch rib and tie girder result in slender tie girder sections. Structures designed to resist the bending result in much larger tie girders. Recent field measurements on the I24 tied arch bridges at Paducah, Kentucky, have demonstrated that the bow-string-girder type structure develops much more bending stress than axial stress under live load[1]. The tie girders are, in general, connected to the floor systems at each panel point (floor) beam location), and the deflection

of the tie girder under live loads, caused by the deflection of the arch and the distortion of the floor system, is the primary reason for this bending. Because of the slender sections adopted for the tie girder, very high bending stress variations develop, which can substantially reduce the fatigue life of the details involved. This casts serious doubt on the validity of the philosophy adopted, in the design of tie girders acting as primary tension members.

In the study reported here, an analysis of the tied arch bridge span, Unit II, over the Ohio River near Paducah, Kentucky, on I24, was carried out. The purpose of this study was to determine the response and magnitude of bending stress variations in the tie girder. The finite element method of analysis was adopted for this study. The general purpose finite element program, SAP IV, was utilized for the analysis[2]. The maximum bending stress range was determined for sections at various distances from a selected panel point, to study the nature of the bending. A comparison between the contributions of the bending mode and tension mode of stress variation to the total stress cycle was made. Also, the susceptibility to crack growth, or several transverse cracks detected in the longitudinal fillet welds, at the tie girder box corners, was investigated. The cracks were discovered in box corner welds during field inspections and were likely caused by the presence of hydrogen[3]. An attempt was made to determine the fatigue life of these details for various assumed crack sizes.

1.2 Description of the Bridge

The bridge under study is the four lane interstate I24 bridge across the Ohio River between McCracken County, Kentucky and Massac County, Illinois. The 2110.13 m crossing consists of six units. Unit II and V of the bridge are simple tied-arch spans 192 m and 222.5 m long, respectively. The rest of the units consist of continuous steel plate girder spans. The bridge was fabricated and erected by the Nashville Bridge Company, Nashville, at a cost of $18.5 million. It was constructed in the period 1969-74. It was designed in accord with the 1965 AASHO Specification and applicable supplements as amended by the Kentucky Department of Transportation. The structure was fabricated using the 1967 AWS Welding Code as modified by supplemental requirements of the Kentucky Department of Transportation. The bridge was opened to traffic on October 18, 1974. In 1978, cracking was detected in the floor beam-tie girder connections of the tied arch spans. No adverse experience was reported in the tie girders until the discovery of groove weld cracking in August 1979. The bridge was closed down because of the lack of redundancy in the system, to undertake further inspection and study and to carry out the required retrofit work[4].

1.3 Description of the Structural System for Unit II

The analysis was performed on the Unit II of the bridge, since detailed information and field testing results were available for

this span. Figure 1.1 shows the elevation and plan for the Unit II, tied-arch span. Figure 1.2 shows the floor system framing plan. The panel points are identified as T0 to T17. The bottom lateral bracing is not shown in Fig. 1.2 and was not considered in the analysis. Figure 1.3 shows a typical cross-section of tie flooring system at the location of a floor beam. The reinforced concrete deck is supported on the stringers which are continuous except for expansion joints at panel points T6 and T11. The stringers are spaced 3.20 m apart with the distance between the outside stringers equal to 19.20 m. The stringers bear on to the floor beams, the flanges of which are tapered. The hangers are connected between the upper part of the floor beam web and the bottom of the arch rib. The arch is a double box-section of varying flange and web thicknesses. The tie girder frames into the bottom of the web of the floor beam at each panel point, as can be seen in Fig. 1.3. Figure 1.4 shows the arch rib section details. Properties for the arch rib are summarized in Table 1.1. Figure 1.5 shows typical tie sections. Figures 1.6, 1.7, and 1.8 show the plan and elevation for the joints at various panel points on the tie girder.

All the structural details for the analysis reported here were based on the original design. None of the retrofit details were incorporated into this analysis. However, field measurements on the bridge were made after the retrofitting was carried out. So, some of the retrofit details were incorporated into the results of the

analysis, to compare with the field test measurements, and establish the validity of results of the study. Figures 1.9 and 1.10 show typical retrofit details for spliced panel points on the tie girder.

2. FINITE ELEMENT MODEL OF THE BRIDGE

2.1 Introduction to the Analytical Model

The purpose of the finite element modeling of the tied arch span was to determine the live load stress variation in the tie girder near splice panel point T6. The analysis was done in two stages: (a) a global analysis, and (b) the substructure analysis.

2.1.1 Global Analysis

Since the tied arch bridge is a long span structure, only a quarter of the structure was modeled taking advantage of bisymmetry. However, it was discovered that there were several drawbacks in the use of symmetry to develop the model. Whenever a load is applied to the analytical model, symmetrically sitated loads are created in all quadrants of the structure. Hence, the calculated stress resultants would be due to identical loads in all four quadrants of the structure. Study of field test results showed that the presence of these fictitious loads due to symmetry, affected the stresses significantly. However, these effects were compensated suitably as discussed in later chapters.

The finite element model for the global analysis consisted of 779 active nodes, and was made up of 49 truss elements, 168 beam elements, 416 plane stress elements, and 403 plate bending elements. It is probable that a more crude discretization of the bridge would

still give good results, in describing the overall behavior of the bridge. This would also eliminate the need to use symmetry, thus removing the effects of fictitious, symmetrically placed loads. This was not attempted in the present study due to the time required to develop an alternate finite element model.

The reinforced concrete deck slab was assumed to behave compositely with the stringers. A concentric slab-stringer system was developed, which accounted for the composite action and was located at the neutral axis of the composite section. Plate bending elements were used for the deck slab and beam elements for the stringers. The bearing joints, between the stringers and the floor beams, were simulated with rigid, truss elements between the beam elements used for the stringers and the top flange of the floor beams. The limitation of the use of rigid, truss elements is that no moment transfer is possible between the stringers and the floor beams. However, the use of rigid beam elements would provide a fixed connection between the stringers and the floor beams. Neither of these types of links simulate the actual behavior of the structure. However, the use of truss elements is expected to be in closer agreement with the actual behavior. The expansion joint at T6 was simulated by the use of two sets of superimposed, deck slab nodes, each set of which was connected to the floor beam by rigid truss elements, but were not mutually connected, thus permitting differential horizontal movement at this location. Plate bending elements were used for the flanges of

the floor beam, and plane stress elements were used for the web. The inspection walk opening in the floor beam was not considered in the analysis. Only the floor beam stiffeners at the stringer locations were included in the model.

The arch rib was modeled with beam elements, since the stresses in the arch rib were not of interest, and the use of beam elements would still simulate the overall behavior of the arch rib. The arch rib was assumed to be straight between the panel points, which is also the way it was constructed. Equivalent beam properties for the various sections of the arch, given in Table 1.1, were determined by first converting the arch rib section to a simple double box-section. All the attachments were included in the web plates and central plate of this double box-section so that an equivalent area and moment of inertia resulted. This simplified the computation of torsional inertia for the arch rib. The top lateral bracing at the arch level was also modeled with beam elements.

The hangers between the arch and the floor beams were modeled with truss elements. The hangers on the actual structure are made up of cable strands, which are only effective in tension. It is possible, though highly unlikely, that some of the cables are slack under some loading conditions. However, due to the large dead weight of the structural system, all the cables will be, in general, in tension. The results of the present study were examined to determine the nature of forces in the truss elements used for the cables. One

or two truss elements did show compressive forces. However, these forces were small. Also, taking into account that the dead load of the structure was input as zero, it would seem that with the inclusion of dead load, all cables would indeed be in tension, for all the load cases considered. Hence, the compressive forces in the cables were not significant.

Plate bending elements were used for the flanges of the tie girder and plane stress elements for the web. Gross sections were used at the splices in the tie girder. The modeling of the end connection detail, between the arch and tie, was complicated due to the fact that the arch rib had been replaced in the model with beam elements. This was overcome by expanding the tie girder box-section at the end, to the actual size of the end section on the bridge. The arch rib forces were then transferred to the tie girder by the use of a very rigid, plate bending element, connected over the cross-section of the tie girder at the end support. The beam element representing the end of the arch was connected to the rigid plate concentrically with the tie girder. This connection detail in the model was expected to simulate the transfer of thrust from the arch rib, axially to the tie girder.

The finite element mesh for the model used for the global analysis is shown in Fig. 2.1. It should be noted again that all dead loads were input as zero, since only the live load stresses were of interest. Twenty load load cases were run, four at each of the panel points T4, T5, T6, T7, and T8.

2.1.2 Substructure Analysis

A substructure was isolated from the global system, located around the panel point T6. The tie girder was isolated at sections 3.3782 m to the left of T6 and 4.1148 m to the right of T6. Boundary displacement cards for the substructure were prepared directly from the output of the global analysis, with the help of a computer program developed for this. At the boundary, between the hanger assembly and the floor beam, and at the rigid connectors between the stringers and floor beam, the appropriate element forces from the global analysis were input to satisfy the boundary conditions. The substructure incorporated a finer discretization of the tie girder around the panel point T6.

The substructure consisted of 607 nodal points and was made up of 359 plane stress elements, 264 plate bending elements, and 70 boundary elements. Figure 2.2 shows the finite element mesh adopted for the substructure analysis. The analysis was carried out for twenty different load cases. The output from SAP IV, for plate bending elements, were moments for unit length and membrane stresses, as shown in Fig. 2.3.

These were used to calculate the flange stresses in the tie girder, along the x direction, which is parallel to the length of the span. The flange stress was calculated by the use of the following equation, which gives the stress for the fibre farthest away from the neutral axis of the plate element.

$$\sigma_{xx} = S_{xx} + \frac{6\ M_{xx}}{t_f^{\ 2}} \qquad (2.1)$$

Where: σ_{xx} = Flange stress in x direction

S_{xx} = Membrane stress in x direction

M_{xx} = Moment per unit length along an edge perpendicular to the x axis

t_f = flange thickness

In most cases, it was found that contribution to σ_{xx} due to moment M_{xx} was negligible. The contribution of the moment was included only when it was greater than 3%.

3. STUDY OF FIELD TEST RESULTS

3.1 Field Testing

The I24 bridge was reopened to traffic on May 12, 1981, after extensive retrofitting had been carried out. At that time, field testing was carried out on Unit II of the bridge, which was instrumented at panel point locations T6 and T11. Strain gages were mounted on the tie girder, at each of the panel points T6 and T11, on and around the reinforcement splices. At T6 reinforcement splice plates covered all the flanges and webs of the tie girder, and at T11 only the girder web reinforcement splices were added. The reinforcement splices were installed over the original bolted connections.

Figure 3.1 shows the location of gages at T6 and T11. The numbers 1, 2, 3, and 4 represent gage locations at each cross-section. The spacing between the gages at Sections A, B, C, and D is approximately 2.54 m. Two 3D trucks of known weight were used to determine the response of the tie girder. The total weight of the two trucks was 395.6 kN. Figure 3.2 shows the dimensions and the loads on the test trucks. The transverse spacing between wheels on the same axle was 1.829 m. The test trucks were placed side by side, on adjacent lanes and crossed the structure at a speed of 80.5 kph.

Analog strain readings were obtained during the movement of the test trucks, on the same side of the road as the instrumented tie

girder. Readings were also obtained when the test trucks were on the opposite side of the bridge. The analog data obtained at panel point T11 for Section B is shown in Figs. 3.3 to 3.5. The chart speed was 5 mm/sec. considering the truck speed of 80.5 kph, this gives a scale of 4.48 m/mm. The portion of the chart corresponding to the movement of the trucks on the bridge has been marked on Figs. 3.3 to 3.5 The rest of the response on these charts is a result of the vibrational response of the bridge. The maximum negative stress in the top flange of the tie girder, and the maximum positive stress in the bottom flange occurred when the trucks were directly above T11. Figure 3.5 compares the analog data in Gage 2, at Section B, for the test trucks traveling in the opposite direction, on the opposite side of the road, with the response given in Fig. 3.3. It is apparent from the traces given in Figs. 3.3 and 3.4 that the maximum stress range for the top flange is obtained at the inboard top fibre, and the maximum stress range for the bottom flange occurs at the outboard bottom fibre, that is, at gage locations 2 and 4.

3.2 Stress History Study

The average daily truck traffic in 1981 was determined from a 24 hour traffic count to be 7372, which is the total traffic in both directions. The sample may be too small for the number to be very reliable. Stress history measurements were acquired at locations A4, B4, C4, and D4. These are summarized in Table 3.1. The maximum

stress response was obtained at A4. The stress response for gage location A4 is shown in Fig. 3.6 in the form of a histogram. This was used to determine the fatigue life of the tie girder box corner weld detail, as discussed in Chapter 5.

4. RESULTS OF THE ANALYTICAL STUDY

4.1 Development of Influence Lines

Based on the results of the finite element analysis, influence lines for the stresses in the tie girder were developed. These influence lines covered load locations between panel points T4 and T8. The center lines of the two lanes of traffic were located by assuming equal width of traffic lanes between the center and outer stringers. Figure 4.1 shows the assumed location of the traffic lanes on the deck, and the finite element model used for the deck, between two adjacent panel points, in the global analysis. The influence lines were based on the twenty load cases, used for the finite element study. As shown in Fig. 4.1, the deck was divided into three plate elements parallel to the direction of the road, between the center and edge of the roadway. In obtaining the influence lines, loads at any position between T4 and T8 were redistributed to the corners of the plate bending element on which they were located. This distribution was done on the basis of simple statics, which is based on static equivalence of loads, for the particular deck element. Figure 4.2 shows the redistribution of loads, for a general load P, to the corners of the rectangular deck element it is situated on. P1, P2, P3, and P4 are the equivalent loads for P. In the longitudinal direction, the loads were directly redistributed to the panel point nodes, ignoring the line of nodes at

the center section between any two panels. This was done to reduce the number of load cases required. The distance between panel points is about 11.28 m. Here, considering the axle spacings of the trucks assumed in this analysis, the above redistribution seems to be reasonable.

Axle loads were placed directly on the center line of the lanes, rather than considering each wheel load separately. Trial studies were carried out to determine if this loading was satisfactory. The two wheels of the same axle were not always located on the same deck element. The trial studies showed that considering axle loads directly yielded almost identical results to case when the wheel loads were considered separately.

The use of simple statics to redistribute loads to the nodal points, has one serious limitation. It can be mathematically shown that for any number of loads located on the same element of the deck slab, they can be replaced by a single load located at the centroid of the loads. The resultant redistributed load to any particular nodal point would be identical in the two cases. Here, the resultant stress obtained, for any particular structural element, by considering all loads separately, should be identical to the stress obtained by using the resultant force. Since the relationship between the locations of the system of forces and the resultant force is linear, this suggests that the corresponding influence line should also be linear between the sections along the span, which contain the

redistribution points. Since, in the present case, the redistribution points were at the panel locations, the influence lines will be linear between the successive panel points. This is an approximate condition, especially in cases where the actual influence line is non-linear. The closer the points of redistribution are located, the more accurate the influence line will be.

The influence lines for loads between panel points T4 and T8, for the two traffic lanes, were developed using a 10 kN axle load. Stresses due to any arbitrary truck location were obtained from superposition, by combining the values of the particular influence line appropriately. The locations on the tie girder at panel point T6, for which influence lines were developed are shown in Fig. 4.3. These locations are marked 0 to 7. In the substructure analysis, the flanges of the tie girder were divided into five elements, at each cross-section. It was found in the substructure analysis, that the elements in the same flange, at any particular cross-section, did not have identical stress conditions. The variation was quite significant. The inboard top flange element and the outboard bottom flange element develop the maximum stress. This behavior was observed in the field test measurements as well. Major axis bending, combined with axial tension, alone does not explain the differences in stress in the elements of the same flange. However, considering biaxial bending and torsion complicates the analysis. To simplify the computations, the stresses were averaged for the outer and center

elements of the flanges, at any particular location. Thus, the influence lines were developed for the average stress in the top and bottom flange of the tie girder.

A computer program was developed to plot the influence lines for the top and bottom fibers of the tie girder. The influence lines obtained at various locations are shown in Figs. 4.4 to 4.17. It might be emphasized that these influence lines are really based on the superimposed effects of the fictitious loads created due to the assumption of bi-symmetry, in the finite element model. This results in a magnification of the stresses developed, especially due to the loads on adjacent lanes, on the opposite side of the road. These effects have been taken into account appropriately.

4.2 Comparison with Field Test Measurements

An attempt was made to compare the results of the analytical study with the field test measurements. An important difference between the analytical study and the field study was that while the analytical study reported here was carried out on the original structural system, the field study was performed on the retrofitted structure. Hence a direct comparison of the results of the two studies was not possible. However, an approximate method of converting the results of the analytical study to suit the retrofitted details was developed. The stresses in the flanges of the tie girder at location 1 (Fig. 4.3) were compared with the stresses measured on

the field at gage location B (Fig. 3.1). The test-trucks used for this comparison are shown in Fig. 3.2.

The stress at any location on the tie girder is given by:

$$\sigma = \sigma_T + \sigma_b \qquad (4.1)$$

where σ_T is the stress due to axial force and is equal to $\frac{P}{A}$, where P is the axial force, and A is the area of cross-section. σ_b is the major axis bending stress given by $\pm\left(\frac{MC}{I}\right)$, where M is the bending moment, I is the moment of inertia of the cross-section, and C is the distance from the neutral axis of the section. Equation (4.1) does not account for the presence of biaxial bending and torsion and is used to simplify the analysis.

The retrofitting carried out on the bridge is expected to create only local effects. Under these conditions, it was assumed that the axial force P and bending moment M are not altered significantly from the original details. Hence, the bending stress and tensile stress for the retrofitted sections, can be computed from the following relationships.

$$\sigma_{TR} = \frac{P}{A_R} = \sigma_T \left(\frac{A}{A_R}\right) \qquad (4.2)$$

$$\sigma_{bR} = \pm\frac{MC}{I_R} = \sigma_b \left(\frac{I}{I_R}\right) \qquad (4.3)$$

where A_R and I_R are, respectively, the area and moment of inertia of the retrofitted sections.

The resultant stress would then be given by:

$$\sigma_R = \sigma_{TR} + \sigma_{bR} \tag{4.4}$$

At the panel point T11, only web splice retrofit plates were installed. The size of these plates was 762 mm x 28.575 m, one on each web. Based on these plate sizes, A_R and I_R were computed. The ratio $\frac{A}{A_R}$ was determined to be 0.585 and $\frac{I}{I_R}$ was 0.715.

Table 4.1 gives the summary of the average flange stresses for the original finite element model, for the passage of test trucks over the bridge. Maximum and minimum stresses in the top and bottom flange of the tie girder at location 1 were determined, for outside lane and inside lane, truck loads. The stress response was then separated into axial tension σ_T and major axis bending σ_b. These stresses were then used in Eqs. (4.2) and (4.3) to obtain axial tension stress σ_{TR} and bending stress σ_{bR}, for the retrofitted section. These were then combined according to Eq. (4.4) to obtain the corresponding top and bottom flange stresses for the retrofitted tie girder at location 1.

Table 4.2 gives the modified stresses assuming the presence of retrofit splices. Figure 4.18 shows a schematic for the corresponding superposition of the stress diaphragms from the analytical study, for the test truck on the inside lane.

Based on the analysis, the average stress range for the top flange of the retrofitted section, with test rucks on both lanes, was

found to be 20.06 MPa, and for the bottom flange, it was 21.24 MPa. Because of the effects of symmetry, these stresses correspond to two test trucks traveling in both the northbound and southbound directions of the bridge. Hence, to compare with the field study, the field response for the northbound and southbound trucks would have to be superimposed. Also, the analytical study takes into account only the static response of the bridge. Figures 3.3 to 3.5 show that the vibrational response accounts for as much as 20% of the total stress cycle. However, it is not possible to completely separate the analog strain measurements into static and vibrational response. Hence, a band was established corresponding to the lower and upper limits of the static response. The lower limit of this band corresponds to the condition when the vibrational response magnifies the static response for each load position. The upper limit corresponds to the case when the vibrational response creates compensatory stresses to the static response, at all load positions. In general, the lower limit of this band corresponds more closely to the actual structural behavior. These computations, based on the field study, are presented in Table 4.3, for gage locations 1B and 2B. The responses due to northbound and southbound trucks were added together to correspond to the condition obtained from the analytical model. The static stress range for gages 1B and 2B were averaged to obtain the top flange stress response. Only the top flange stresses were compared between the analytical model and field study, since strain measurements for southbound trucks were not available for gage locations 3B and 4B.

The field study gave top flange static-stress-response limits of 25.51 MPa to 40.68 MPa. The analytical study gave a static stress range of 20.06 MPa. This comparison does not account for all the differences between the structural behavior and the analytical model. The estimates for the vibrational response of the structure are only approximate. Also, minimization of the twist of the floor beam due to the truss links assumed between the stringer and floor beams could be another cause of discrepancy. However, the general shape of the response from field study conforms to the response obtained from the analytical model, once the effects of vibration are removed.

4.3 Study of the Stress Variations in the Tie Girder

This study was done using the original design conditions on comparison of the influence lines developed for outside lane and inside lane loads, shown in Figs. 4.4 to 4.17, it is apparent that the behavior is similar for loads on both lanes. The outside lane loads create slightly more severe stress conditions. Hence, for this part of the study, only outside lane, truck loading was considered. Also, the effect of loads on the southbound lanes, which developed due to symmetry, were not considered, since these only magnify the stress, and the type of stress response would still remain the same. A HS20 truck was adopted for this study. Figure 4.19 shows the axle spacing and loads for such a truck.

Table 4.4 shows the critical stresses obtained for the various sections. The truck location at T6 produces maximum negative stress

in the top flange and maximum positive stress in the bottom flange. The maximum positive stress for the top flange and the corresponding bottom flange stress were obtained when the truck load was concentrated at T8. The response was separated into the response due to bending and due to tension forces. It is seen from Table 4.4, as well as Figs. 4.4 to 4.10, that while the top flange experiences a stress reversal, the bottom flange does not. Hence, the stress ranges for the top and bottom flanges are controlled by different load locations. The contributions of bending and tension to the total stress range were also determined. These are plotted in Figs. 4.20 and 4.21, for the top flange and bottom flange respectively. It is apparent that tension contributes more significantly to the total stress range for the bottom flange, than for the top flange. However, in both cases, bending is still the predominant mode of stress vibration. The sudden drop in stress ranges at locations 4, 5, and 6 is due to the increased section of the tie girders; these are located on the splice at T6. Location 7 is immediately after the splice and thus shows an increase in stress range due to the reduced cross-section.

It is also apparent from Table 4.4 that when the truck is at panel point T6, bending is the dominant stress rangel mode. However, as the truck moves to T8, axial tension becomes the dominant mode of stress. Hence, the mathematical model also indicates that bending of the tie girder is a local effect. This is directly comparable to the measured stress range shown in Figs. 3.3 to 3.5.

5. ESTIMATED FATIGUE DAMAGE OF THE BOX CORNER WELD DETAIL

5.1 Fatigue Life of Structural Details

The primary factors governing the fatigue strength of any structural detail are the applied stress range, the number of cycles and the type of detail[5]. All welding processes invariably introduce small discontinuities in or near the weldment. These discontinuities, with the added presence of stress concentration conditions at the detail, propagate by fatigue until crack instability results. The presence of cracks in welded structures is more significant because of the continuous path provided by the welded connections and because high residual tensile stresses exist.

Members and details on bridges are arranged into five basic classes for fatigue design purposes[6]. A number of typical bridge etails are classified in Ref. 7. Design fatigue resistance curves have been developed, to be applied to various categories of details.

In the initial stages of fatigue crack growth in an as welded structure, most of fatigue life occurs in regions of high tensile residual stress. Under cyclic loading, the material at or near the initial discontinuity will be subjected to a fully effective cyclic stress, even in cases of stress reversal. This is the major reason why stress range alone is the variable describing the fatigue behavior of welded joints. Most of the fatigue life is exhausted by the time the fatigue crack propagates out of this high tensile residual zone.

5.2 Fracture Mechanics Approach

The design fatigue resistance curves are not applicable when large cracks (internal flaws greater than 6.35 mm, and visible weld toe cracks) exist because of fabrication or some other cause. The residual fatigue life must be estimated by the use of fracture mechanics models[8].

The stress intensity range is given as

$$\Delta K = F_e \; F_s \; S_w \; F_g \; (S_r) \; \sqrt{\pi a} \qquad (5.1)$$

Where F_e = Crack shape correction

F_s = Front free surface correction

F_w = Back surface correction

F_g = Stress gradient correction

a = Crack size

S_r = Stress range

The possibility of fatigue crack growth is dependent on the initial flaw size. Tests have shown that below he crack growth threshold steels (ΔK_{Th} = 3.3 MPa $\sqrt{m}$), crack propagation does not occur under constant cyclic stress. However, in the case of random variable loading, as occurs on a bridge, if any of the stress cycles create a stress intensity range greater than ΔK_{Th}, all stress cycles seem to participate in the crack propagation.

5.3 Variable Amplitude Load Spectrum

Test results by Schilling, et al.[9] showed that variable amplitude loading with a random sequence stress spectrum, can be represented by a single constant amplitude effective stress range that would result in the same fatigue life as the variable amplitude stress range spectrum.

The effective stress range is given by

$$S_{re} = \left[\gamma_i \; S_{ri}{}^{n}\right]^{1/2} \tag{5.2}$$

where S_{ri} is the i_{th} stress range and γ_i is the frequency of occurrence of the i_{th} stress range. Two popular ways of computing the effective stress range are the root mean square (RMS) method (n = 2), and the Miner's effective stress range (n = 3). Using n = 3, is equivalent to the Miner's law[10].

$$\sum \frac{n_i}{N_i} = 1 \tag{5.3}$$

In the present study, the Miner's effective stress range was adopted.

5.4 Fatigue Crack Propagation

The fatigue crack propagation or crack growth rate, $\frac{da}{dN}$ is usually related to the variation of stress intensity factor by the Paris Power Law[11,12]

$$\frac{da}{dN} = C\Delta K^n \tag{5.4}$$

C and n are material constants for the steels, n can be taken as 3.0 for most structural steels, and C is equal to 2×10^{-10} for a mean value and 3.6×10^{-10} for an upper bound fit to available crack growth data when the units are ksi $\sqrt{in}$.

Equation (5.4) can be integrated to obtain the number of cycles required to propagate a crack a_i to some larger value a_f.

$$\Delta N = \int_{a_i}^{a_f} \frac{da}{C\Delta K^n} \tag{5.5}$$

In general, a closed form integration is not possible, and approximate numerical integration techniques have to be used.

Crack instability is often the limiting condition in the fatigue life of a detail. The maximum stress intensity factor is given by

$$K_{max} = F_e\ F_s\ F_w\ F_g\ S_{max}\ \sqrt{\pi a} \tag{5.6}$$

Large cracks normally have a negligible stress concentration factor, and hence f_g can be taken equal to 1.0. S_{max} is the maximum stress. When the crack tip is in a residual tensile zone, a conservative value for S_{max} is equal to σ_y. When K_{max}, the estimated maximum stress intensity factor, equals K_c, the fracture toughness of the connected material, brittle fracture occurs. Hence, for the detail to be safe and develop the full fatigue resistance, K_{max} should always be less than K_c when the crack is smaller than the plate thickness.

Hence, the material fracture toughness will often control the size of the largest crack that can be tolerated before a fracture of the member or component will occur. This crack size is normally used in Eq. 5.5 as a_f, to determine the fatigue life of the detail.

5.5 Fatigue Life of the Tie Girder Box Corner Weld Detail

5.5.1 Crack Geometry

Examination of the box corner weld at crack locations showed that the crack was elliptical in shape which was partly exposed to the surface along the major axis[2]. Embedded, penny shaped cracks were also found. However, since the surface crack provides the more severe condition, the propagation of this type of crack is examined in this study. Figure 5.1 shows the idealized corner crack.

The crack shape correction factor was taken as

$$Fe = \frac{1}{E(K)} \left[\left(\sin^2 \phi + \left(\frac{a}{c} \right)^2 \cos^2 \phi \right) \right]^{1/4} \qquad (5.7)$$

Where a and c are, respectively, the semi-minor and semi-major axis of the elliptical crack, and ϕ is the location, from the major axis where the stress intensity factor is required.

E(K) is the complete elliptical integral of the second kind:

$$E(K) = \int_0^{\frac{\pi}{2}} \left[1 - \left(1 - \frac{a^2}{a^2} \right) \sin^2 \theta \right]^{1/2} d\theta \qquad (5.8)$$

K is defined as:

$$K = 1 - \frac{a^2}{c^2} \tag{5.9}$$

E(K) can be evaluated by the use of the following equation[13]:

$$E(K) = \frac{\pi}{2}\left\{1 - \left(\frac{1}{2}\right)^2 \frac{K^2}{1} - \left[\frac{(1)\ (3)}{(2)\ (4)}\right]^2 \frac{K^4}{3} - \left[\frac{(1)\ (3)\ (5)}{(2)\ (4)\ (6)}\right]^2 \frac{K^6}{5} - - - -\right\} \tag{5.10}$$

The combined finite width and back surface correction was taken as

$$F_w = \left(1 + 0.122\ \cos^4 \frac{\pi a}{2b}\right)\left(\frac{2b}{\pi a} \tan \frac{\pi a}{2b}\right)^{1/2}$$

where "b" the dimension shown in Fig. 5.1.

The crack shape relationship was assumed as follows[9]

$$C = 1.088a^{0.946} \tag{5.11}$$

5.5.2 Susceptibility to Crack Growth

The susceptibility of a given crack to fatigue crack propagation depends on the maximum stress range developed. From the field stress history study, the maximum stress range developed was 52.40 MPa. When the stress intensity factor range, with the maximum stress range acting, exceeds ΔK_{Th}, crack propagation can occur. ΔK_{Th} was assumed conservatively to be 3.0 MPa $\sqrt{m}$, to represent a high residual stress condition.

The smallest crack size "a", susceptible to crack growth was determined to be 2.03 mm, where "2a" is the minor axis diameter of the elliptical crack.

5.5.3 Fatigue Life Estimate

The effective stress range, based on the stress history study shown in Fig. 5.2, is 12.48 MPa. The fatigue life was determined based on the number of cycles required for the crack to propagate through the entire box corner thickness, that is when "a" approaches 25.4 mm (Fig. 5.1).

Fracture was not considered as a limit of fatigue life, since the residual stress distribution at the box corner weld is complicated. Hence, a fracture analysis would be complex and require a knowledge of the residual stress field. Various crack sizes were examined. The fatigue life study is summarized in Table 5.1.

6. CONCLUSIONS

The finite element study shows that the tie girders experience significant bending stresses. These bending stresses are, primarily, localized effects and are caused mainly by the distortion of the floor system at the panel points. Bending is the major contribution to the stress range cycles.

The present study suggests there is a need to modify the current design philosophy which assumes the tie girders to be primary tension members. The presence of various weld discontinuities and defects and the unaccounted bending stresses reduce the fatigue life of the details involved significantly. An analytical method for including the presence of bending of tie girders is required.

The correlation between the field study and the analytical model was limited, since it was not possible to account for all the differences in the behavior of the structure and the response provided by the model. Among the factors contributing to the variation was the dynamic vibrational response of the structure, the differences in loading, and the assumed truss connections between the stringers and the floor beams. The vibrational response made it difficult to superimpose the measured response for the separate north and southbound measurements. Since the analytical model made use of symmetry, the precise superposition of the north and southbound measurements was limited by knowning their precise location, along the structure.

The truss connections used between the stringers and floor beams minimized the twisting of the floor beams.

The fatigue life studies of the longitudinal fillet welds at the box corners show that any crack greater than 2.03 mm (semiminor diameter) in size is susceptible to fatigue crack propagation. In the present study, fracture was not considered as a limiting condition to the fatigue life. Hence, the fatigue life estimates presented, may not be accurate.

To get a better estimate of the fatigue life, the residual stress distribution at the box corner weld detail would have to be obtained and considered in the determination of the maximum stress at the detail. A terminal crack size, at which fracture would occur, could then be determined based on the fracture toughness of the material.

TABLE 1.1 PROPERTIES FOR ARCH RIB

Section Designation	Flange Thickness (cm)	Modified Web Thickness (cm)	I_{xx} (cm^4) $x10^4$	I_{yy} (cm^4) $x10^4$	Area (cm^2) $x10^2$	K_T (cm^4) $x10^4$
RA	2.54	2.16	1617.1	284.0	18.72	771.7
RB	2.54	1.68	1453.2	231.1	16.13	632.7
RC	2.54	2.48	1726.3	319.3	20.45	857.4
RD	3.65	2.48	2108.6	333.5	22.48	926.6
RE	3.65	1.68	1835.5	245.3	18.16	669.6
RF	4.13	1.68	1999.4	251/3	19.03	680.0
RG	3.81	1.68	1890.2	27.3	18.45	673.3
RH	3.02	1.68	1617.1	237.2	17.0	651.3

TABLE 1.1 PROPERTIES FOR ARCH RIB

Section Designation	Flange Thickness (cm)	Modified Web Thickness (cm)	I_{xx} (cm^4) $x10^4$	I_{yy} (cm^4) $x10^4$	Area (cm^2) $x10^2$	K_T (cm^4) $x10^4$
RA	2.54	2.16	1617.1	284.0	18.72	771.7
RB	2.54	1.68	1453.2	231.1	16.13	632.7
RC	2.54	2.48	1726.3	319.3	20.45	857.4
RD	3.65	2.48	2108.6	333.5	22.48	926.6
RE	3.65	1.68	1835.5	245.3	18.16	669.6
RF	4.13	1.68	1999.4	251/3	19.03	680.0
RG	3.81	1.68	1890.2	27.3	18.45	673.3
RH	3.02	1.68	1617.1	237.2	17.0	651.3

TABLE 3.1 STRESS HISTORY MEASUREMENTS

Stress Range (MPa)	Estimated 50 year Count ($x10^6$ Cycles) Gage - Locations A4	B4	C4	D4
7.52	93.64	27.53	20.26	55.17
11.24	18.58	7.44	5.02	15.70
14.96	8.54	4.10	1.44	5.53
18.69	3.65	0.54	0.11	3.77
22.48	3.21	0.08	0.02	2.51
26.20	2.26	0.04	0.01	1.14
29.92	1.24	0.04	--	0.42
33.65	0.43	--	--	0.15
37.44	0.16	--	--	0.02
41.16	0.07	--	--	0.02
44.89	0.02	--	--	0.02
48.61	0.02	--	--	--
52.40	0.02	--	--	--

TABLE 4.1 SUMMARY OF STRESSES DUE TO TEST TRUCKS FROM THE ANALYTICAL STUDY AT LOCATION 1

Test Truck Location	Top Flange Stress (Max. or Min.) (Mpa)	Bottom Flange Stress (Max. or Min.) (MPa)	Axial Tension (MPa)	Bending Stress σ_b (±) (MPa)
Inside Lane	-4.69	+15.65	5.45	10.20
	+9.52	+3.38	6.48	3.03
Outside Lane	-4.96	+16.07	5.58	10.48
	+9.03	+3.86	6.48	2.55

TABLE 4.1 SUMMARY OF STRESSES DUE TO TEST TRUCKS FROM THE ANALYTICAL STUDY AT LOCATION 1

Test Truck Location	Top Flange Stress (Max. or Min.) (Mpa)	Bottom Flange Stress (Max. or Min.) (MPa)	Axial Tension (MPa)	Bending Stress σ_b (±) (MPa)
Inside Lane	-4.69	+15.65	5.45	10.20
	+9.52	+3.38	6.48	3.03
Outside Lane	-4.96	+16.07	5.58	10.48
	+9.03	+3.86	6.48	2.55

TABLE 4.2 MODIFIED STRESSES FROM THE ANALYTICAL STUDY AT LOCATION 1

Test Truck Location	Modified Axial Tension σ_{TR} (MPa)	Modified Bending Stress σ_{BR} (MPa)	Top Flange Stress (Max. or Min.) (MPa)	Bottom Flange Stress (Max. or Min.) (MPa)
Inside Lane	3.17	7.31	-4.137	+10.48
Inside Lane	3.79	2.21	+6.0	+1.59
Outside Lane	3.24	7.52	-4.27	+10.76
Outside Lane	3.79	1.86	+5.65	+1.93

TABLE 4.2 MODIFIED STRESSES FROM THE ANALYTICAL STUDY AT LOCATION 1

Test Truck Location	Modified Axial Tension σ_{TR} (MPa)	Modified Bending Stress σ_{BR} (MPa)	Top Flange Stress (Max. or Min.) (MPa)	Bottom Flange Stress (Max. or Min.) (MPa)
Inside Lane	3.17	7.31	-4.137	+10.48
Inside Lane	3.79	2.21	+6.0	+1.59
Outside Lane	3.24	7.52	-4.27	+10.76
Outside Lane	3.79	1.86	+5.65	+1.93

TABLE 4.3 SEPARATION OF STRESS RESPONSE FROM THE FIELD STUDY INTO STATIC AND VIBRATIONAL RESPONSE

Gage Location	Direction of Traffic	Total Stress Range (MPa)	Estimated Stress Range Due to Vibrational Response (MPa)	Limits of Static Stress Range (Mpa)	Limits of Static Stress Range for N.B. & S.B. Trucks (MPa)
1B	Northbound	16.55	4.14	12.41 to 20.69	22.4 to 36.2
1B	Southbound	12.76	2.76	10.0 to 15.51	
2B	Northbound	20.69	4.83	15.86 to 25.5	28.3 to 44.8
2B	Southbound	15.86	3.45	12.4 to 19.3	

TABLE 4.3 SEPARATION OF STRESS RESPONSE FROM THE FIELD STUDY INTO STATIC AND VIBRATIONAL RESPONSE

Gage Location	Direction of Traffic	Total Stress Range (MPa)	Estimated Stress Range Due to Vibrational Response (MPa)	Limits of Static Stress Range (Mpa)	Limits of Static Stress Range for N.B. & S.B. Trucks (MPa)
1B	Northbound	16.55	4.14	12.41 to 20.69	
					22.4 to 36.2
1B	Southbound	12.76	2.76	10.0 to 15.51	
2B	Northbound	20.69	4.83	15.86 to 25.5	
					28.3 to 44.8
2B	Southbound	15.86	3.45	12.4 to 19.3	

TABLE 4.4 CRITICAL STRESSES FOR HS20 TRUCK LOADING ON THE OUTSIDE LANE

Section Designation	Truck Location	Top Flange Stress (MPa)	Bottom Flange Stress (MPa)	Axial Tension σ_T (MPa)	Bending Stress $\sigma_b^{(\pm)}$ (MPa)
1	T6	-6.69	+24.41	8.83	15.58
1	T8	+14.69	+6.07	10.41	4.31
2	T6	-7.65	+25.51	8.93	16.55
2	T8	+14.82	+6.07	10.48	4.34
3	T6	-8.21	+23.99	7.93	16.07
3	T8	+14.69	+5.86	10.27	4.41
4	T6	-3.65	+11.17	3.79	7.38
4	T8	+6.62	+2.96	4.83	1.79
5	T6	-3.24	+10.89	3.79	7.10
5	T8	+6.62	+2.96	4.83	1.79
6	T6	-2.55	+10.41	3.93	6.48
6	T8	+6.48	+3.10	4.83	1.65
7	T6	-4.69	+22.62	8.96	13.65
7	T8	+13.65	+7.24	10.48	3.17

TABLE 4.4 CRITICAL STRESSES FOR HS20 TRUCK LOADING ON THE OUTSIDE LANE

Section Designation	Truck Location	Top Flange Stress (MPa)	Bottom Flange Stress (MPa)	Axial Tension σ_T (MPa)	Bending Stress $\sigma_b^{(\pm)}$ (MPa)
1	T6	-6.69	+24.41	8.83	15.58
1	T8	+14.69	+6.07	10.41	4.31
2	T6	-7.65	+25.51	8.93	16.55
2	T8	+14.82	+6.07	10.48	4.34
3	T6	-8.21	+23.99	7.93	16.07
3	T8	+14.69	+5.86	10.27	4.41
4	T6	-3.65	+11.17	3.79	7.38
4	T8	+6.62	+2.96	4.83	1.79
5	T6	-3.24	+10.89	3.79	7.10
5	T8	+6.62	+2.96	4.83	1.79
6	T6	-2.55	+10.41	3.93	6.48
6	T8	+6.48	+3.10	4.83	1.65
7	T6	-4.69	+22.62	8.96	13.65
7	T8	+13.65	+7.24	10.48	3.17

TABLE 5.1 FATIGUE LIFE ESTIMATE FOR THE BOX CORNER WELD DETAIL INITIAL CRACK

Size		
Minor Semidiameter "a" (mm)	Major Semidiameter "c" (mm)	Fatigue Life ($x10^6$ Cycles)
6.35	7.44	640
8.89	10.24	394
11.43	12.98	239
13.97	15.70	136

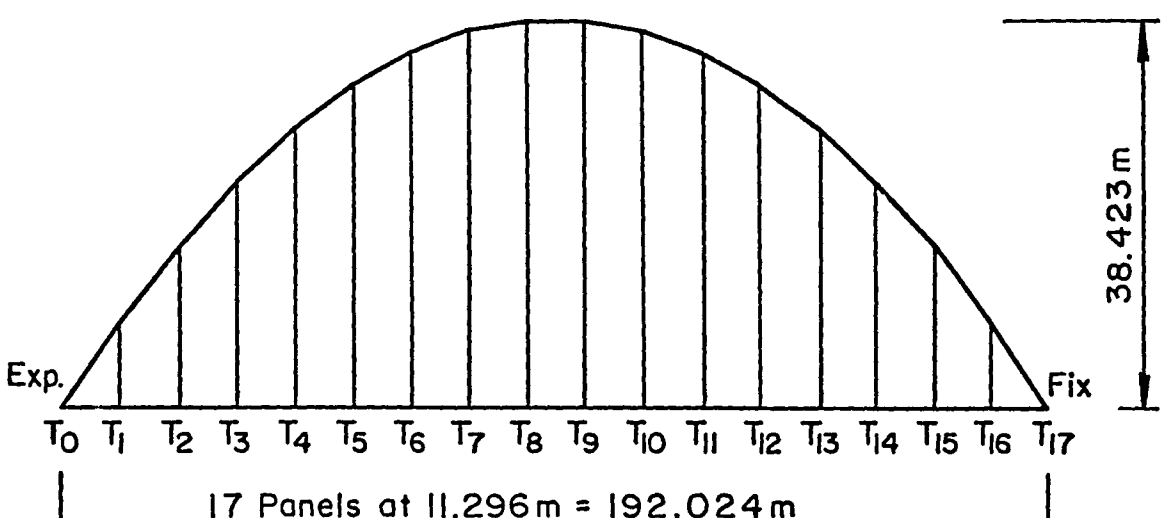

Elevation

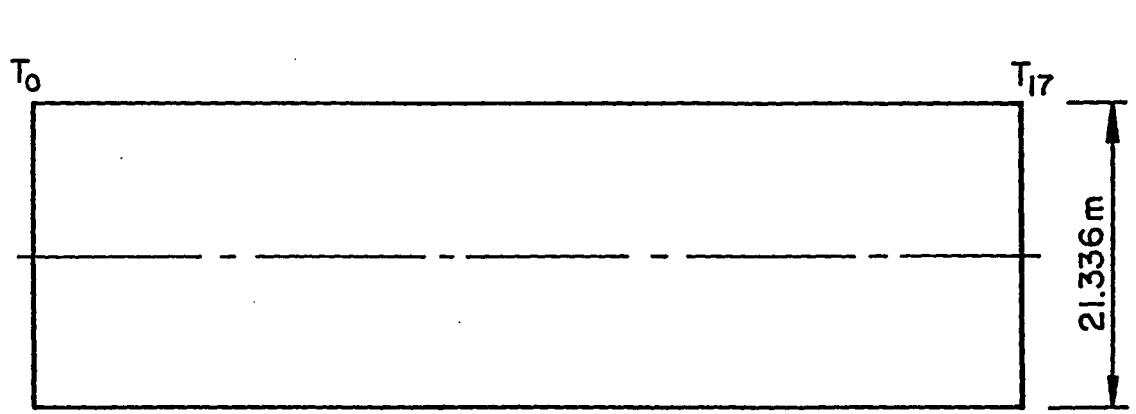

Plan at Floor Beam Level

Fig. 1.1 Plan and Elevation of the Tied Arch Span (Unit II)

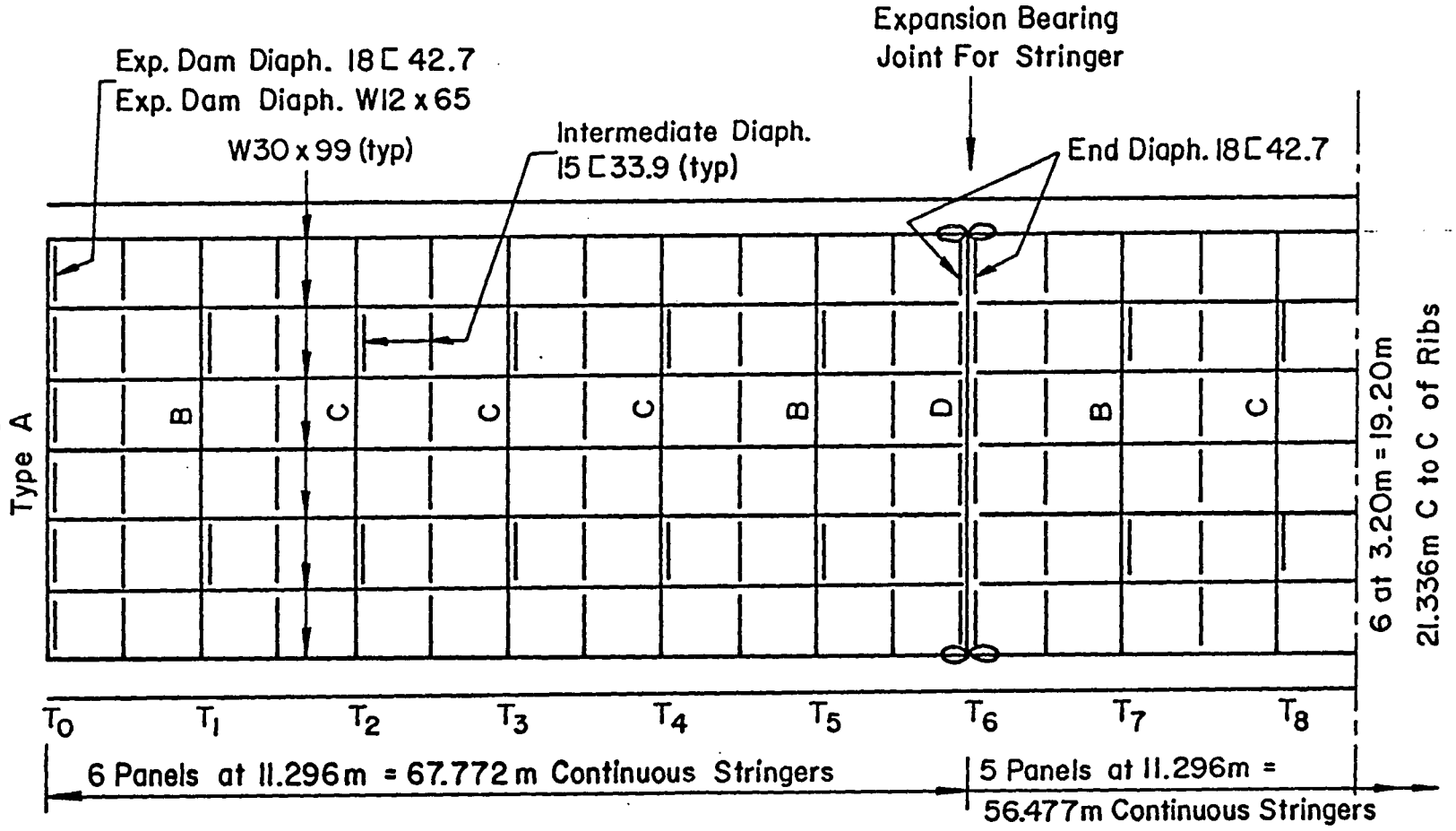

Fig. 1.2 Floor System Framing Plan

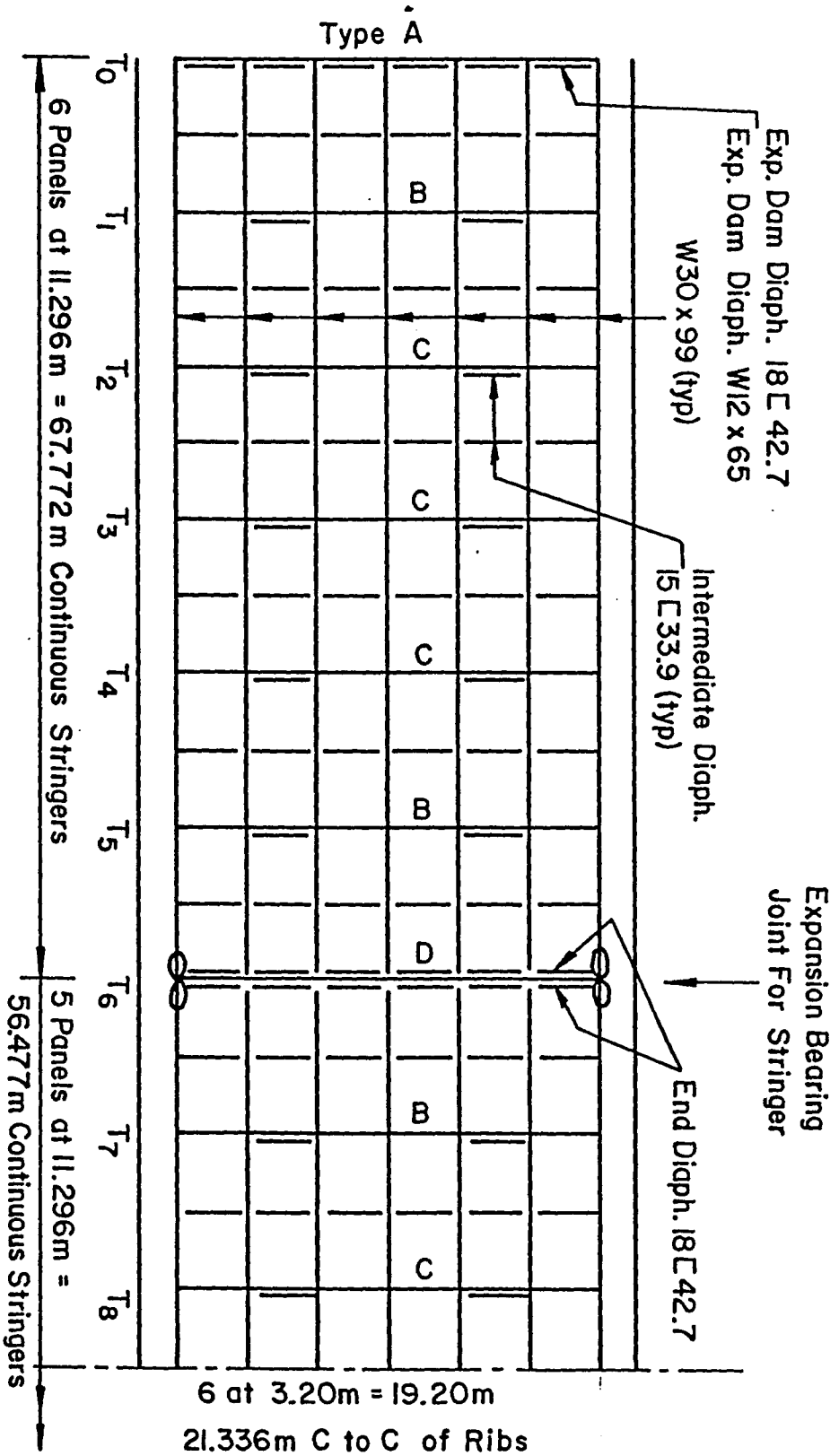

Fig. 1.2 Floor System Framing Plan

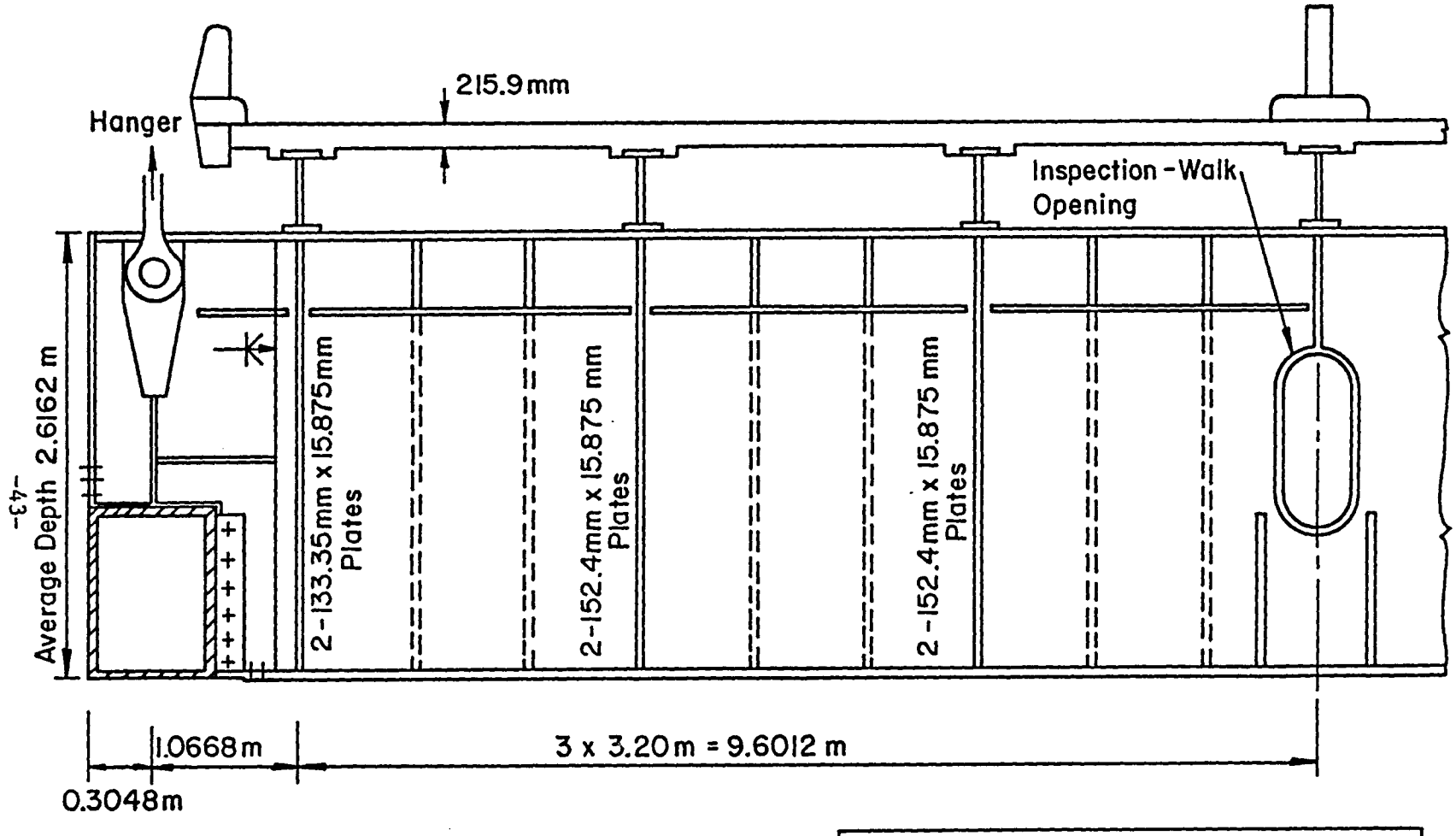

Flange Plate Thickness (mm)				
FL. Beam Type	A	B	C	D
Thickness	41.28	39.69	36.51	28.58

Fig. 1.3 Typical Cross-Section of Floor System

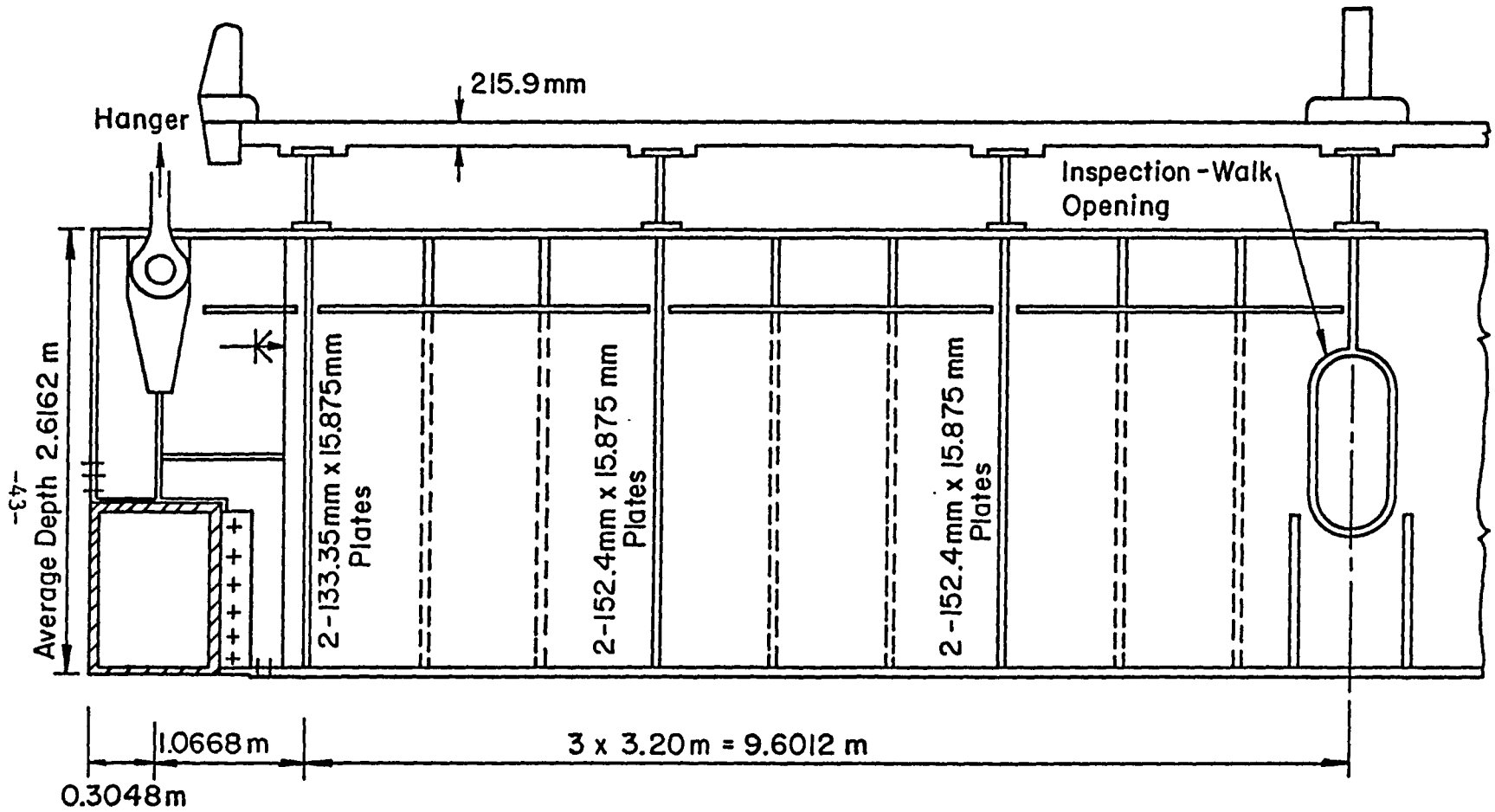

Flange Plate Thickness (mm)				
FL. Beam Type	A	B	C	D
Thickness	41.28	39.69	36.51	28.58

Fig. 1.3 Typical Cross-Section of Floor System

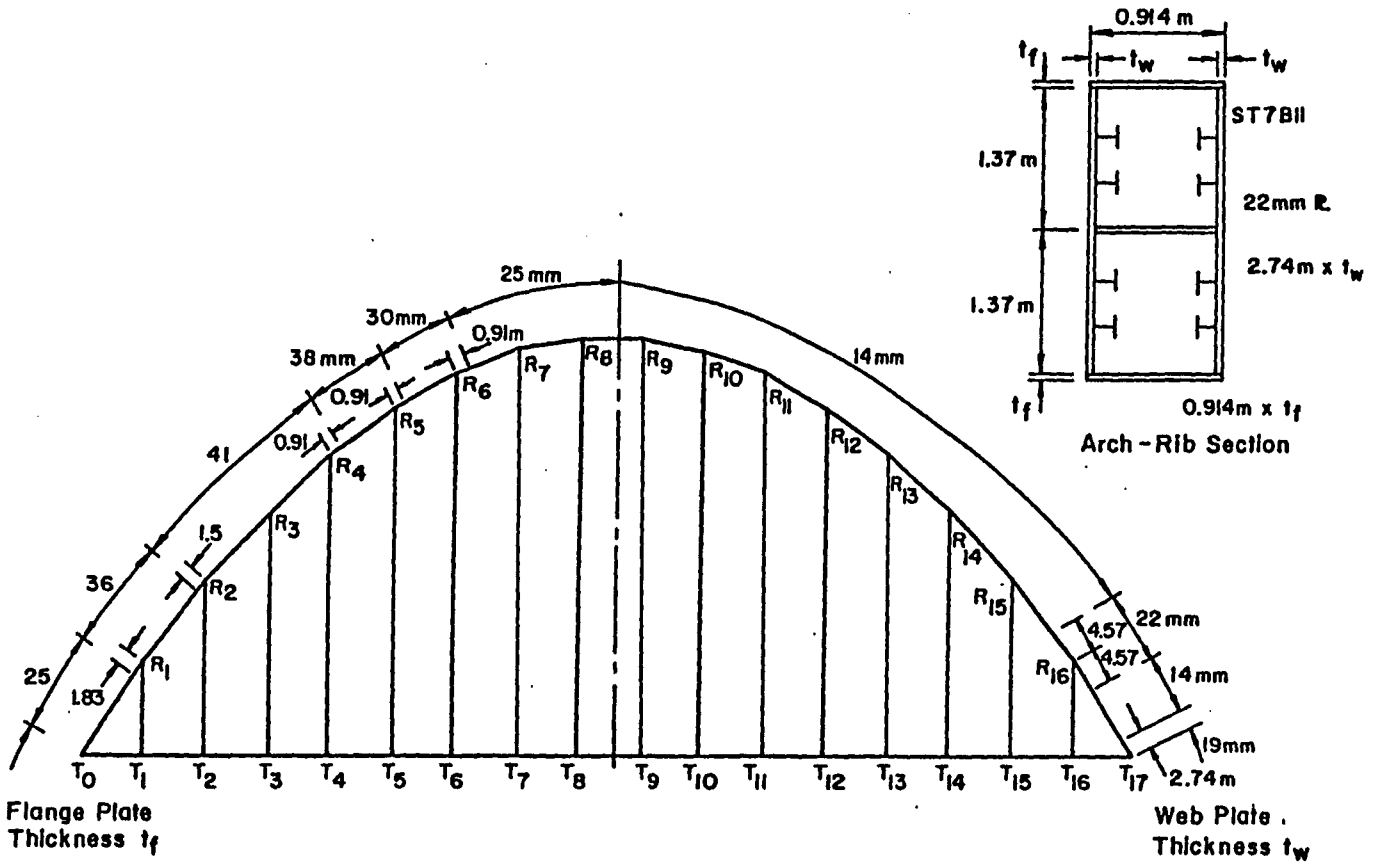

Fig. 1.4 Arch Rib Section Details

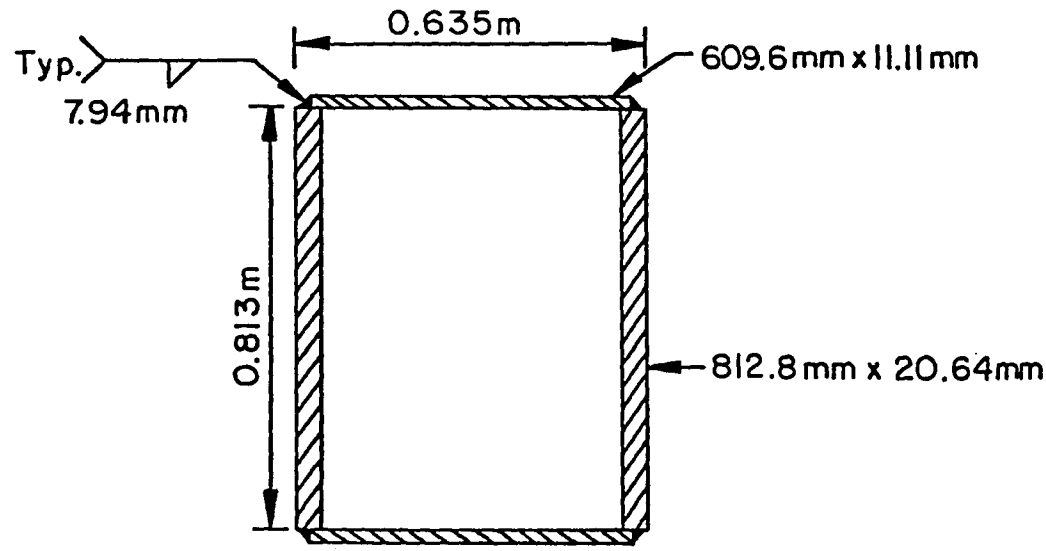

Typical Tie Section

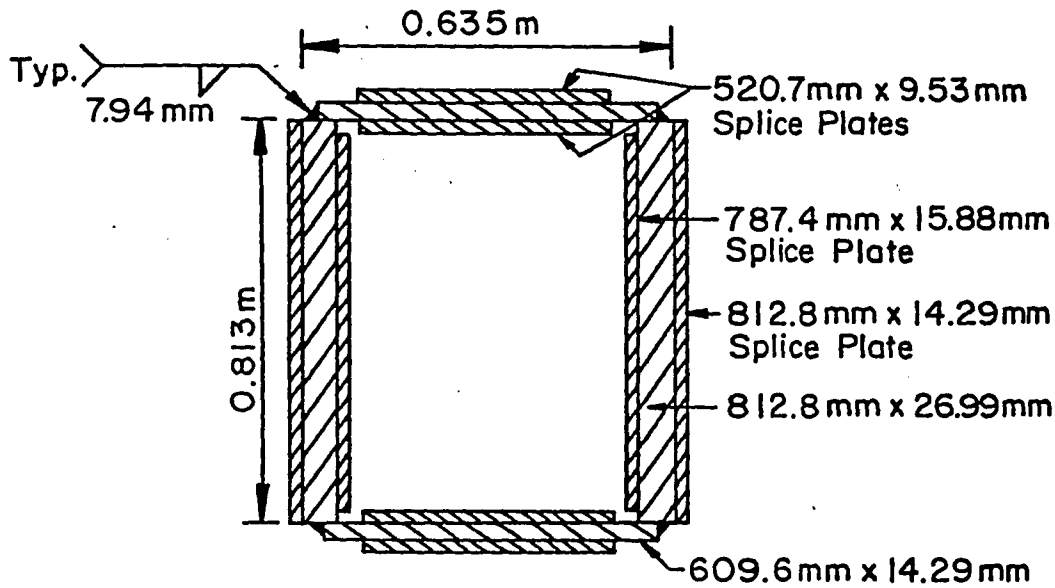

Typical Section Thru Splice

Fig. 1.5 Typical Tie Girder Sections

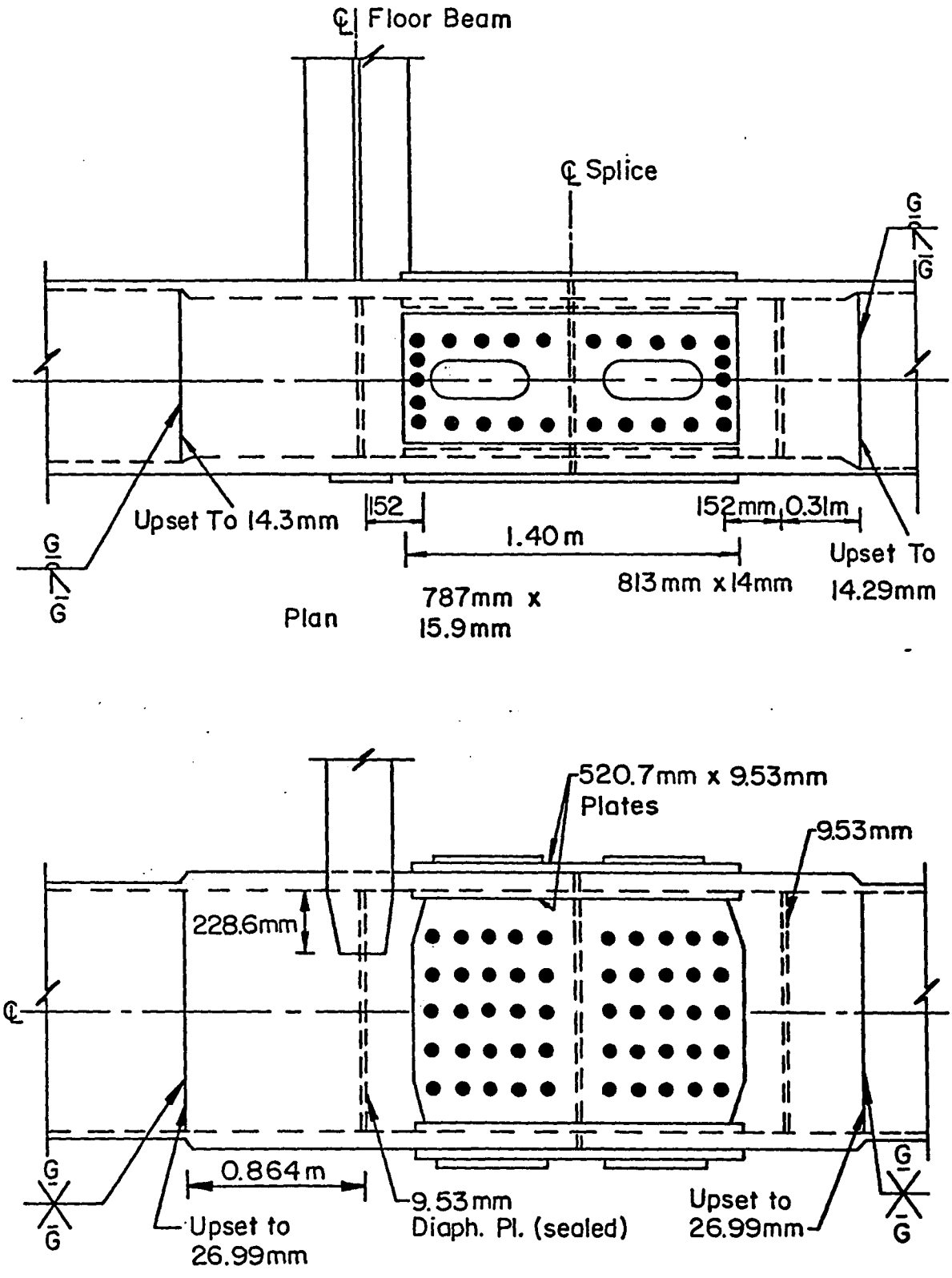

Fig. 1.6 Detail of Spliced Joints T3, T6, T9, T11, and T14

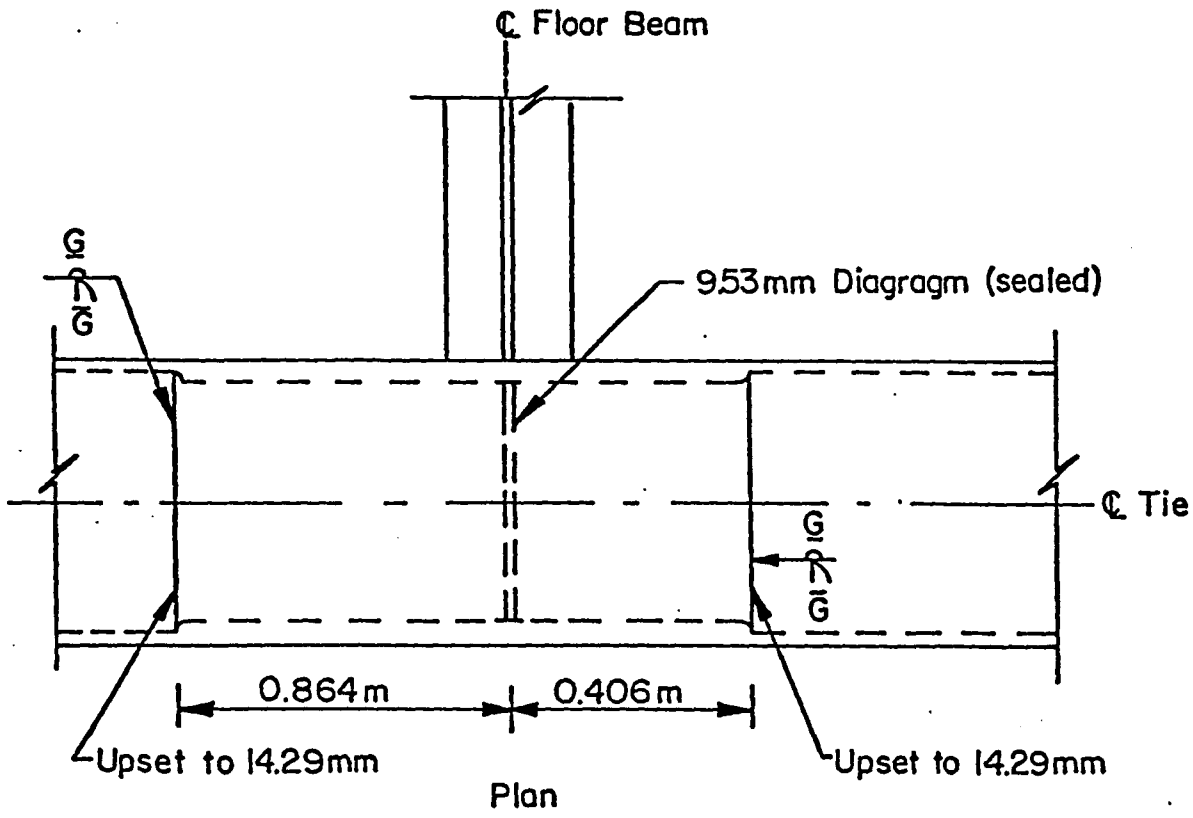

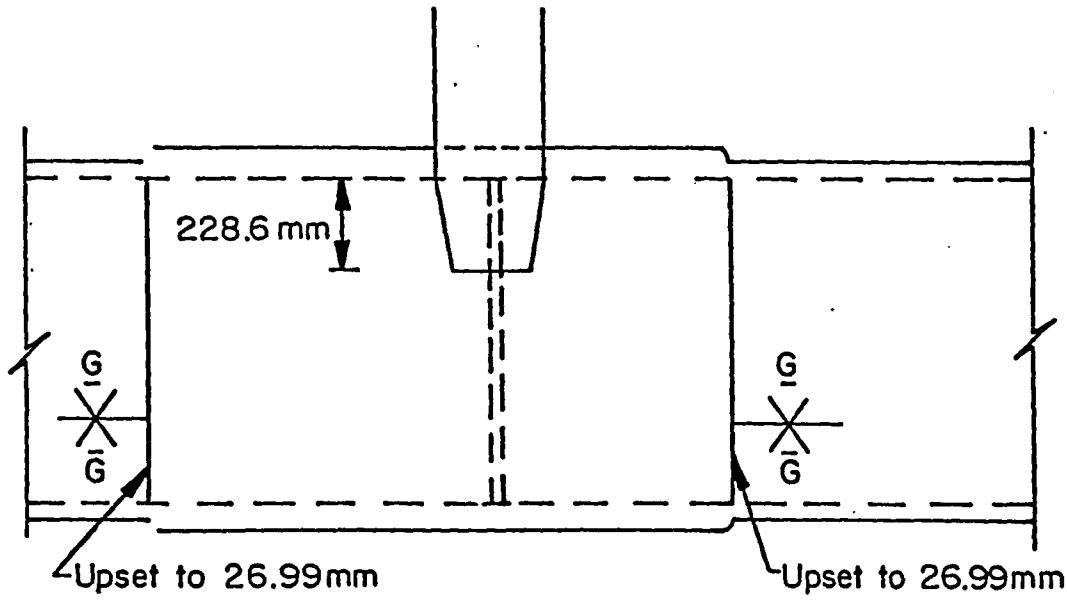

Fig. 1.7 Detail for Joints T1, T2, T4, T5, T7

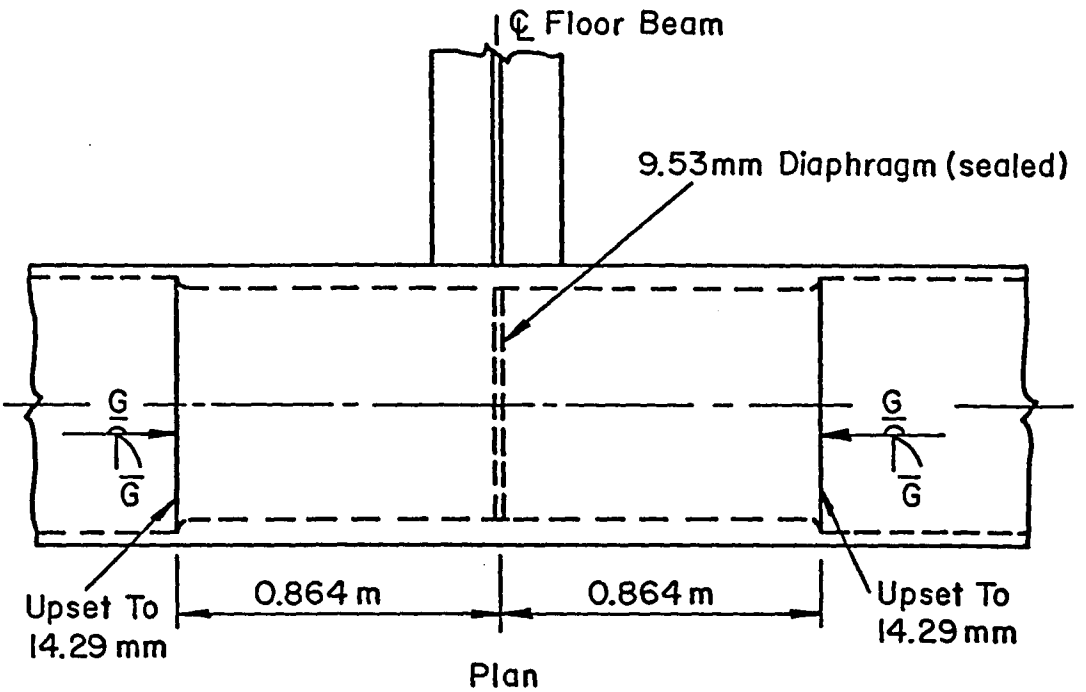

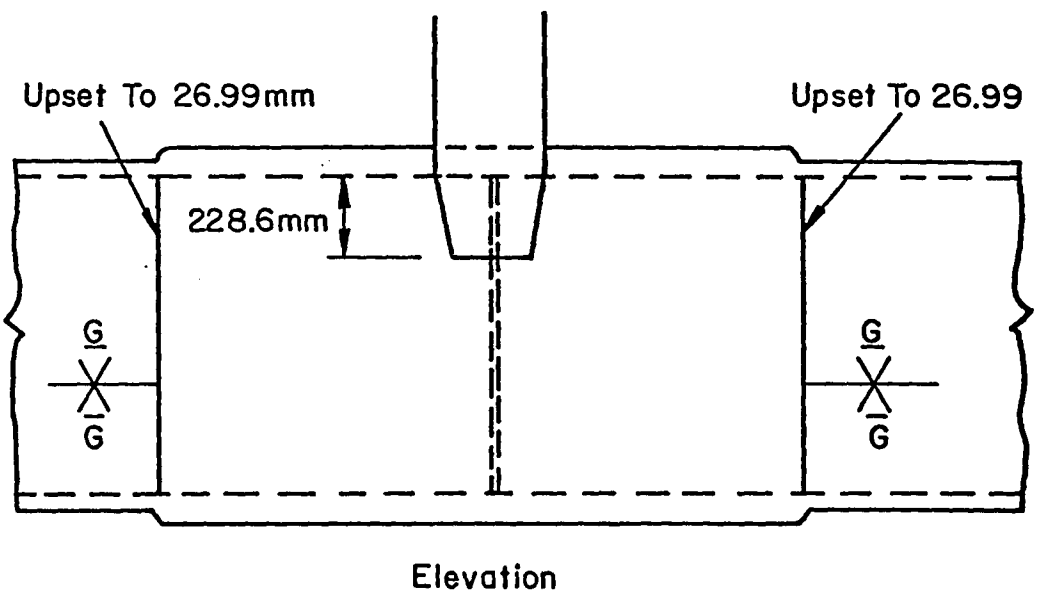

Fig. 1.8 Detail for Joint T8

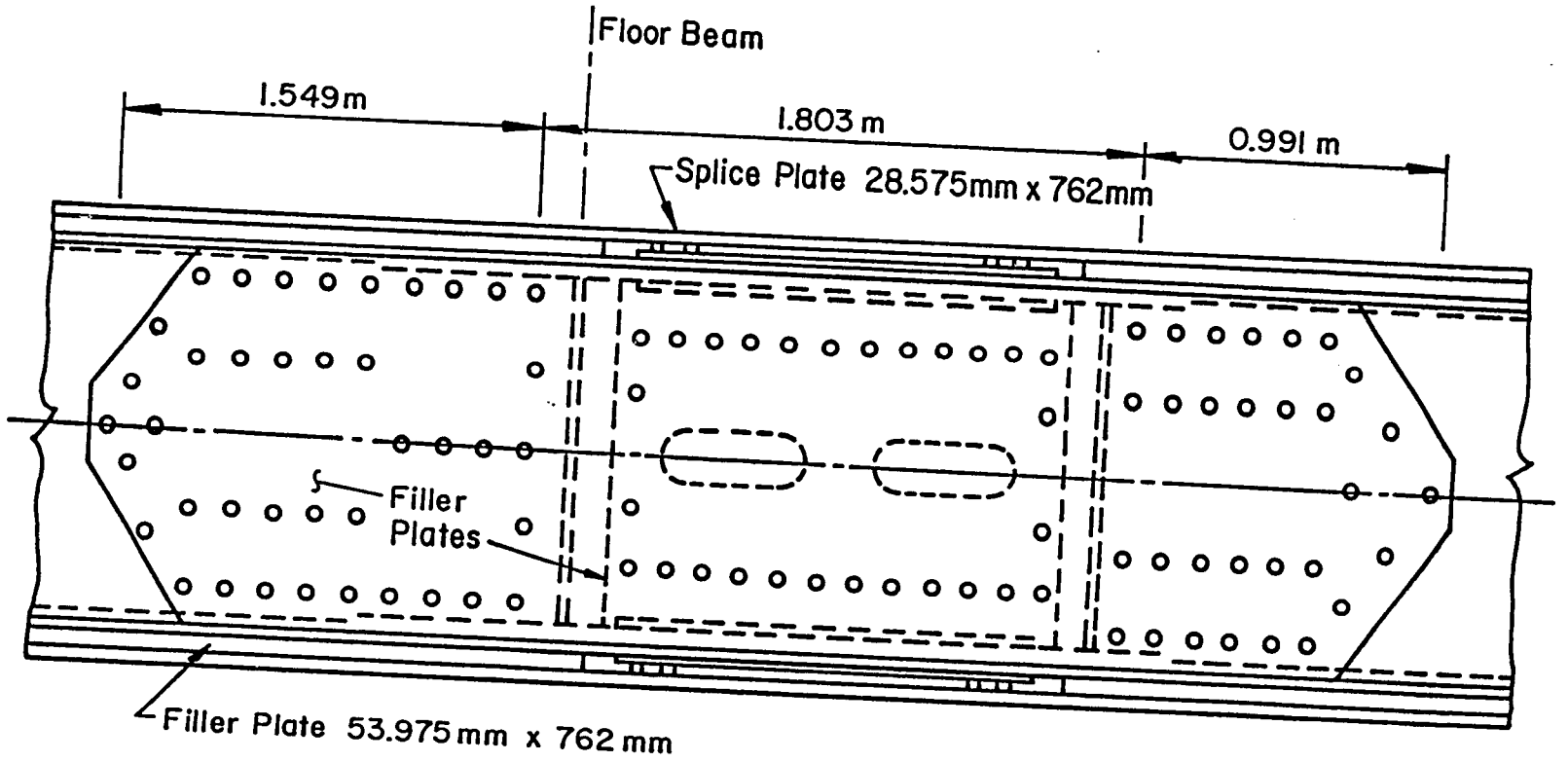

Fig. 1.9 Plan of the Typical Retrofit Detail for Spliced Panel Points on the Tie Girder

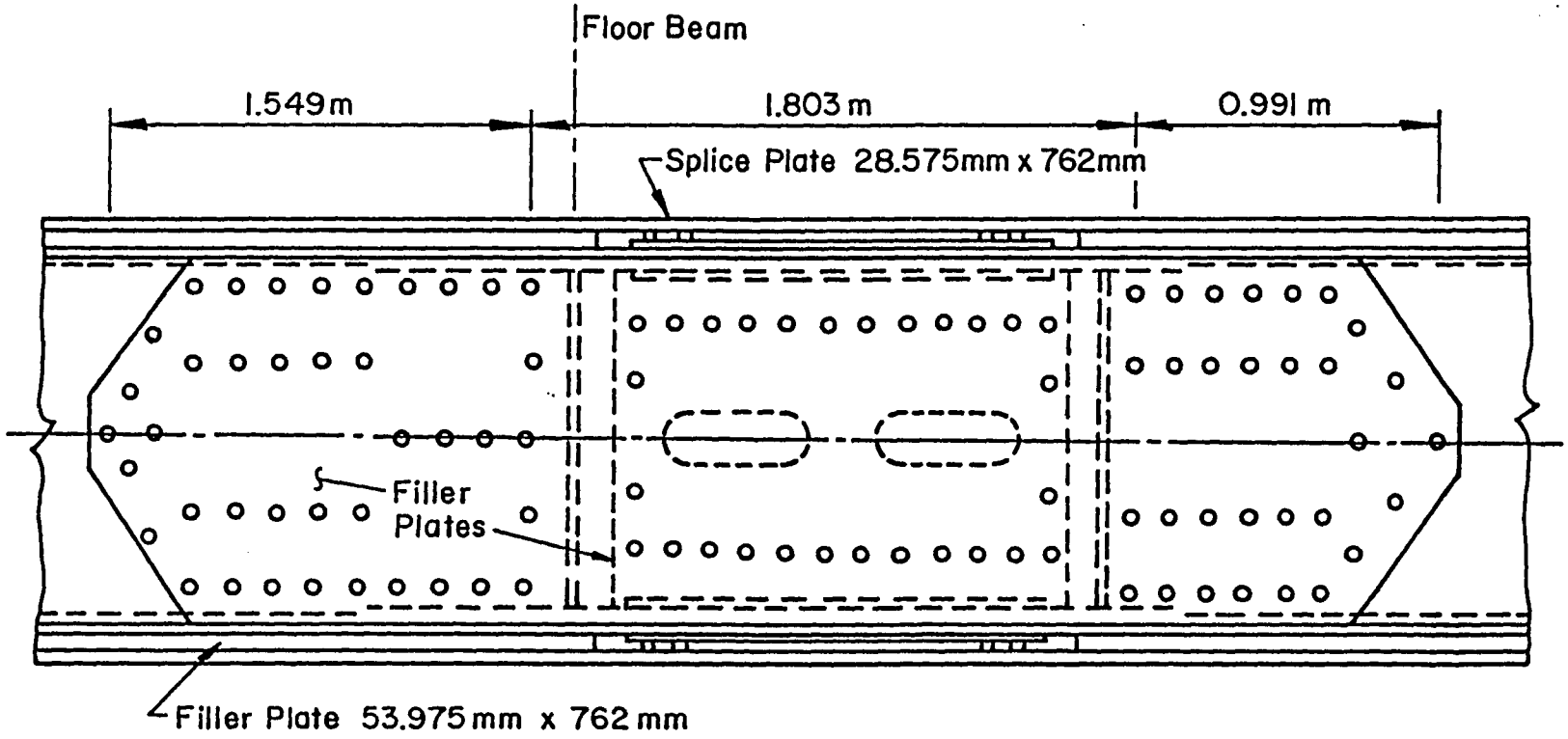

Fig. 1.9 Plan of the Typical Retrofit Detail for Spliced Panel Points on the Tie Girder

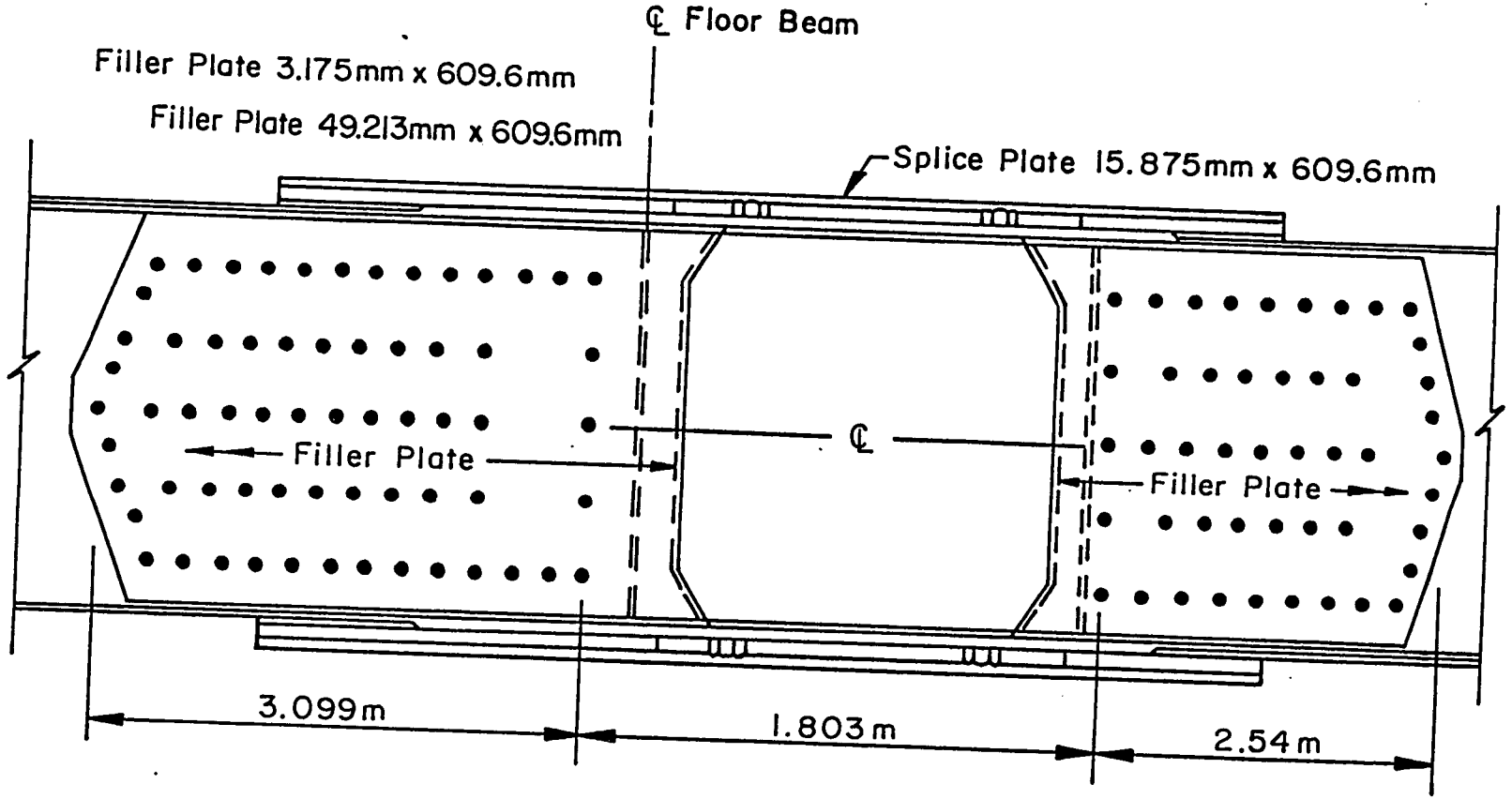

Fig. 1.10 Elevation of the Typical Retrofit Detail for Spliced Panel Points of the Tie Girder

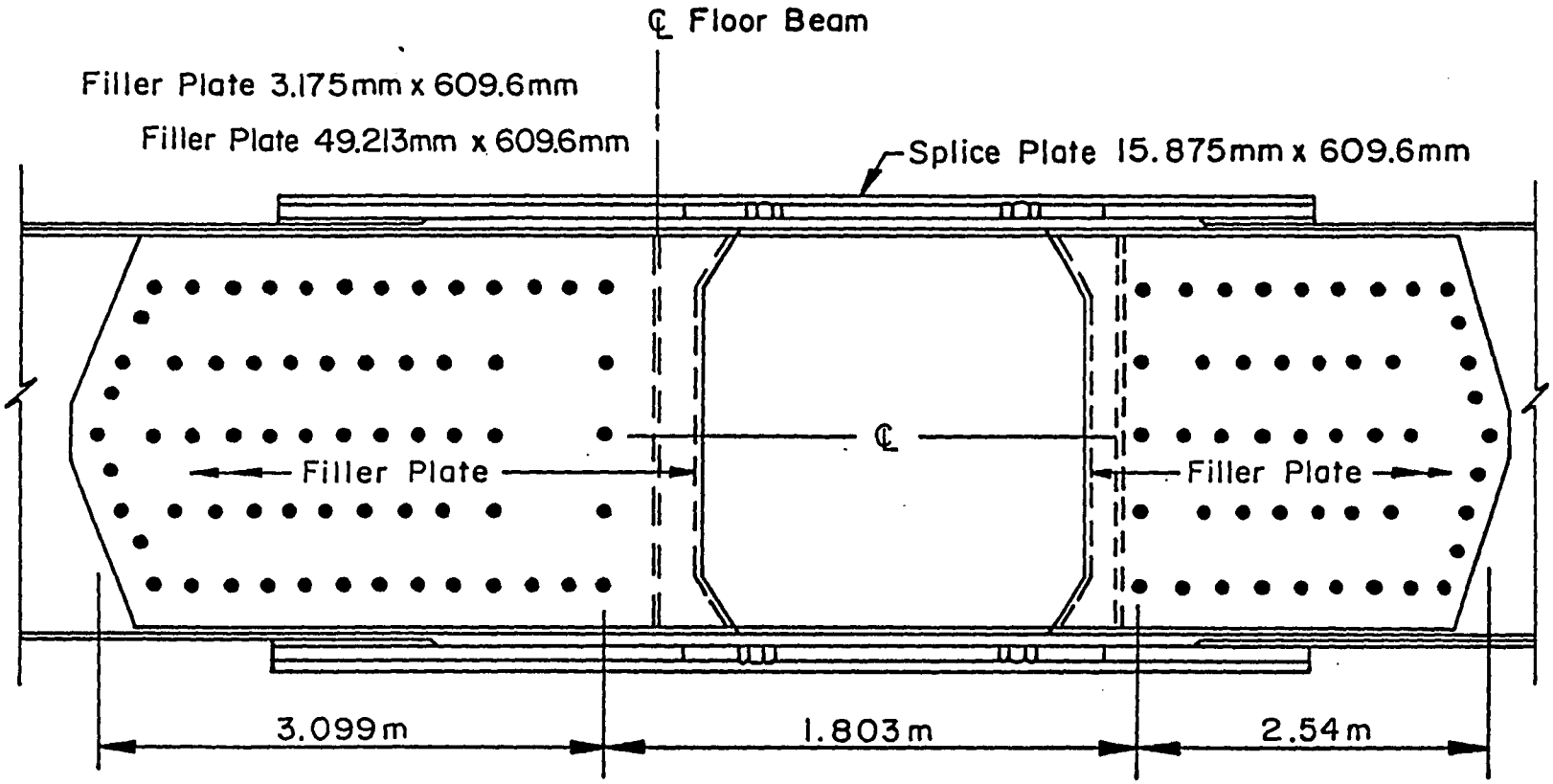

Fig. 1.10 Elevation of the Typical Retrofit Detail for Spliced Panel Points of the Tie Girder

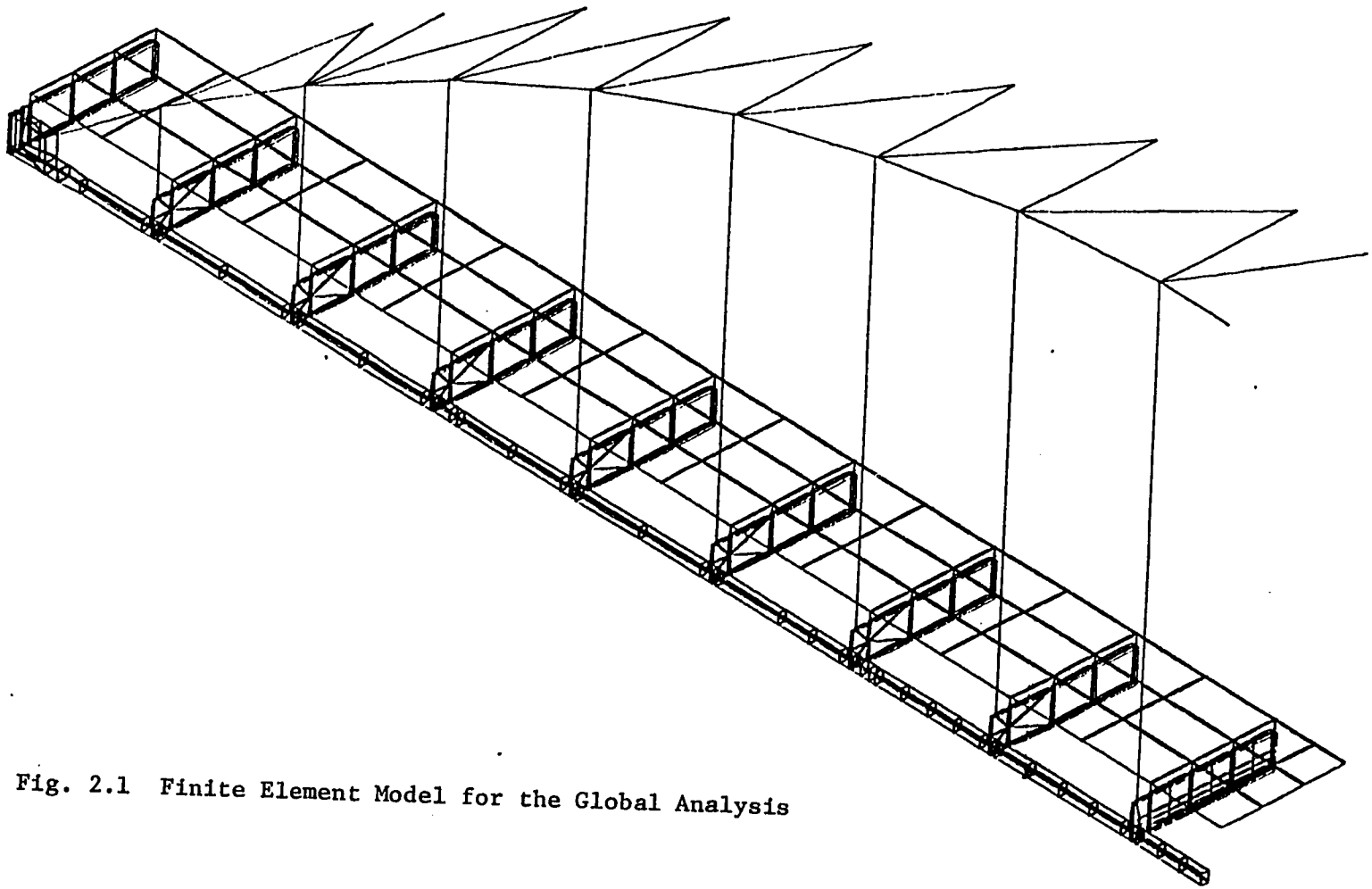

Fig. 2.1 Finite Element Model for the Global Analysis

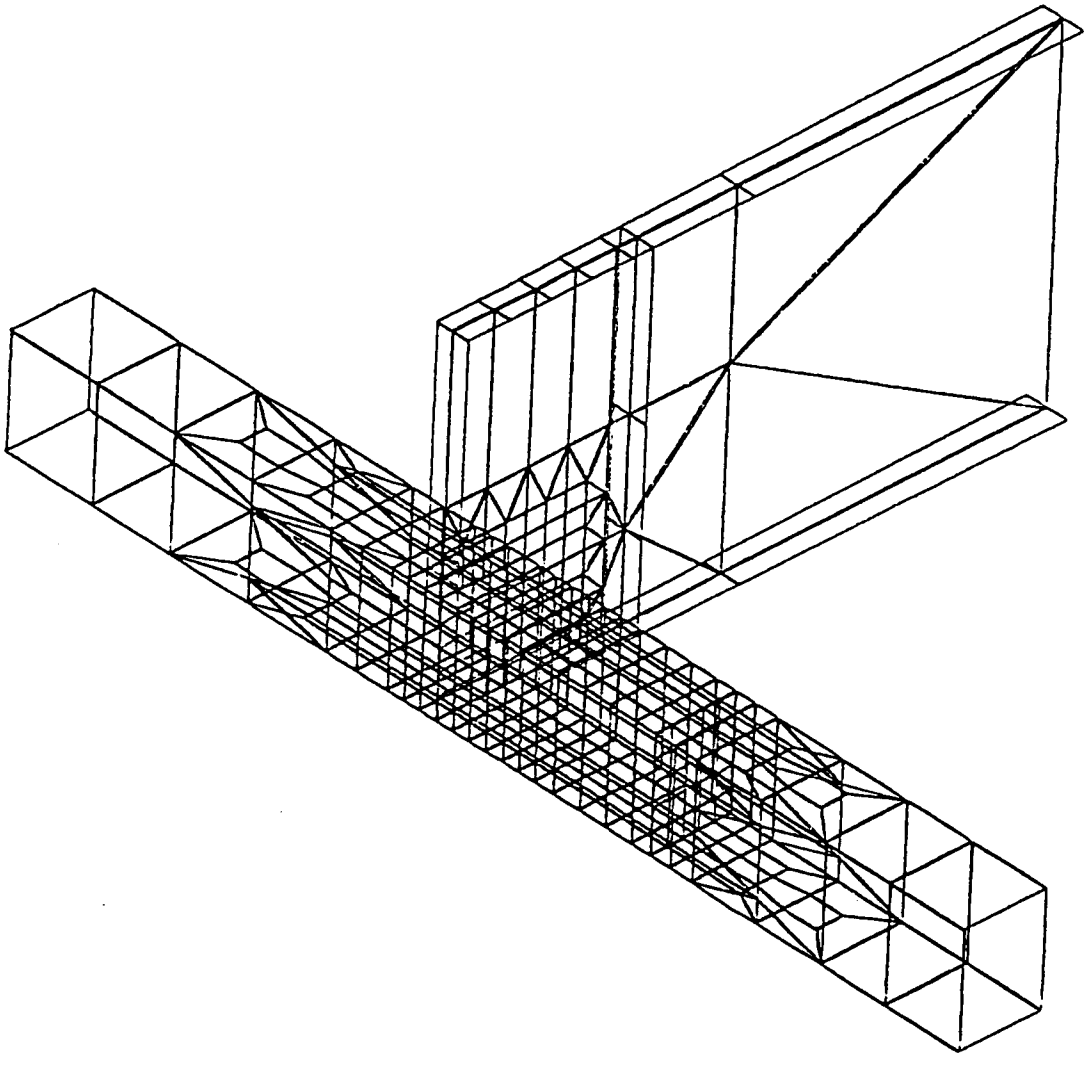

Fig. 2.2 Finite Element Model for the Substructure Analysis

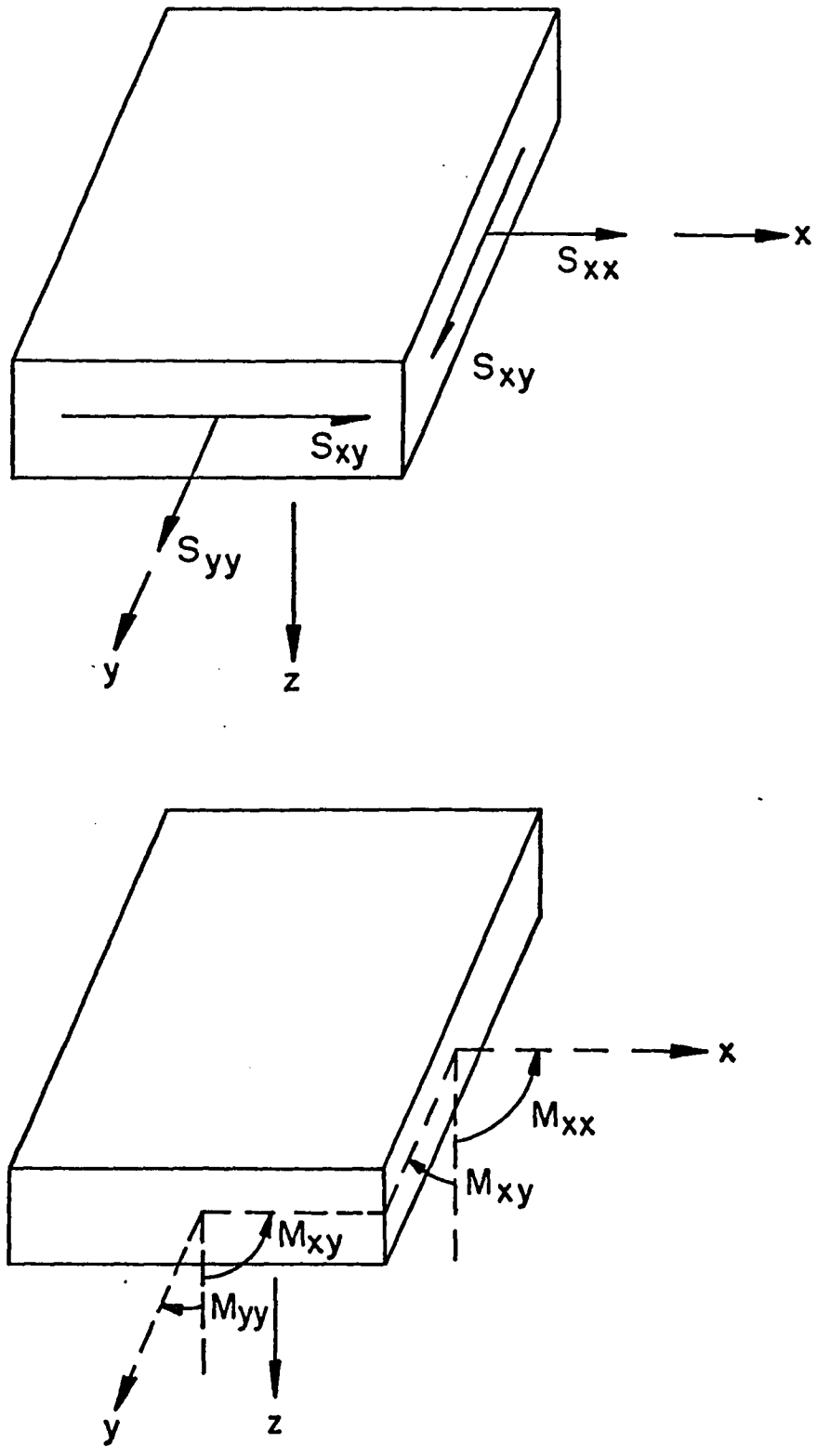

Fig. 2.3 Stress Resultants for SAP IV Plate and Shell Element

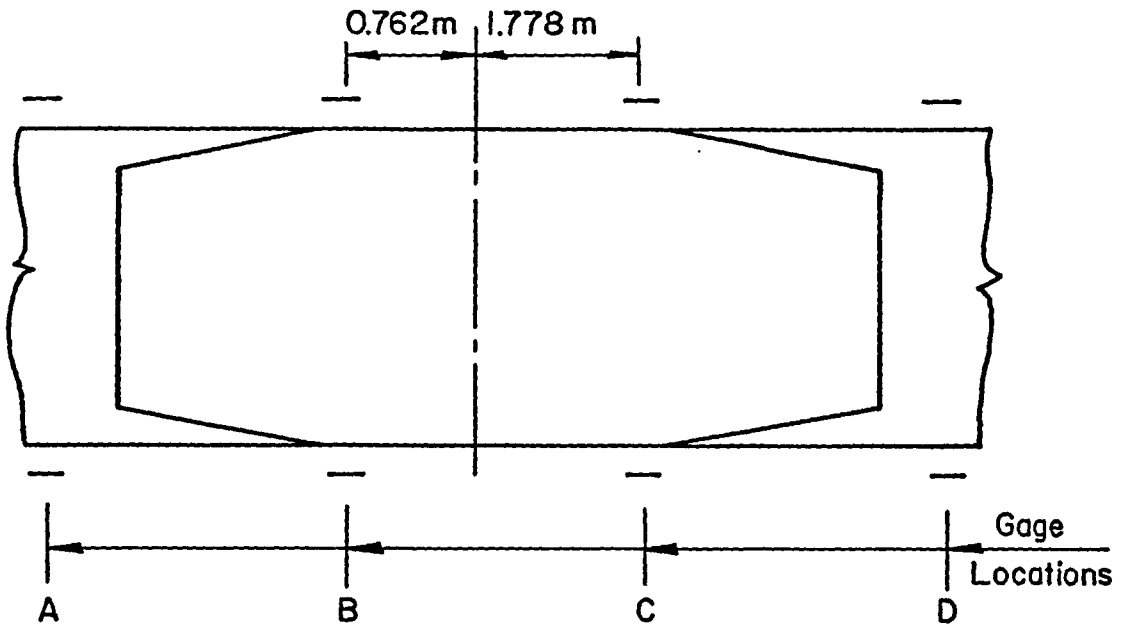

Elevation of Tie Girder at T6 or T11 (opposite hand)

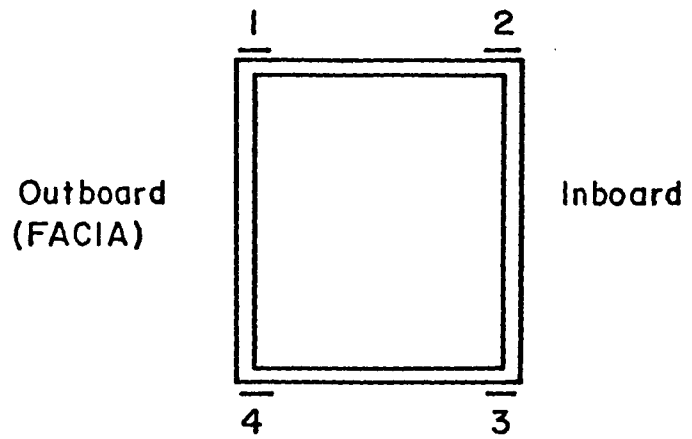

Cross Section

Fig. 3.1 Location of Strain Gages on the Tie Girder

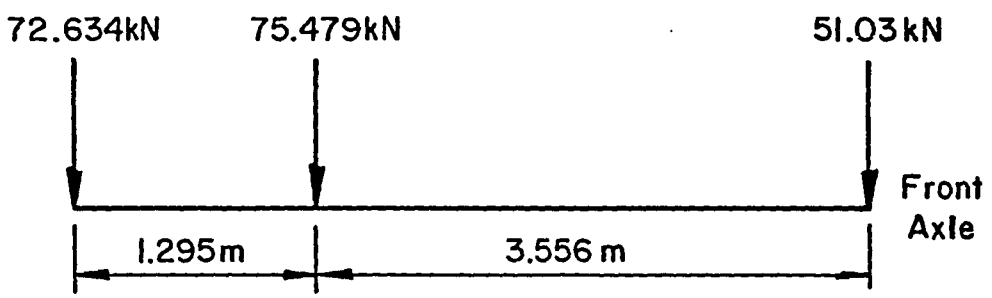

Test Truck on Inside Lane

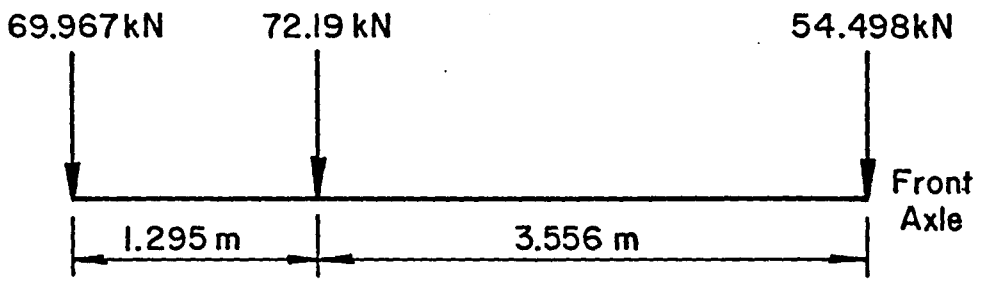

Test Truck on Outside Lane

Fig. 3.2 Test Trucks Used for the Field Study

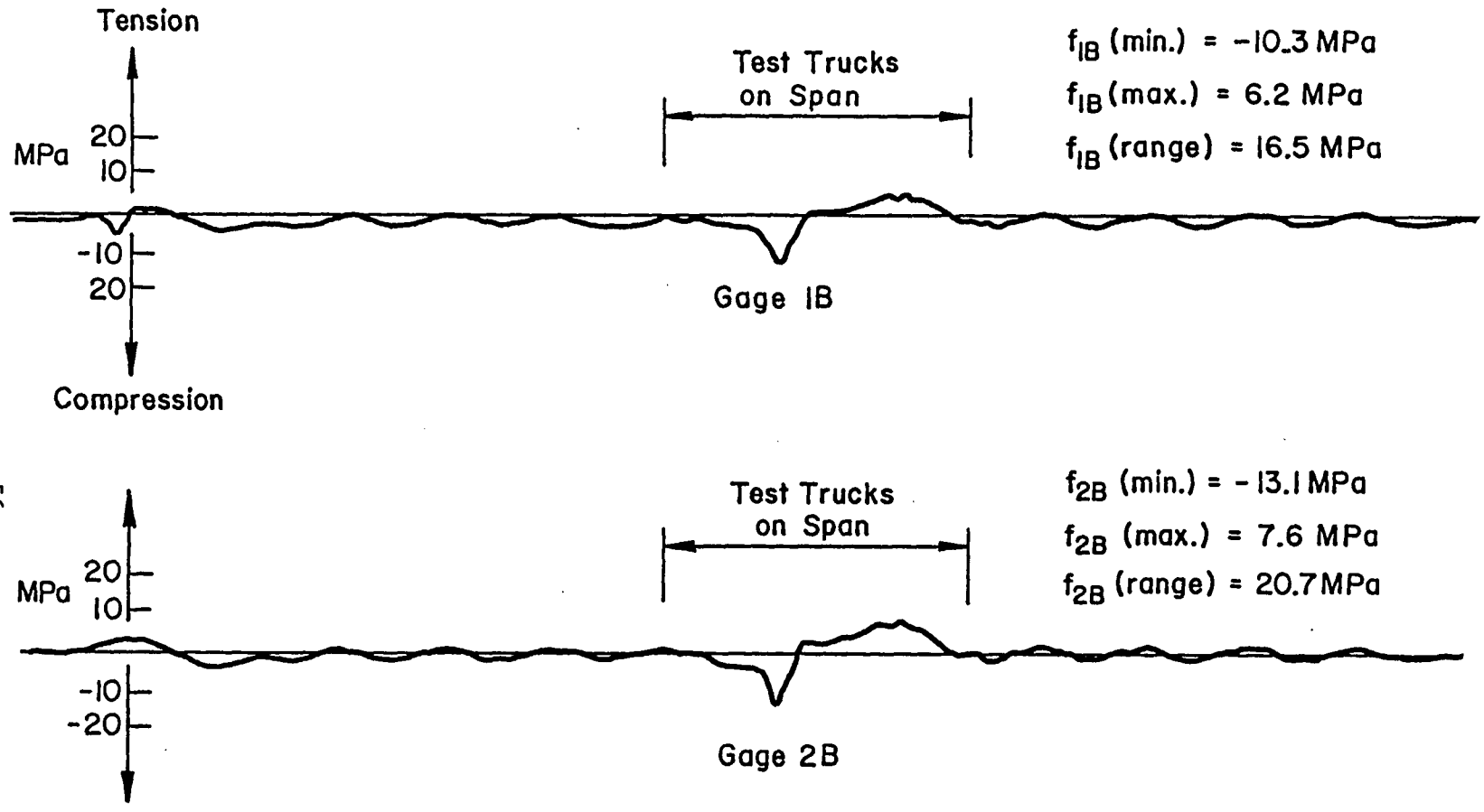

Fig. 3.3 Analog Traces for Passage of Test Trucks over Bridge

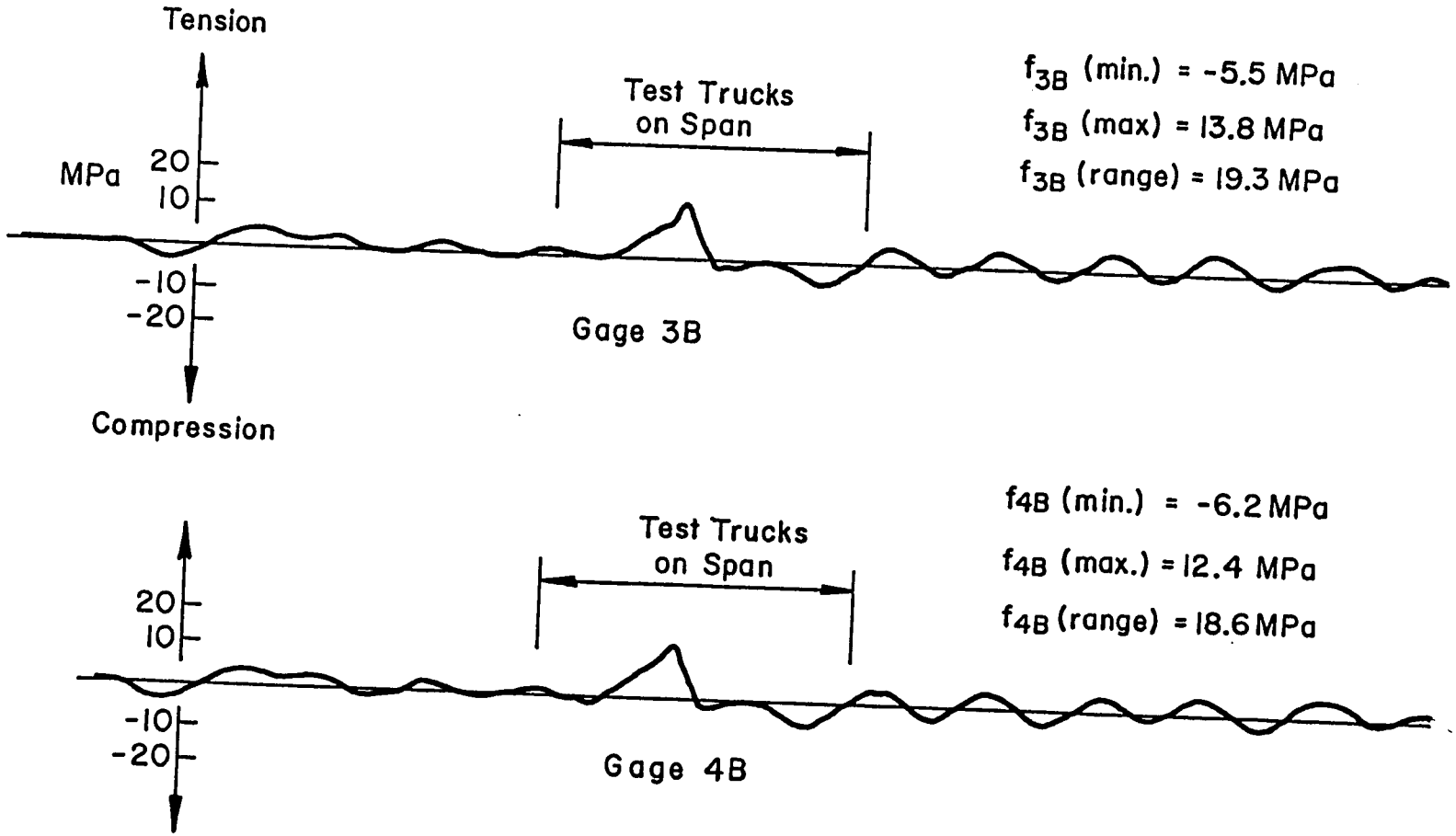

Fig. 3.4 Analog Traces for Passage of Test Trucks over Bridge - Trucks on the Nearer Side of the Road, Northbound

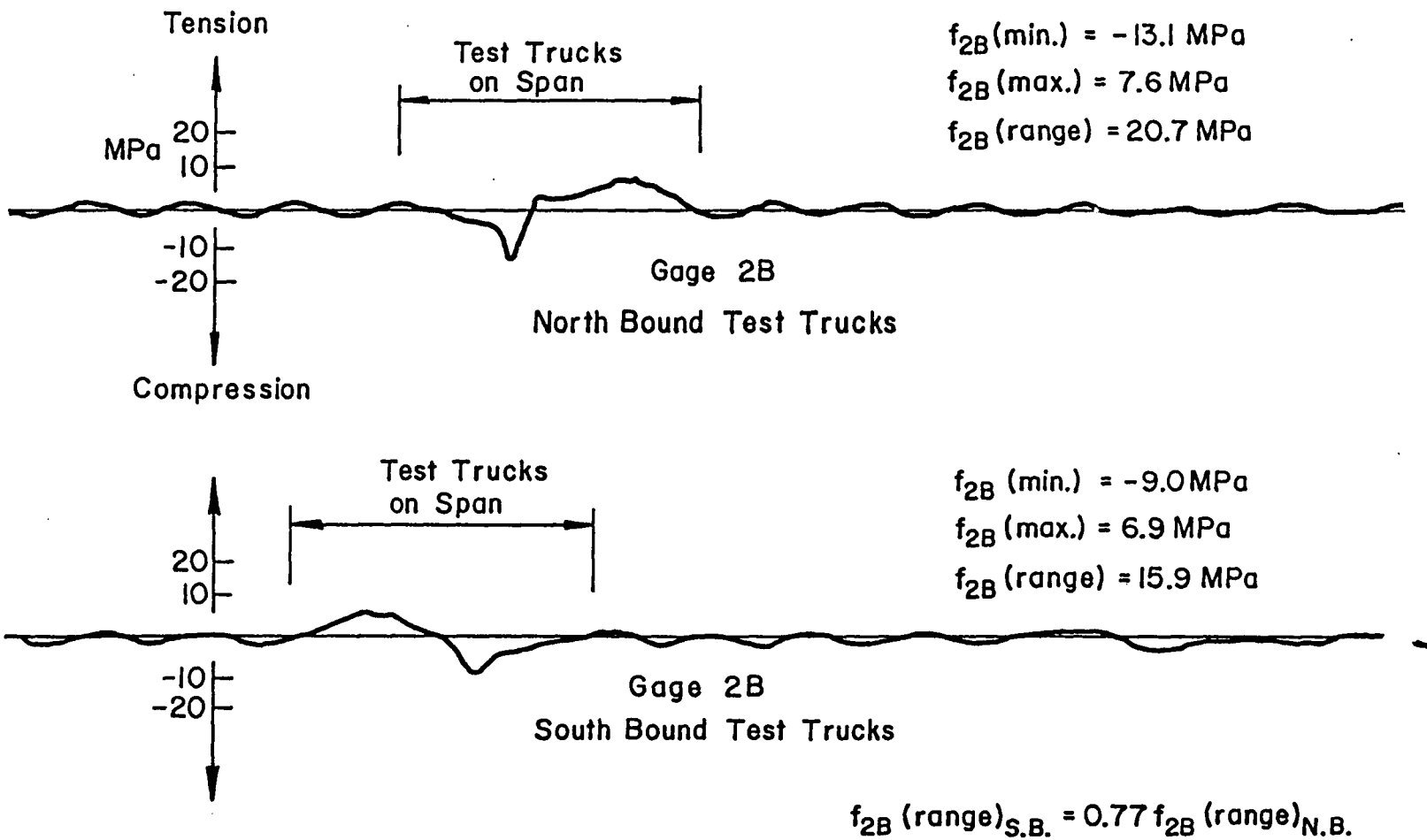

Fig. 3.5 Comparison of Analog Traces for Northbound vs. Southbound Trucks

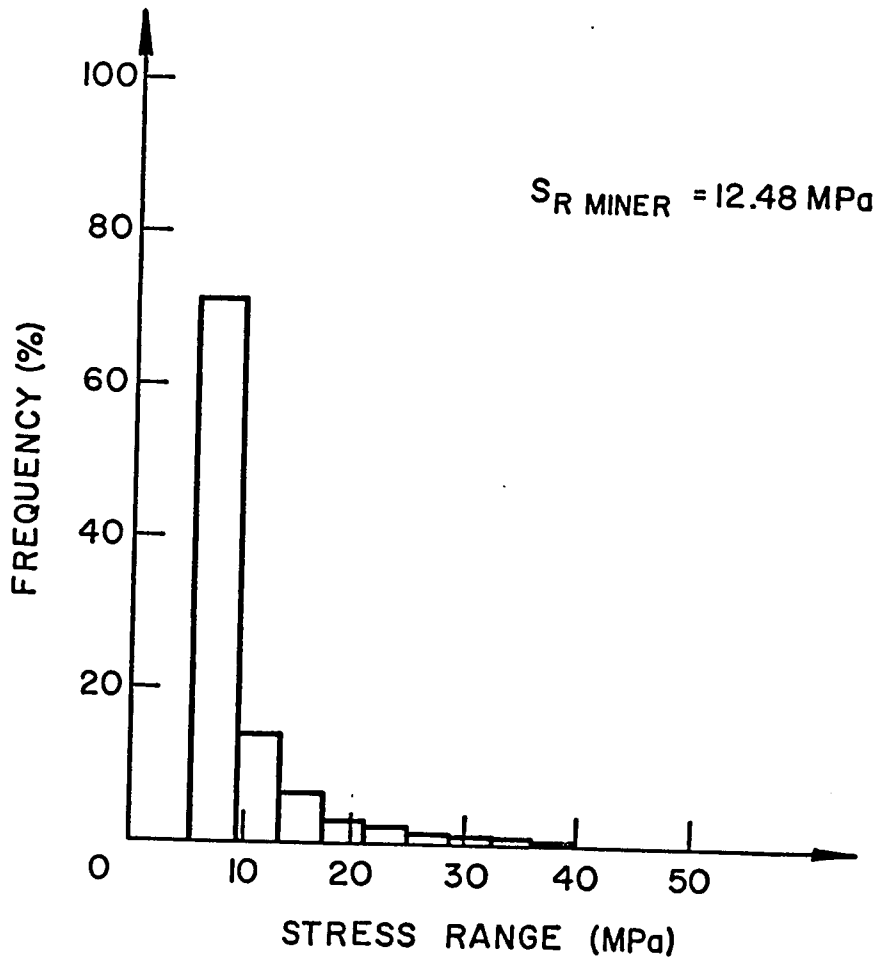

Fig. 3.6 Stress Histogram for Gage Location A4

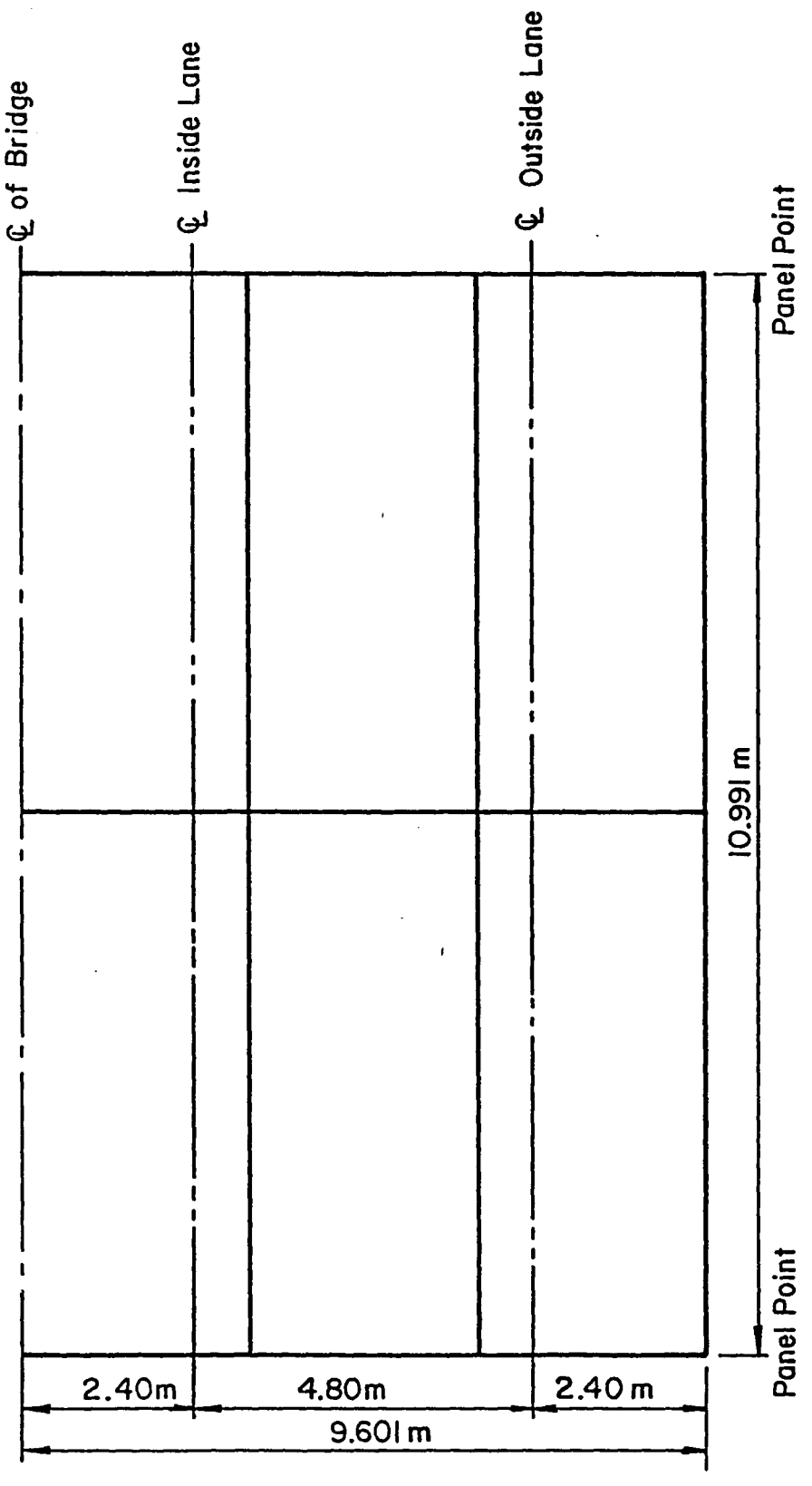

Fig. 4.1 Location of Traffic Lanes on the Bridge

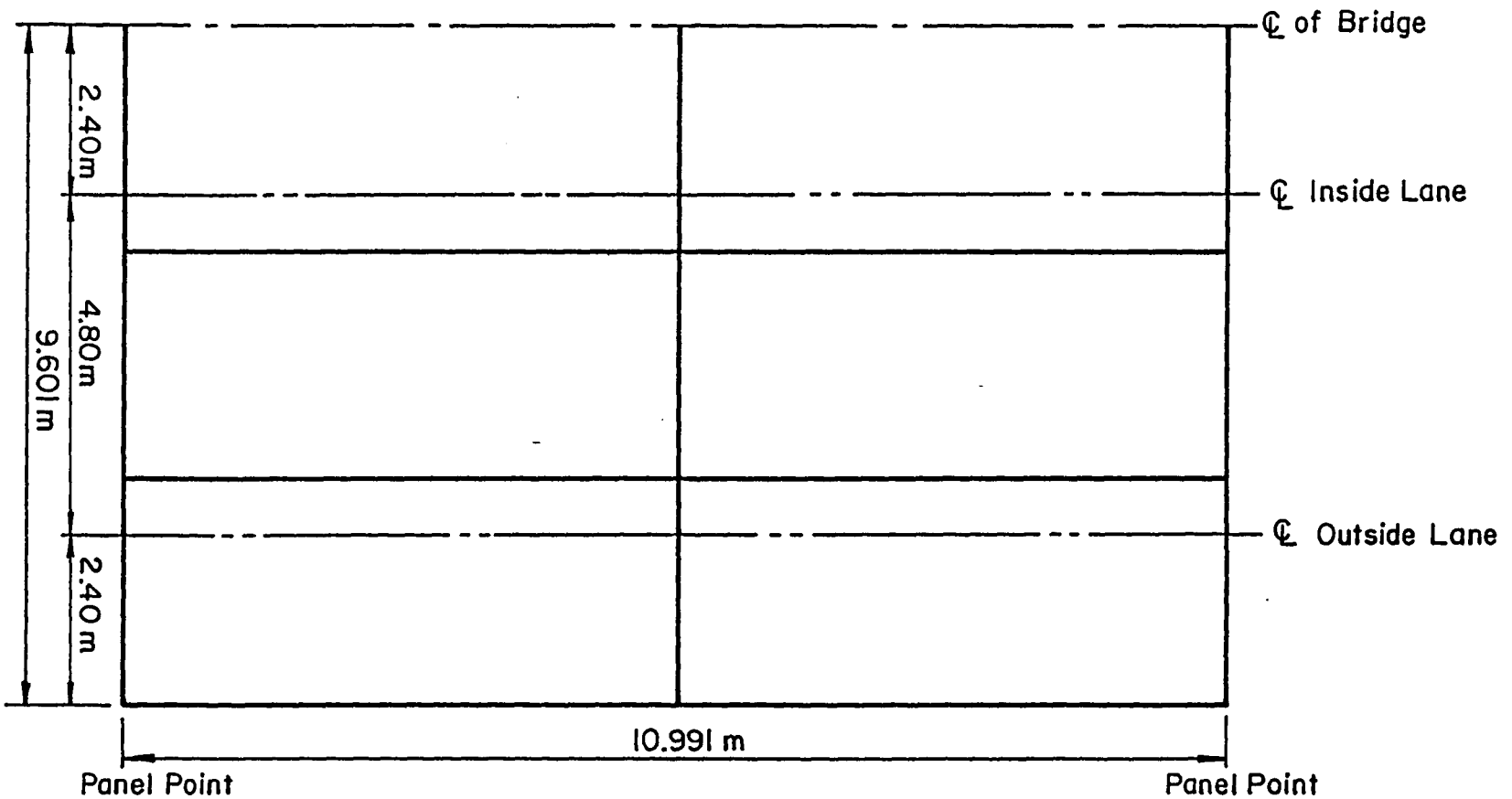

Fig. 4.1 Location of Traffic Lanes on the Bridge

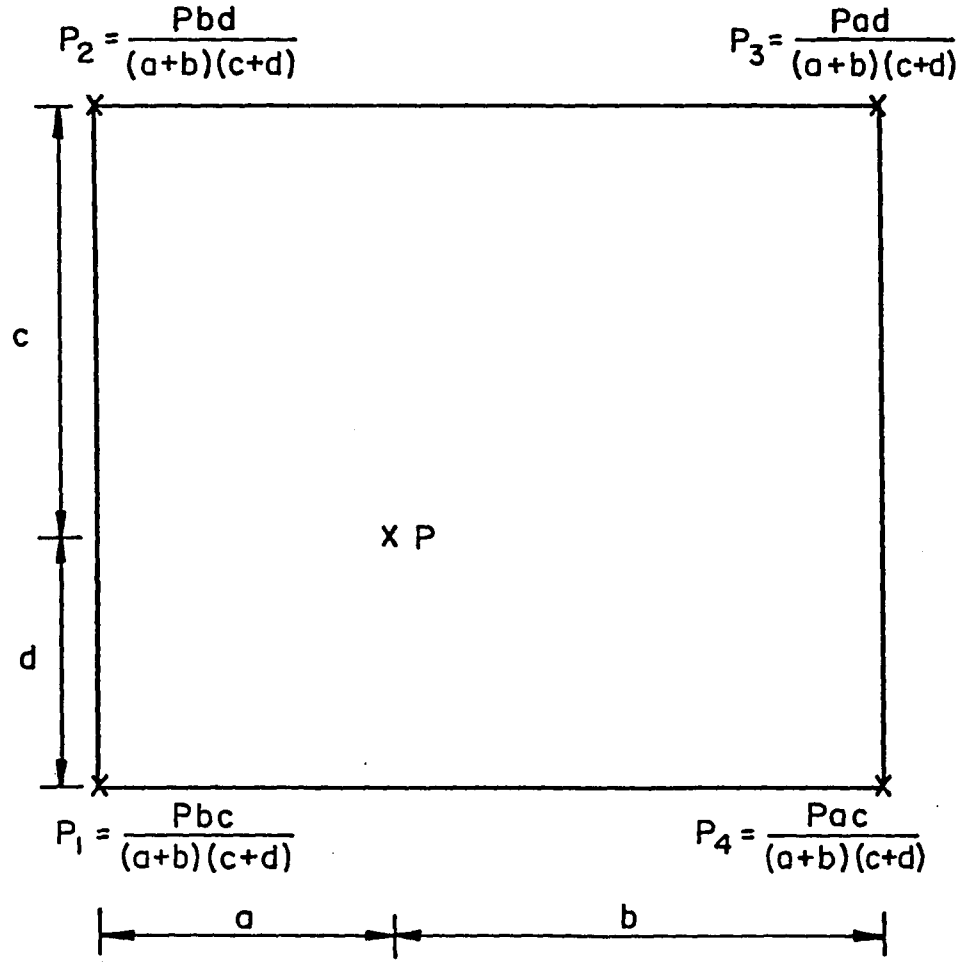

Fig. 4.2 Redistribution of Interior Load P

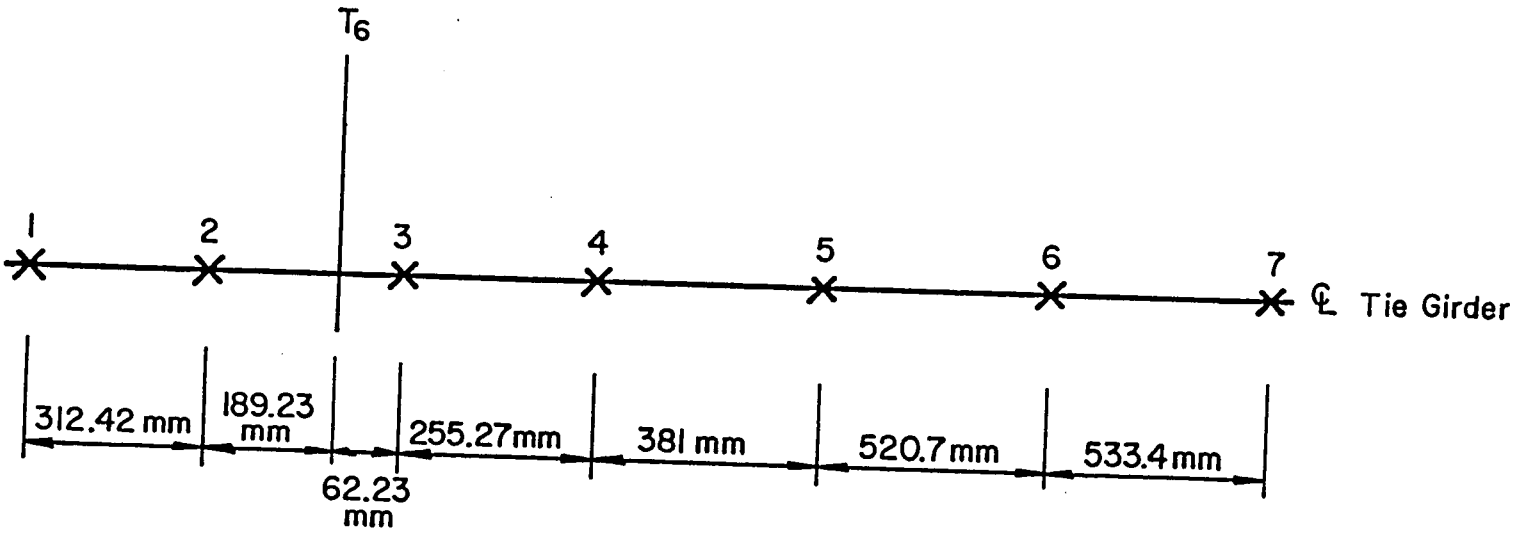

Fig. 4.3 Locations of Sections Along Length of Tie Girder for which Influence Lines were Developed

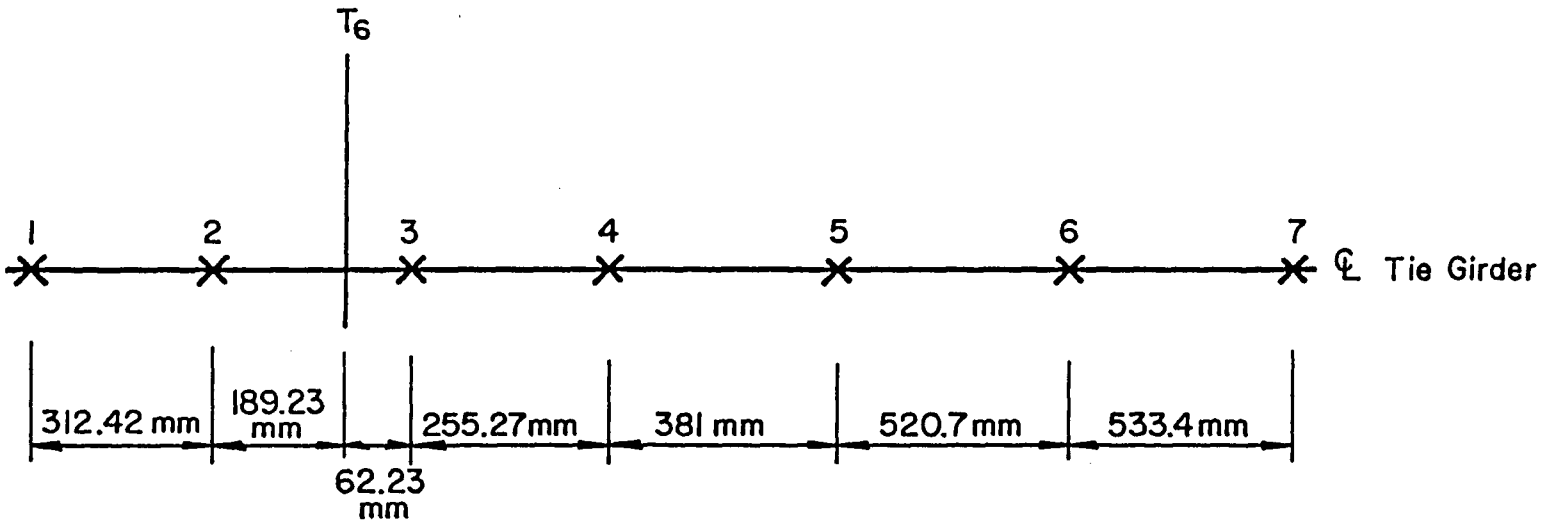

Fig. 4.3 Locations of Sections Along Length of Tie Girder for which Influence Lines were Developed

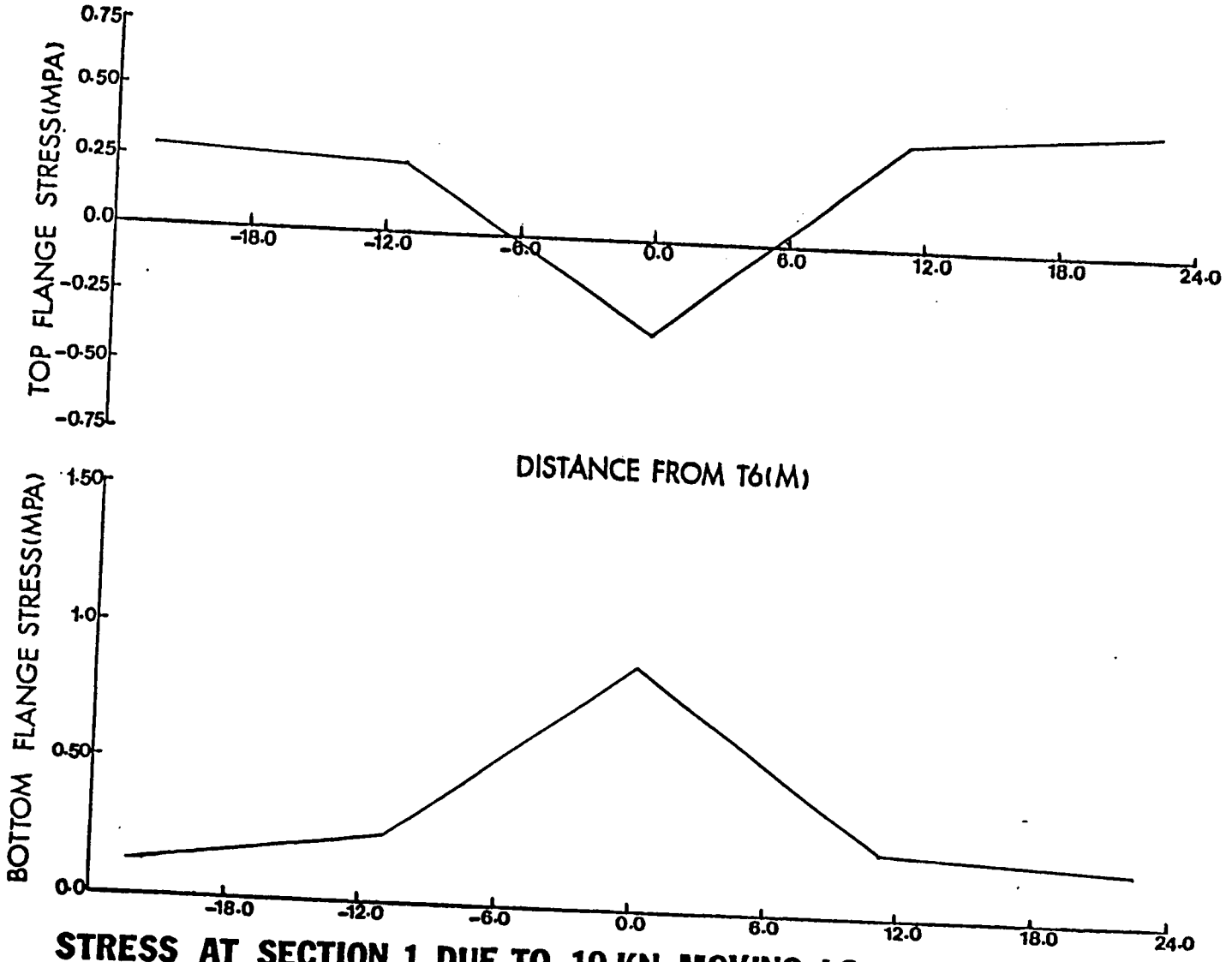

STRESS AT SECTION 1 DUE TO 10 KN MOVING LOAD ON OUTSIDE LANE

Fig.4.4

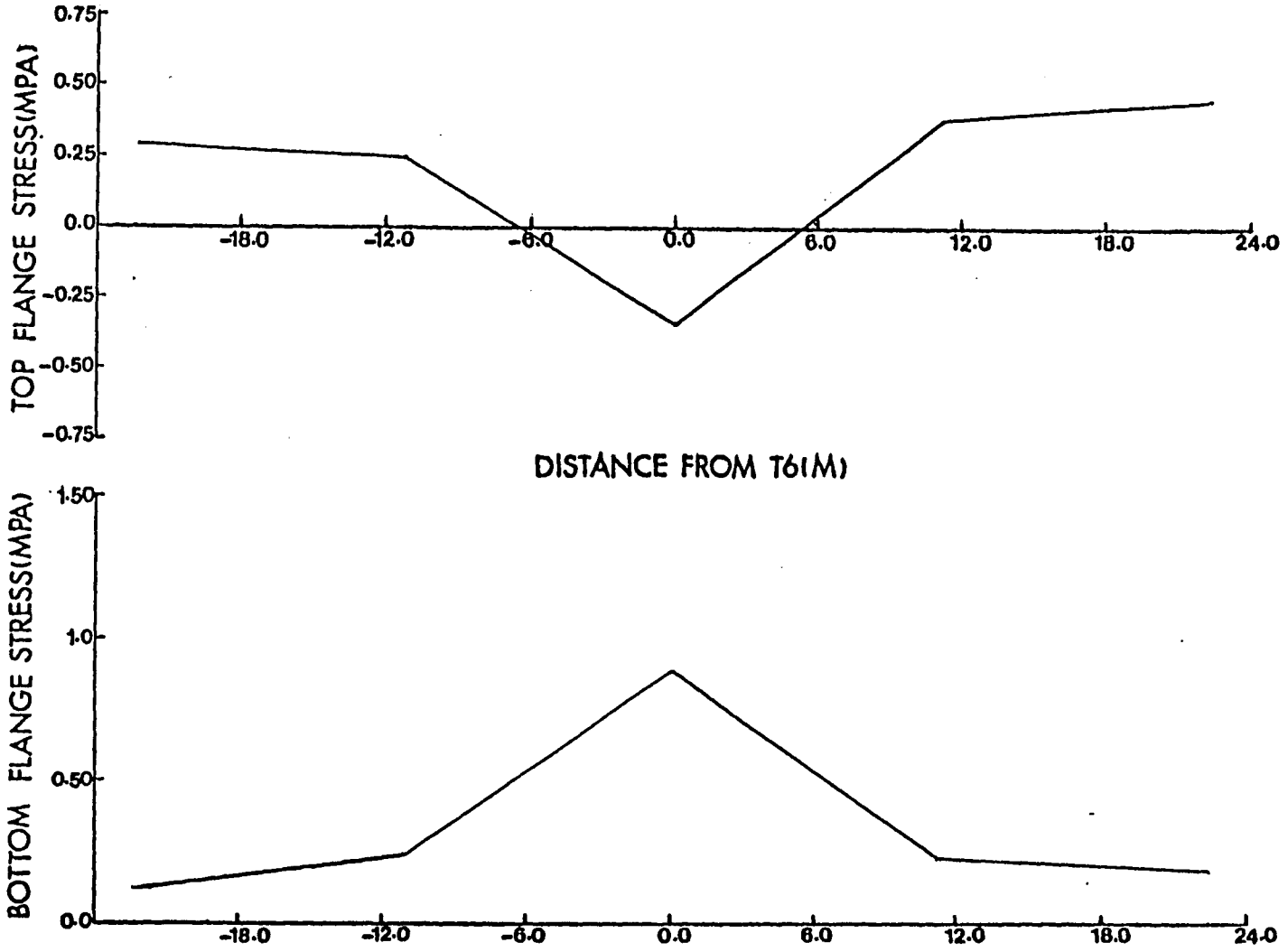

STRESS AT SECTION 1 DUE TO 10 KN MOVING LOAD ON OUTSIDE LANE

Fig.4.4

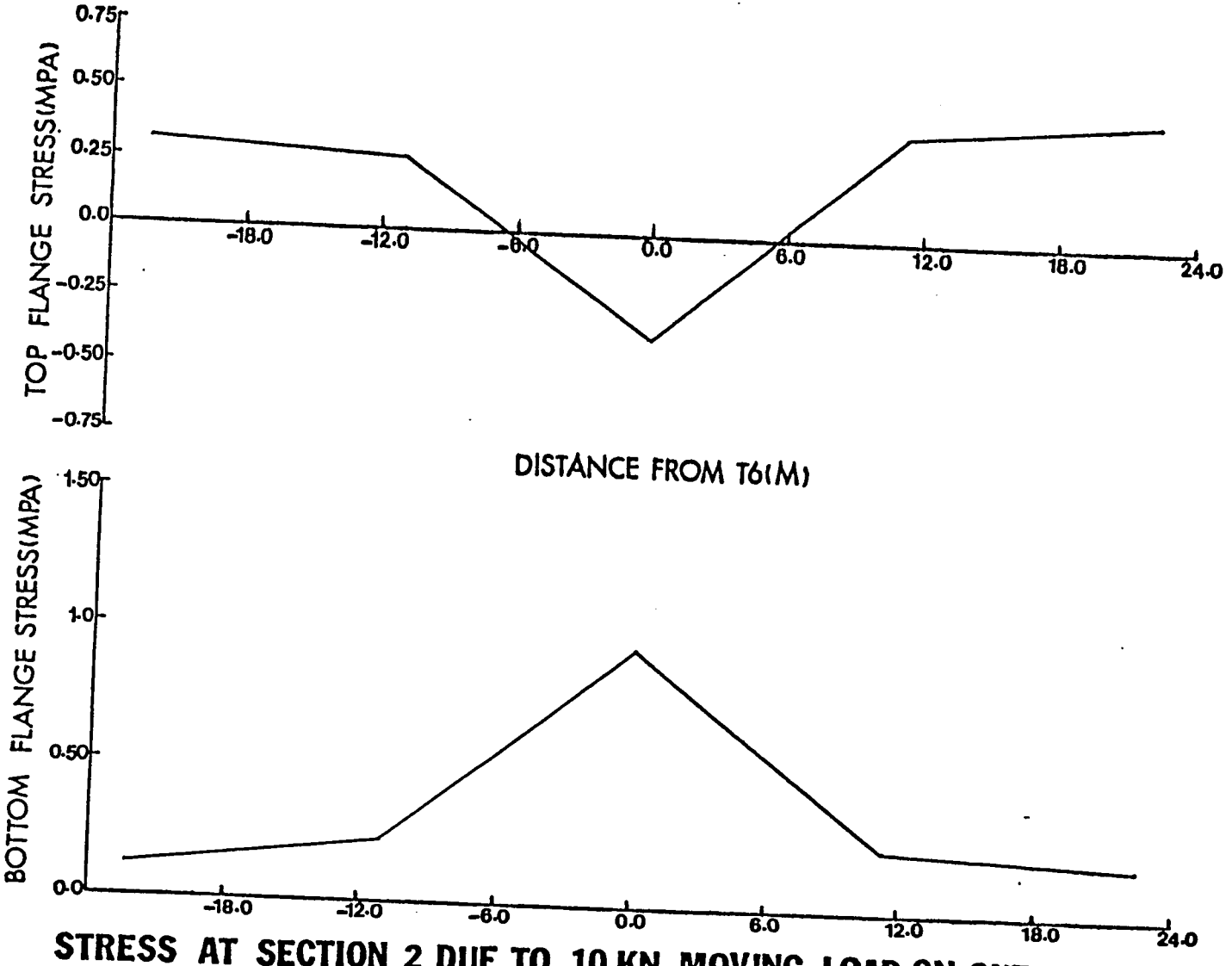

STRESS AT SECTION 2 DUE TO 10 KN MOVING LOAD ON OUTSIDE LANE

Fig.4.5

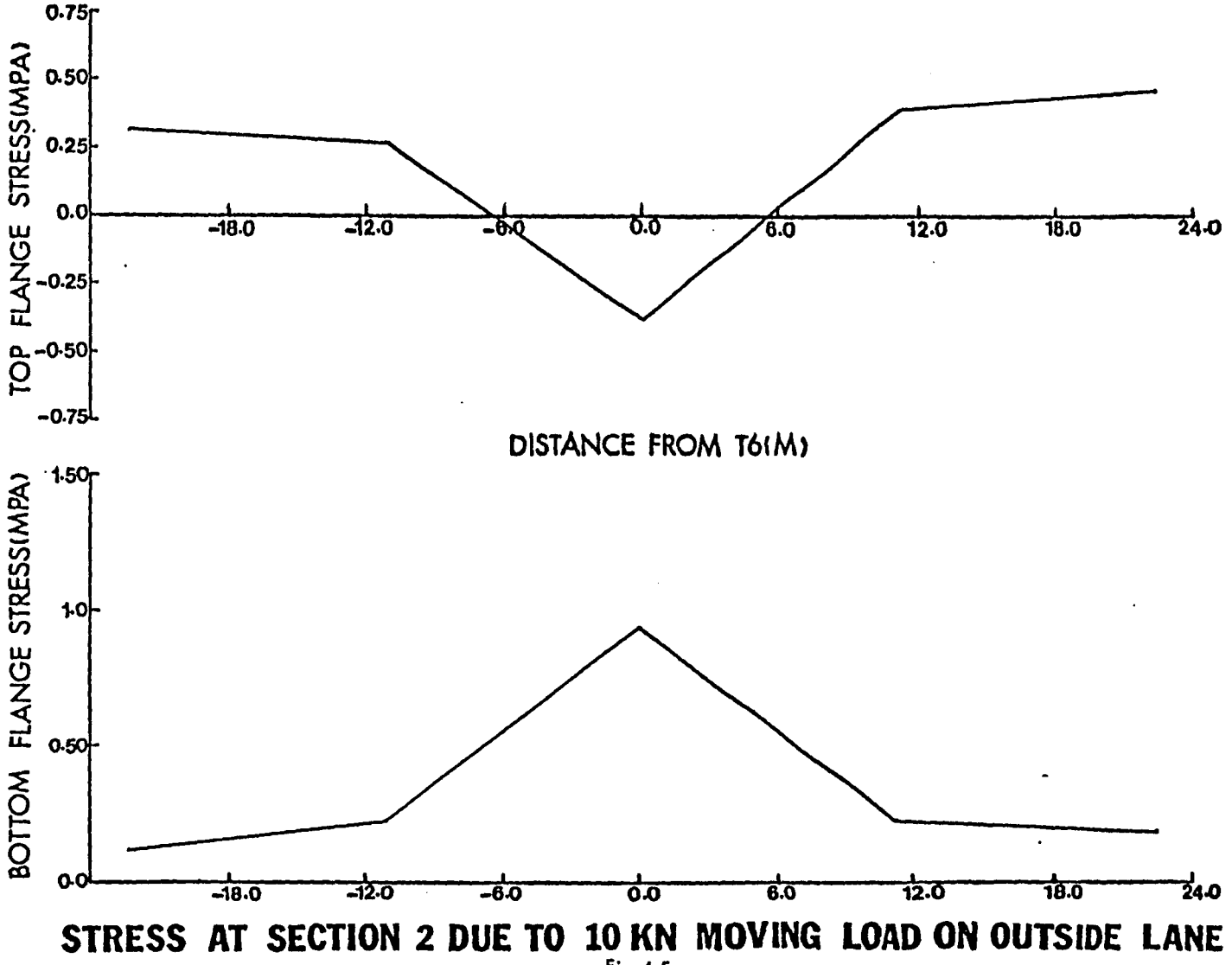

STRESS AT SECTION 2 DUE TO 10 KN MOVING LOAD ON OUTSIDE LANE

Fig.4.5

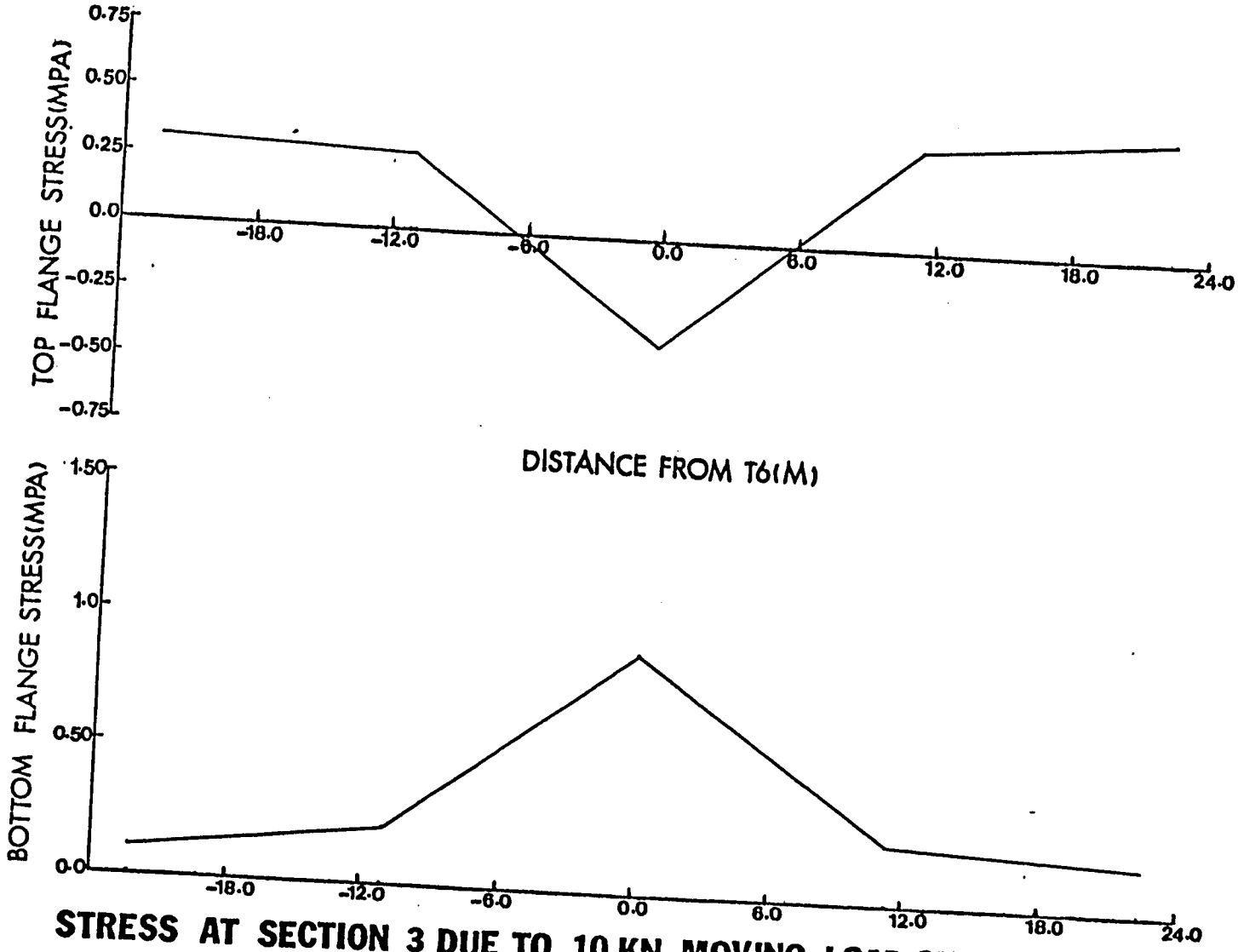

STRESS AT SECTION 3 DUE TO 10 KN MOVING LOAD ON OUTSIDE LANE

Fig.4.6

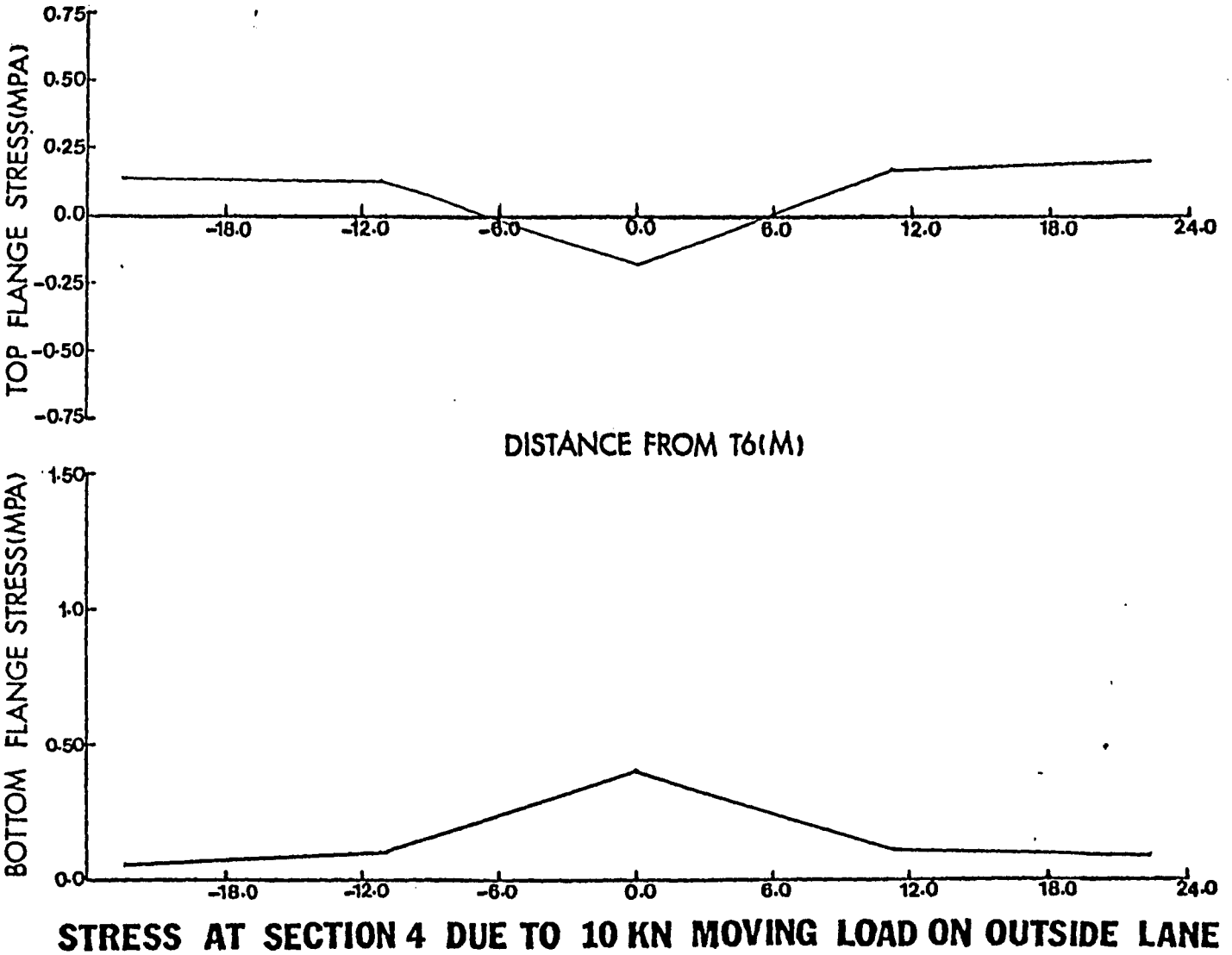

STRESS AT SECTION 4 DUE TO 10 KN MOVING LOAD ON OUTSIDE LANE

Fig.4.7

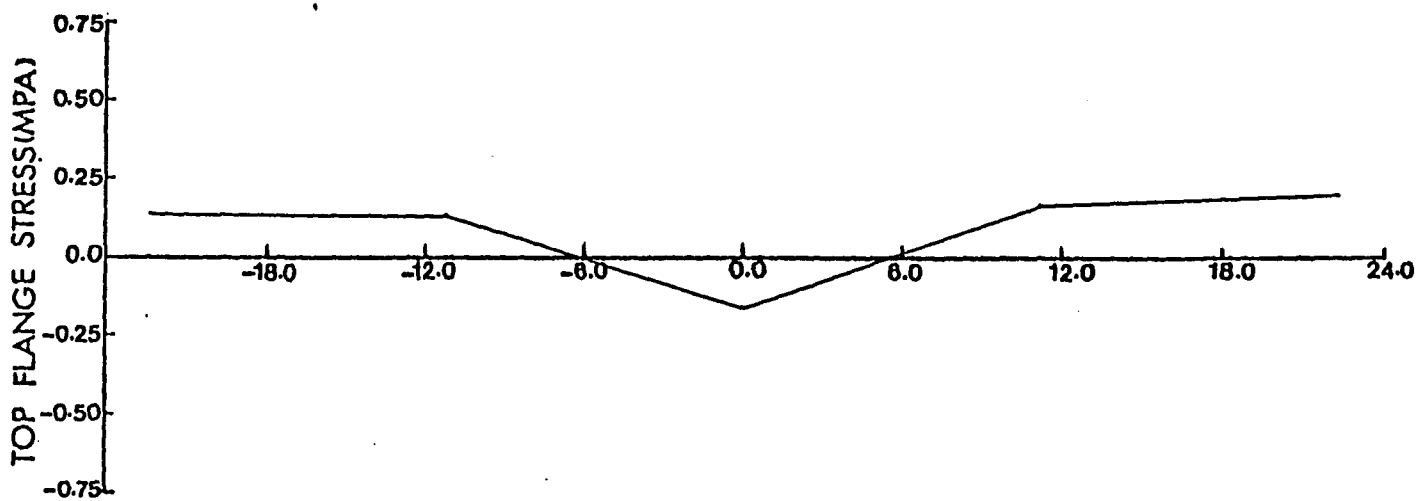

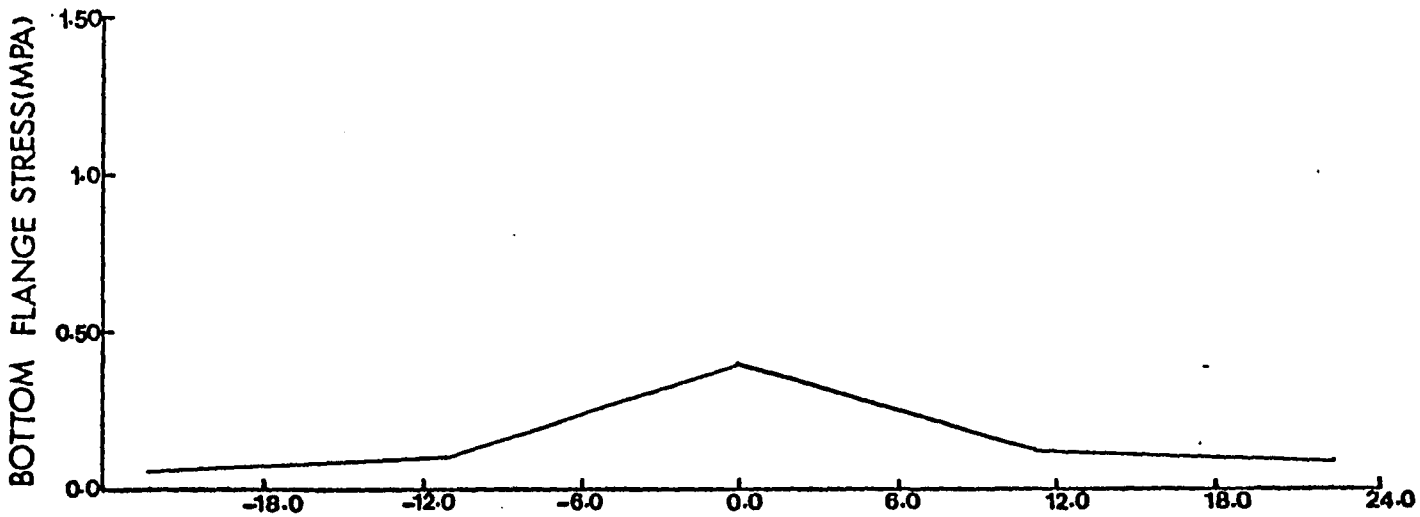

STRESS AT SECTION 5 DUE TO 10 KN MOVING LOAD ON OUTSIDE LANE

Fig.4.8

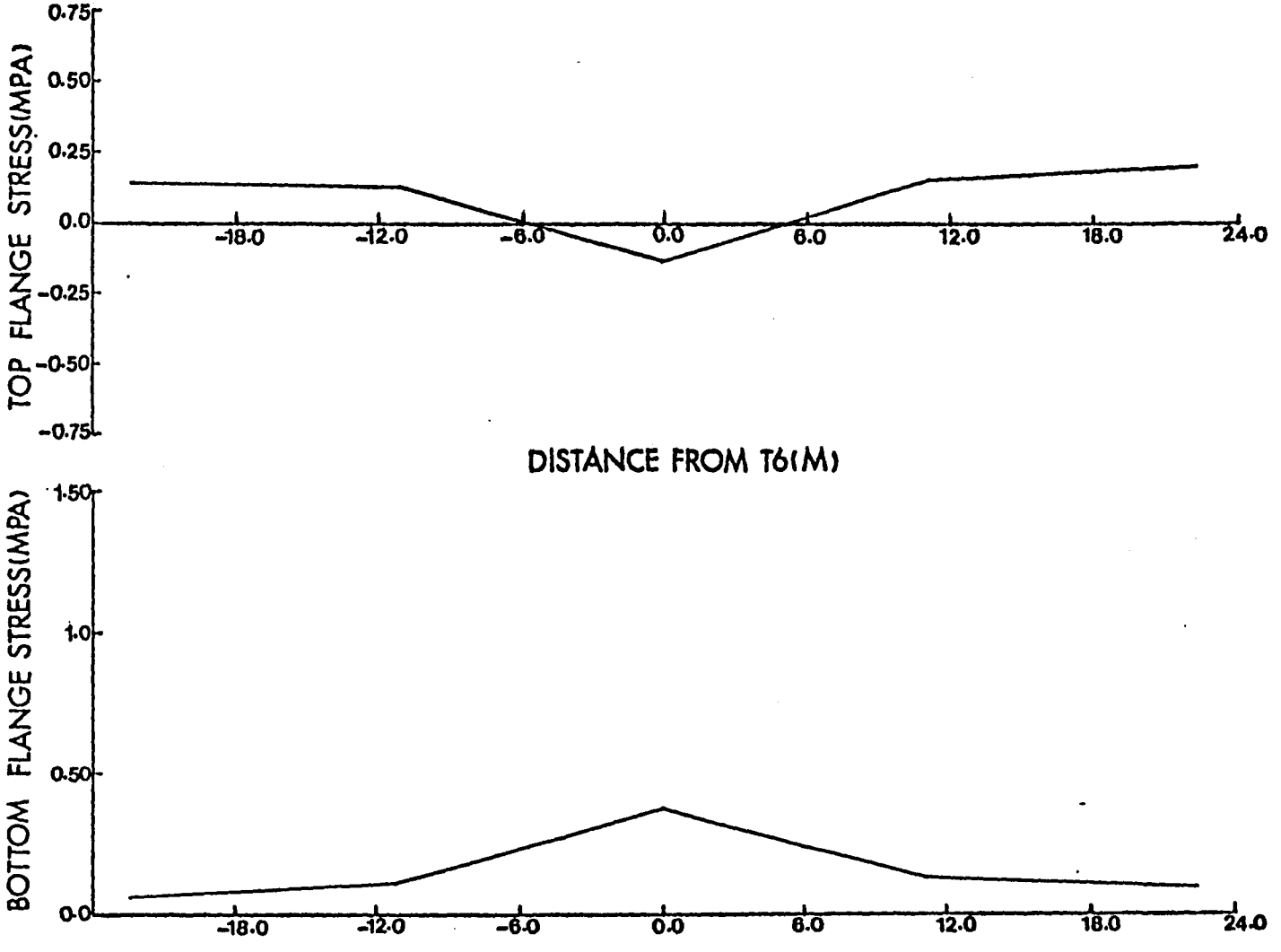

STRESS AT SECTION 6 DUE TO 10 KN MOVING LOAD ON OUTSIDE LANE

Fig.4.9

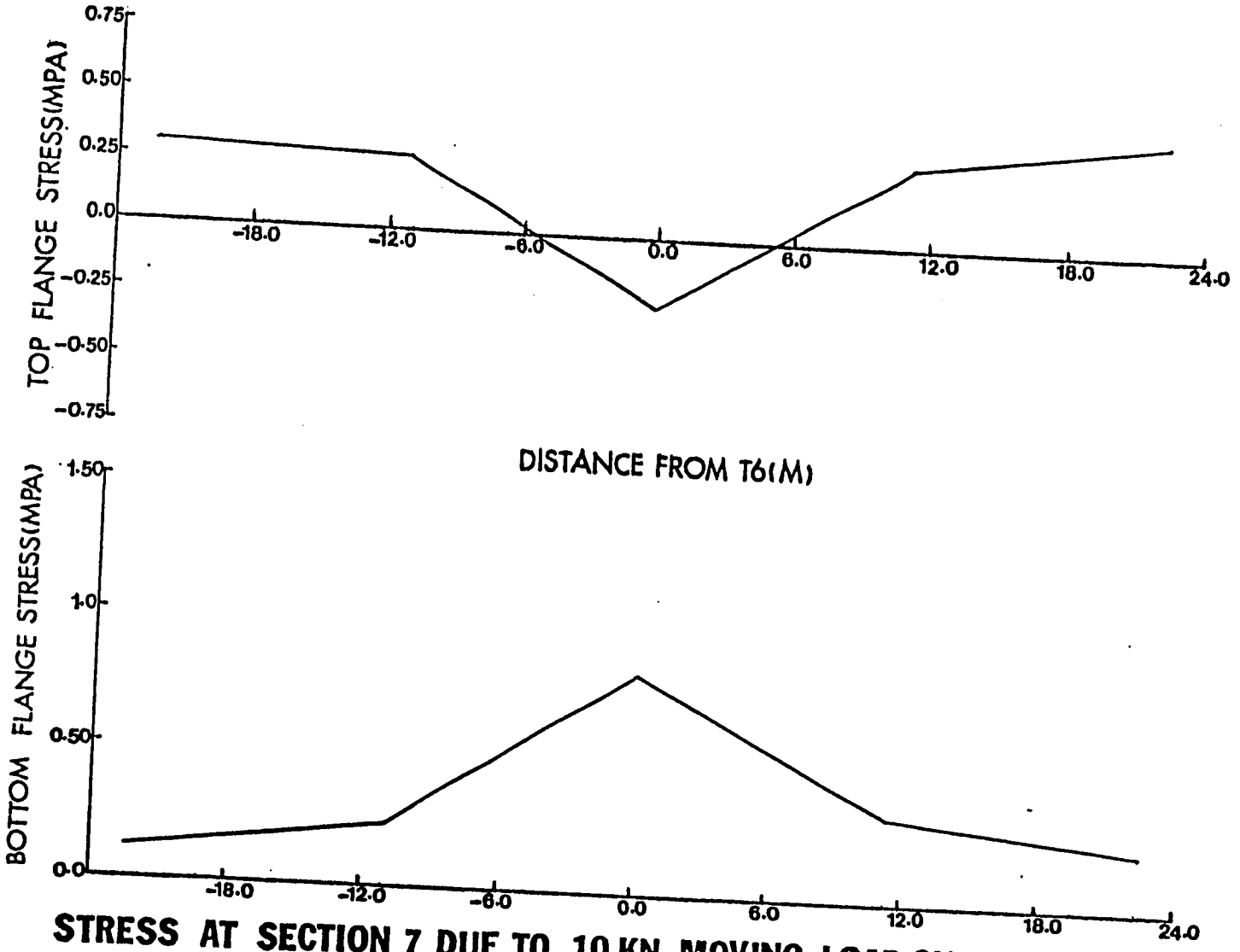

STRESS AT SECTION 7 DUE TO 10 KN MOVING LOAD ON OUTSIDE LANE

Fig.4.10

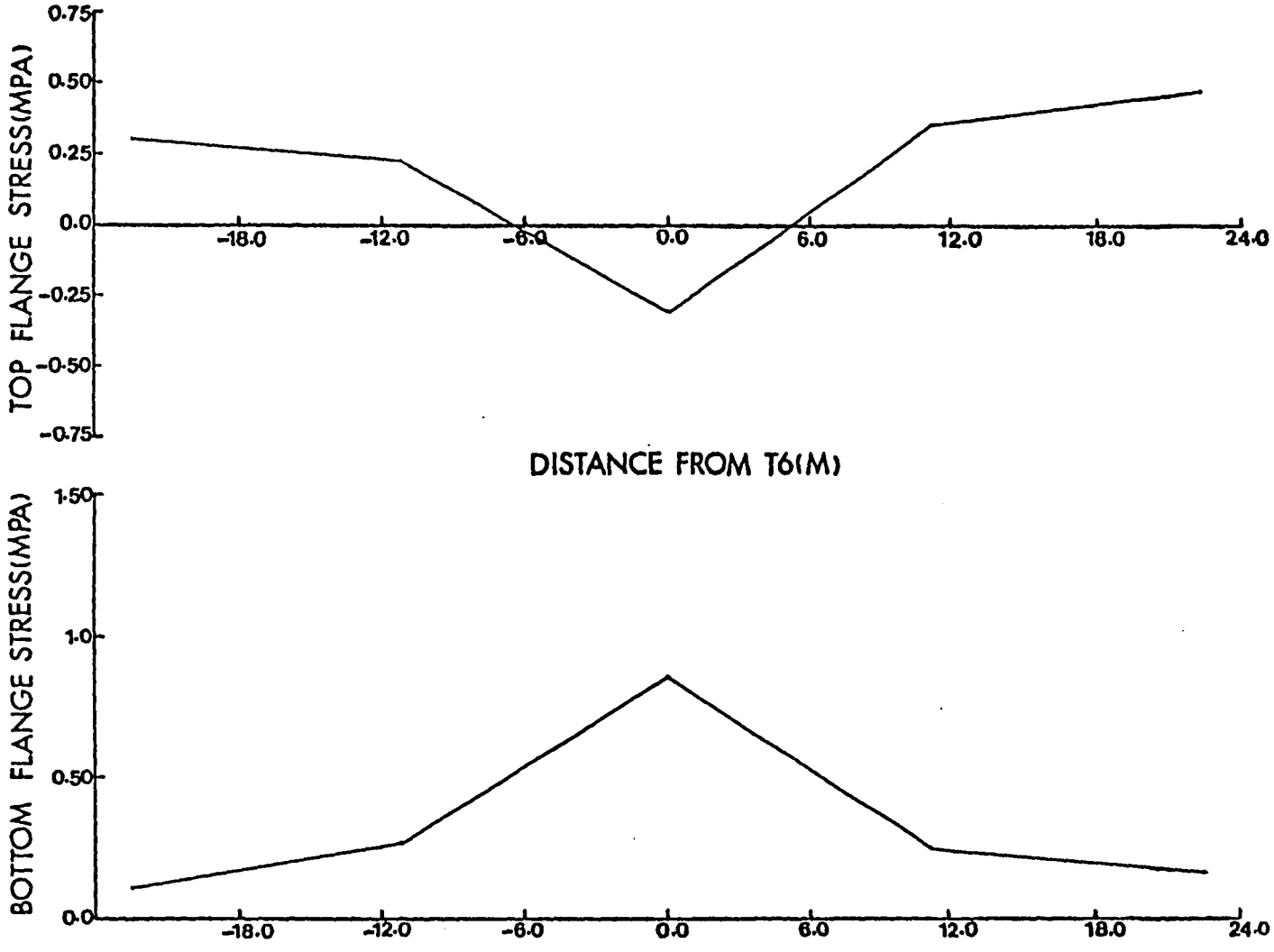

STRESS AT SECTION 1 DUE TO 10 KN MOVING LOAD ON INSIDE LANE

Fig. 4.11

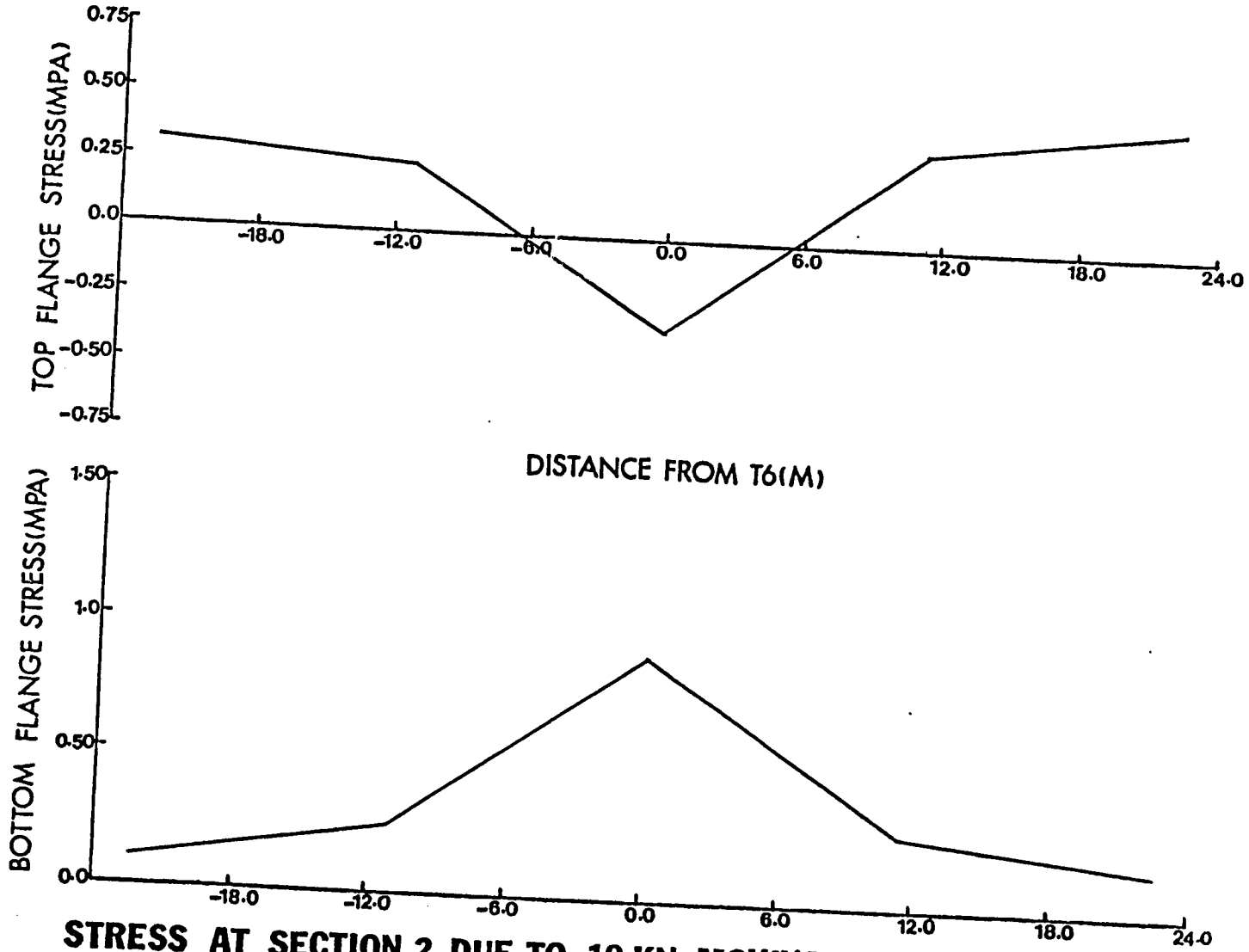

STRESS AT SECTION 2 DUE TO 10 KN MOVING LOAD ON INSIDE LANE

Fig. 4.12

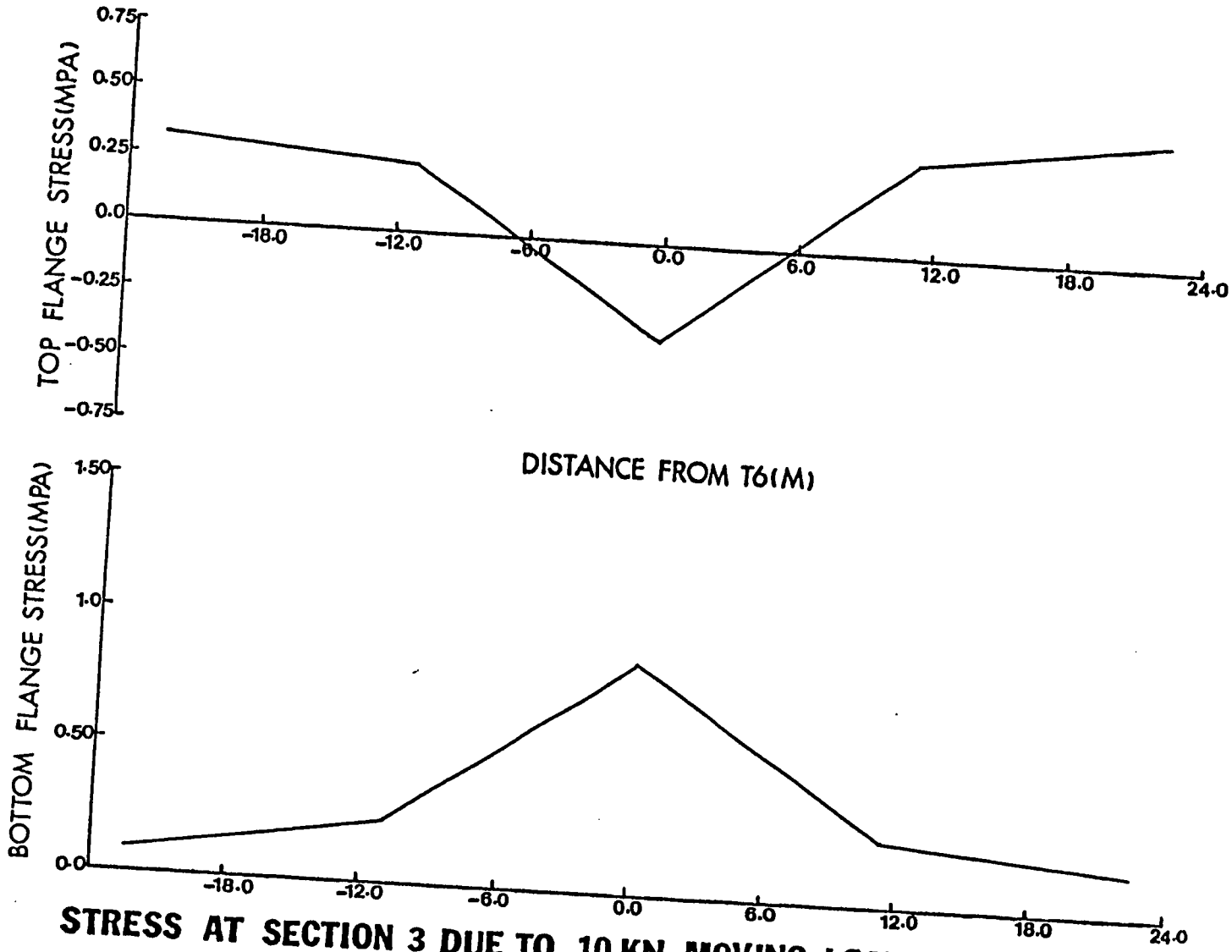

STRESS AT SECTION 3 DUE TO 10 KN MOVING LOAD ON INSIDE LANE

Fig. 4.13

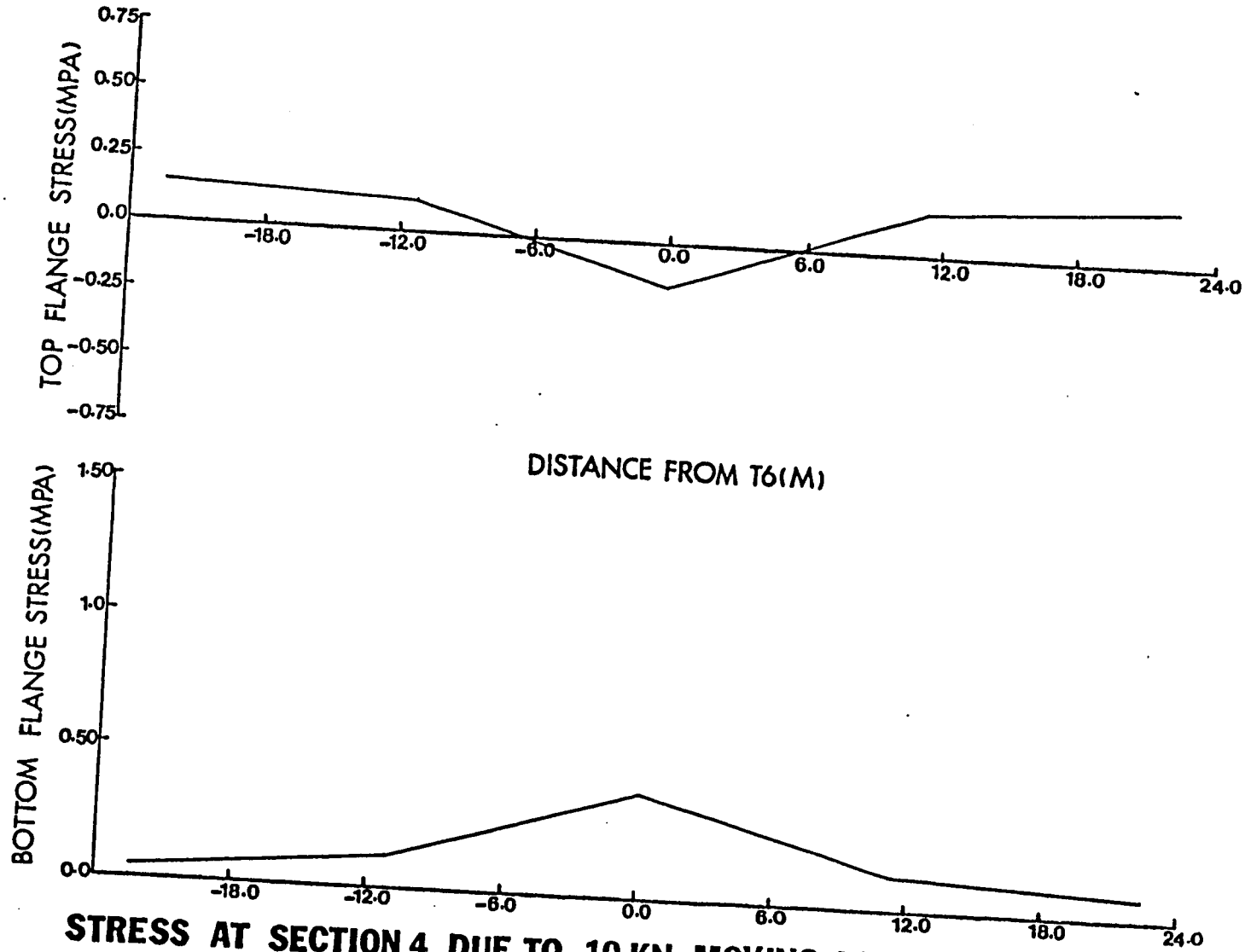

STRESS AT SECTION 4 DUE TO 10 KN MOVING LOAD ON INSIDE LANE

Fig. 4.14

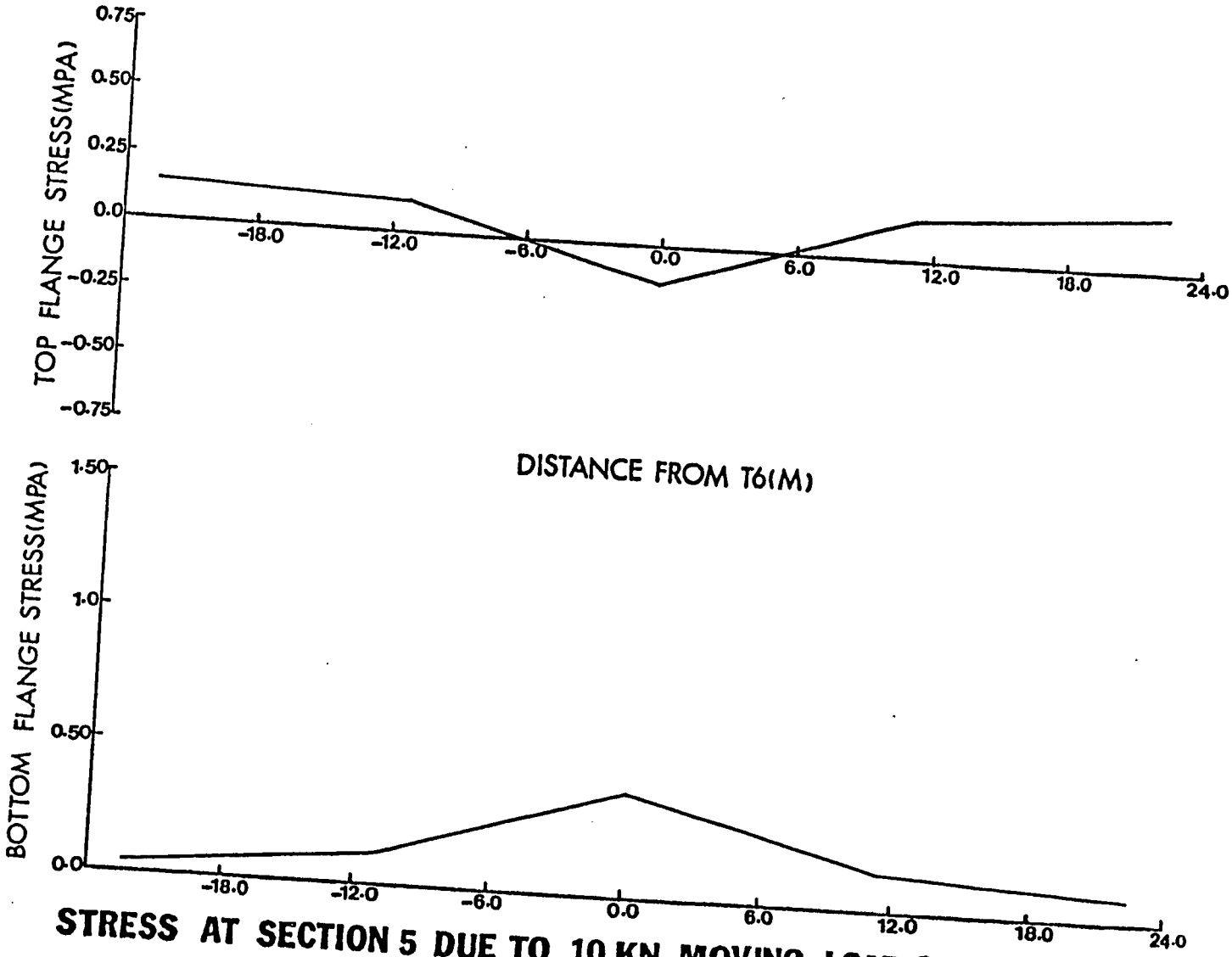

STRESS AT SECTION 5 DUE TO 10 KN MOVING LOAD ON INSIDE LANE

Fig. 4.15

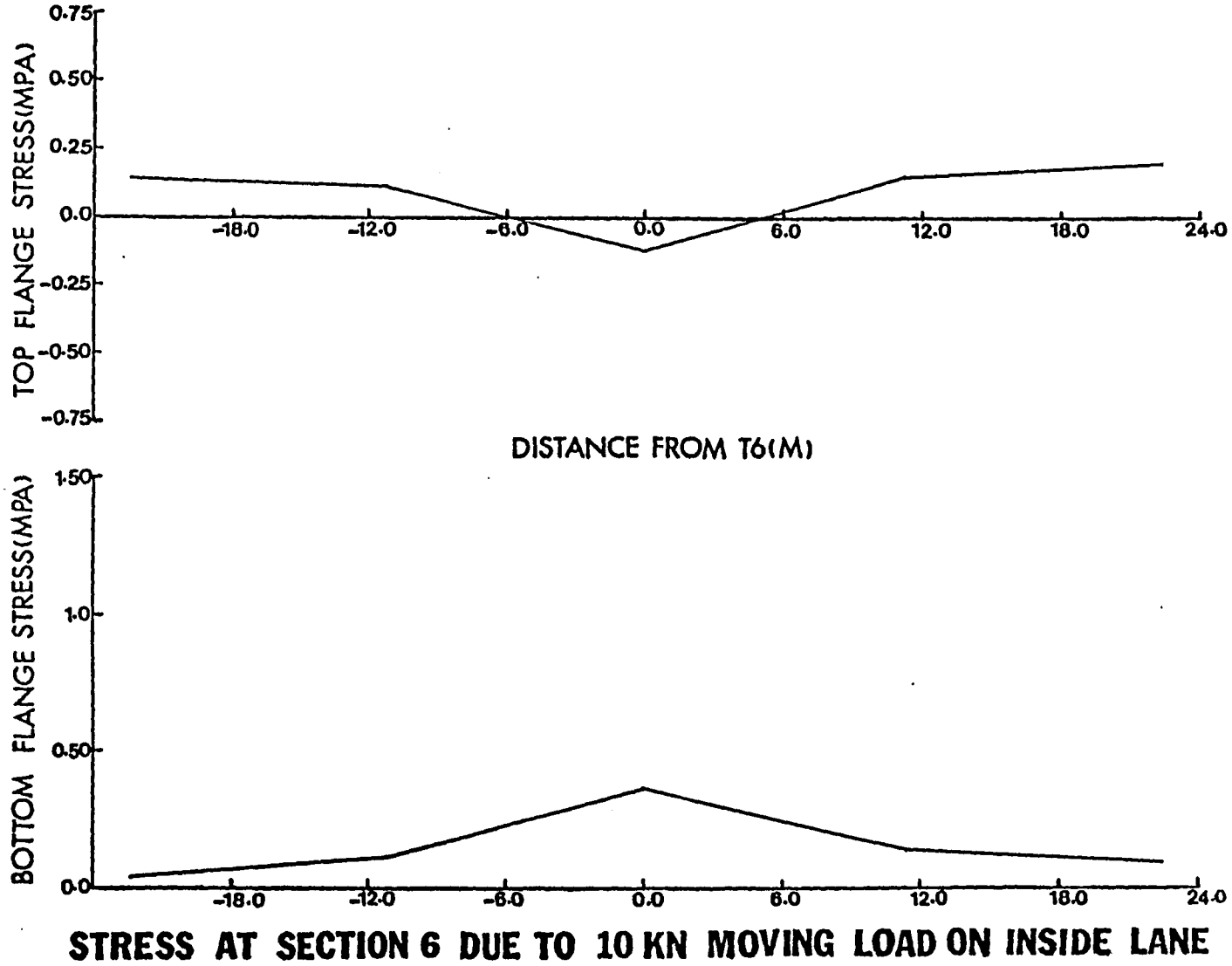

STRESS AT SECTION 6 DUE TO 10 KN MOVING LOAD ON INSIDE LANE

Fig. 4.16

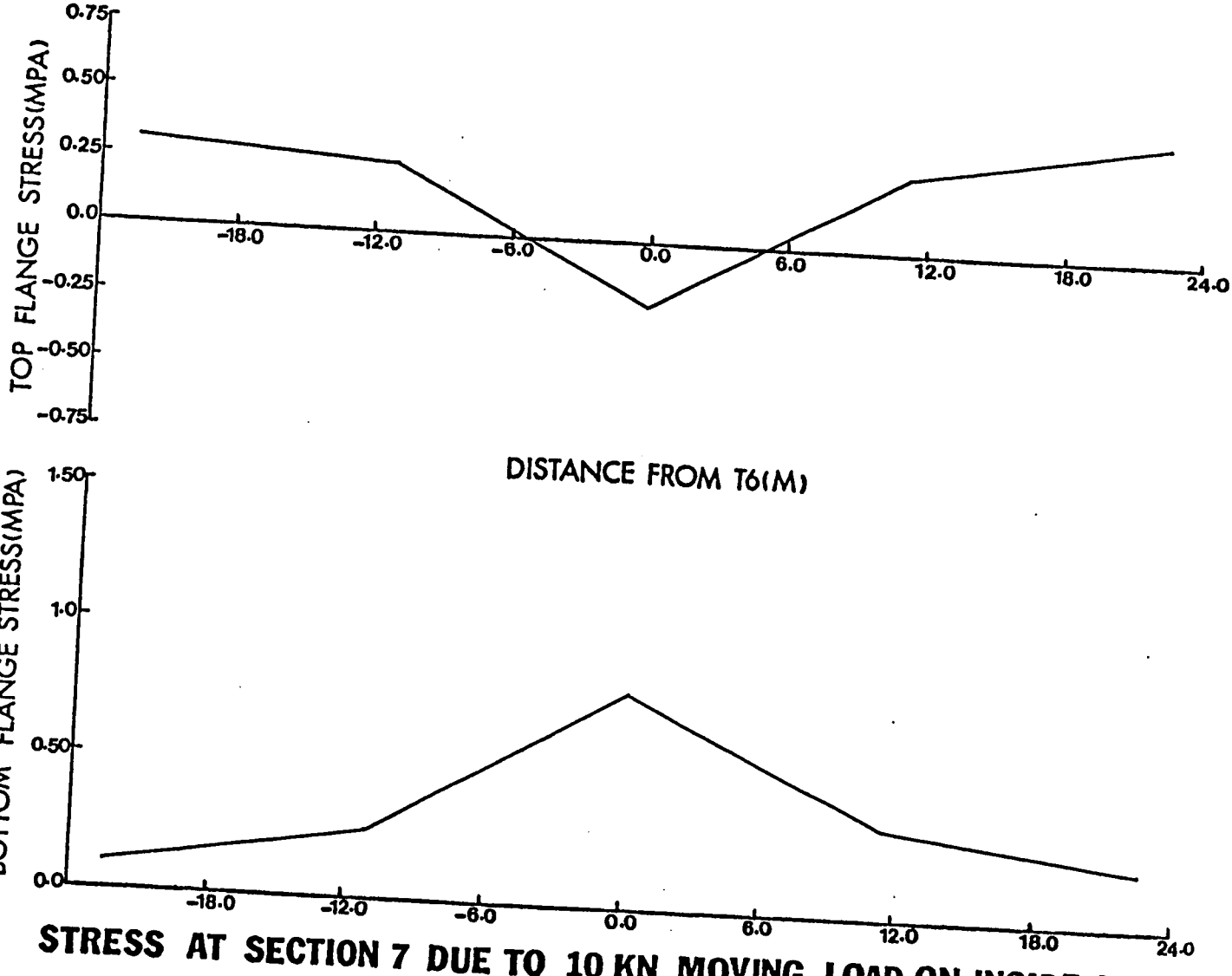

STRESS AT SECTION 7 DUE TO 10 KN MOVING LOAD ON INSIDE LANE

Fig. 4.17

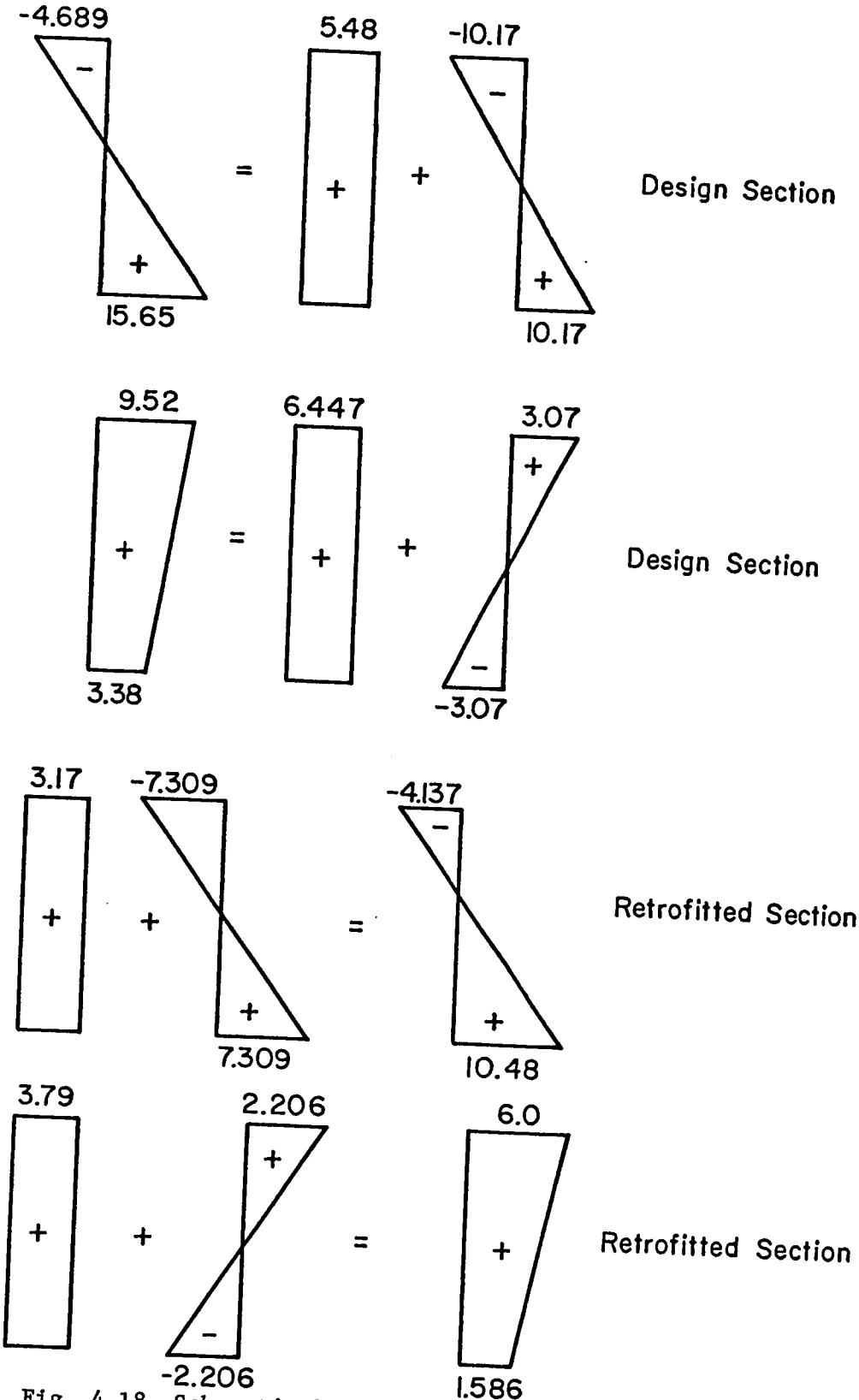

Fig. 4.18 Schematic Superposition of Stress Diagrams from Analytical Study, for Inside Lane Test Truck

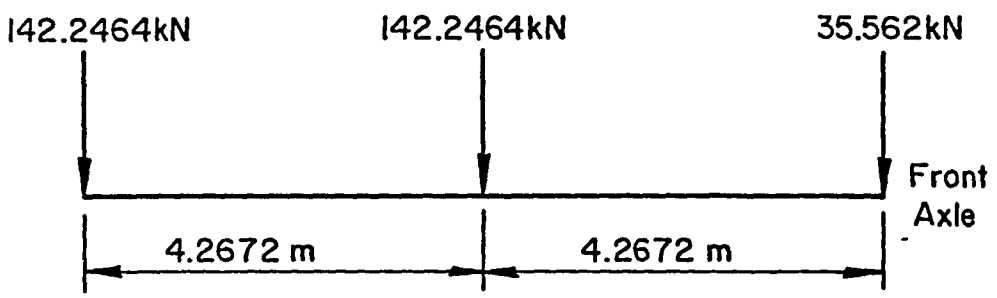

Fig. 4.19 HS20 Truck Loading

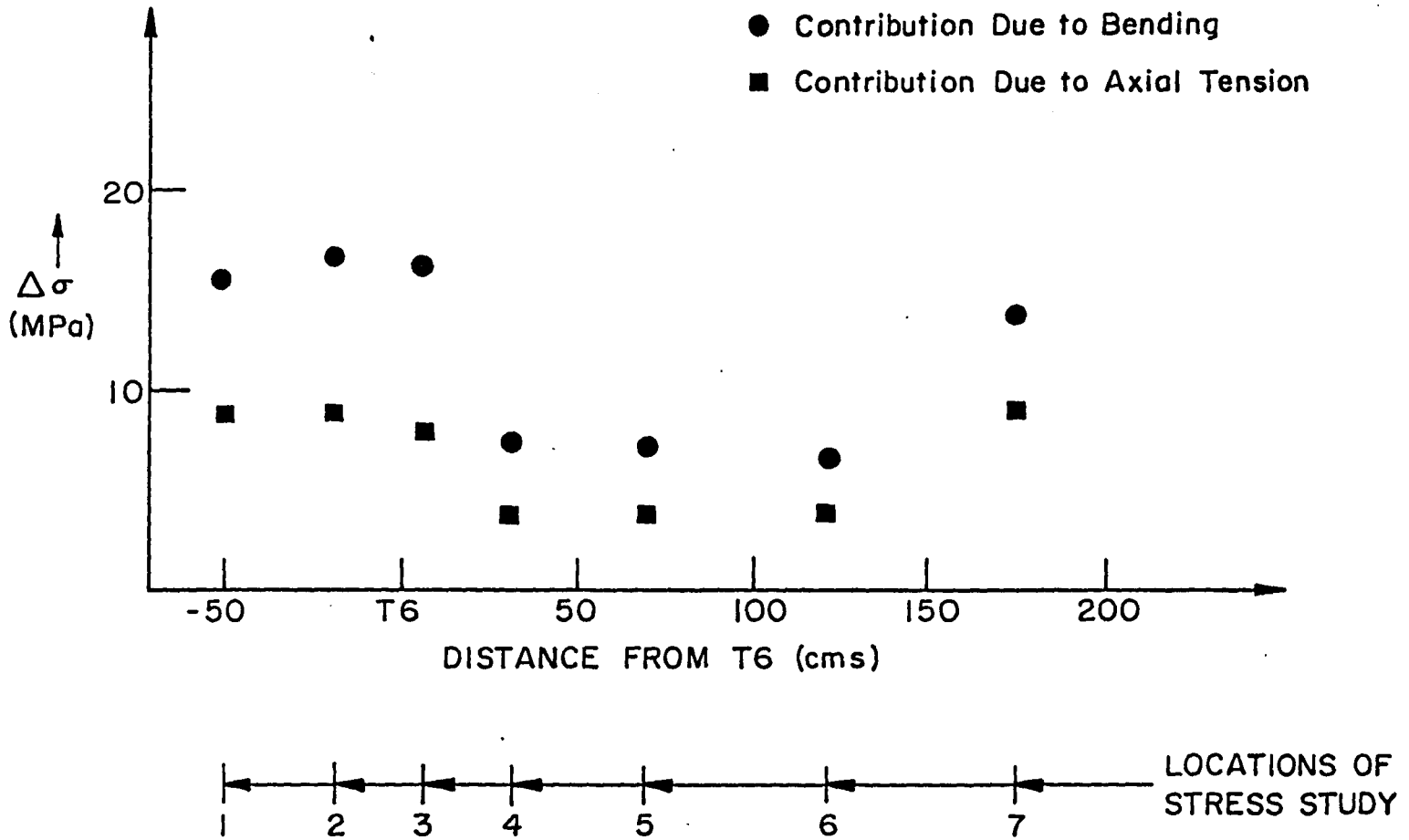

Fig. 4.20 Comparison of the Contributions of Bending and Axial Tension to the Total Stress Range for the Top Flange of the Tie Girder

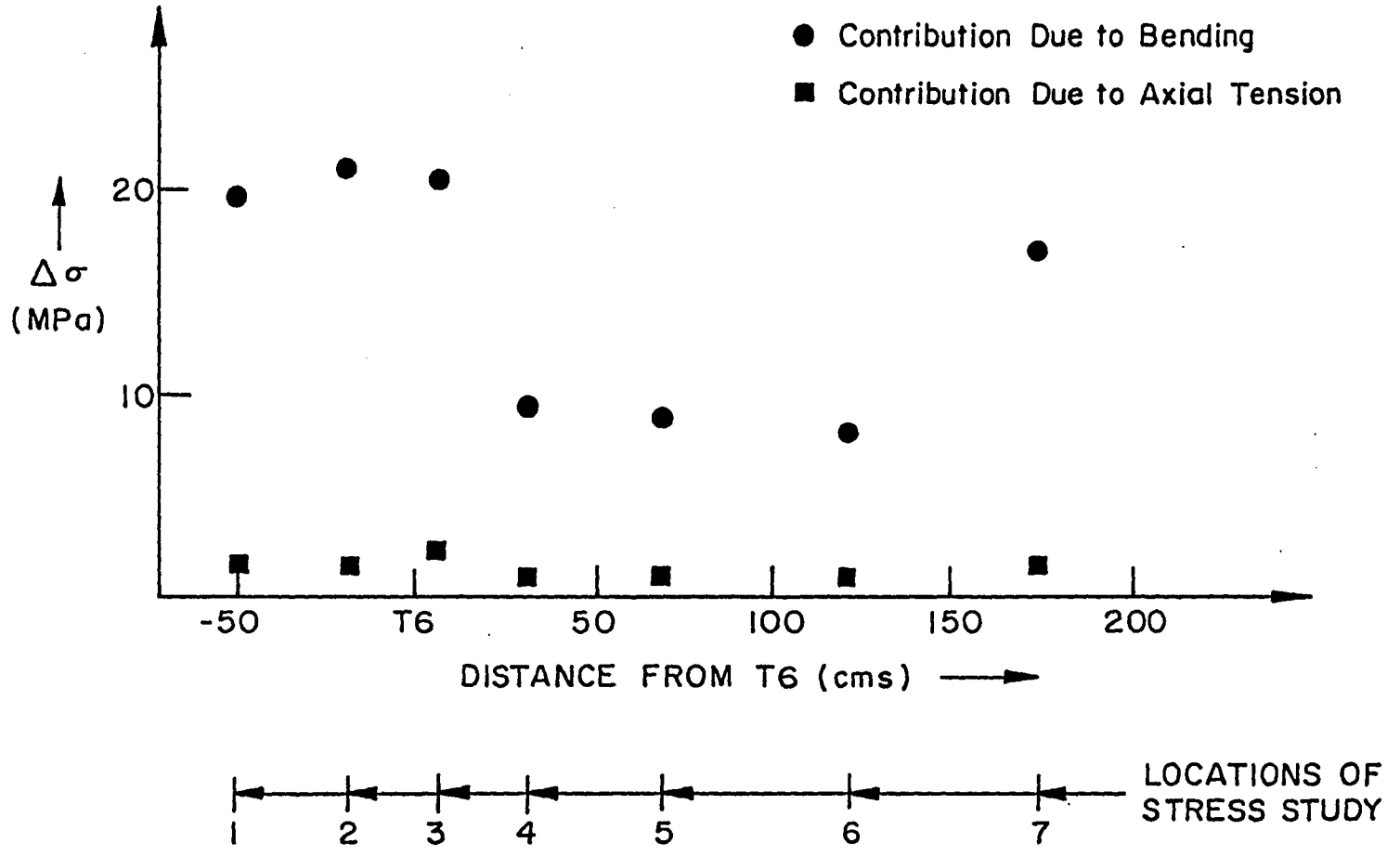

Fig. 4.21 Comparison of the Contributions of Bending and Axial Tension to the Total Stress Range for the Top Flange of the Tie Girder

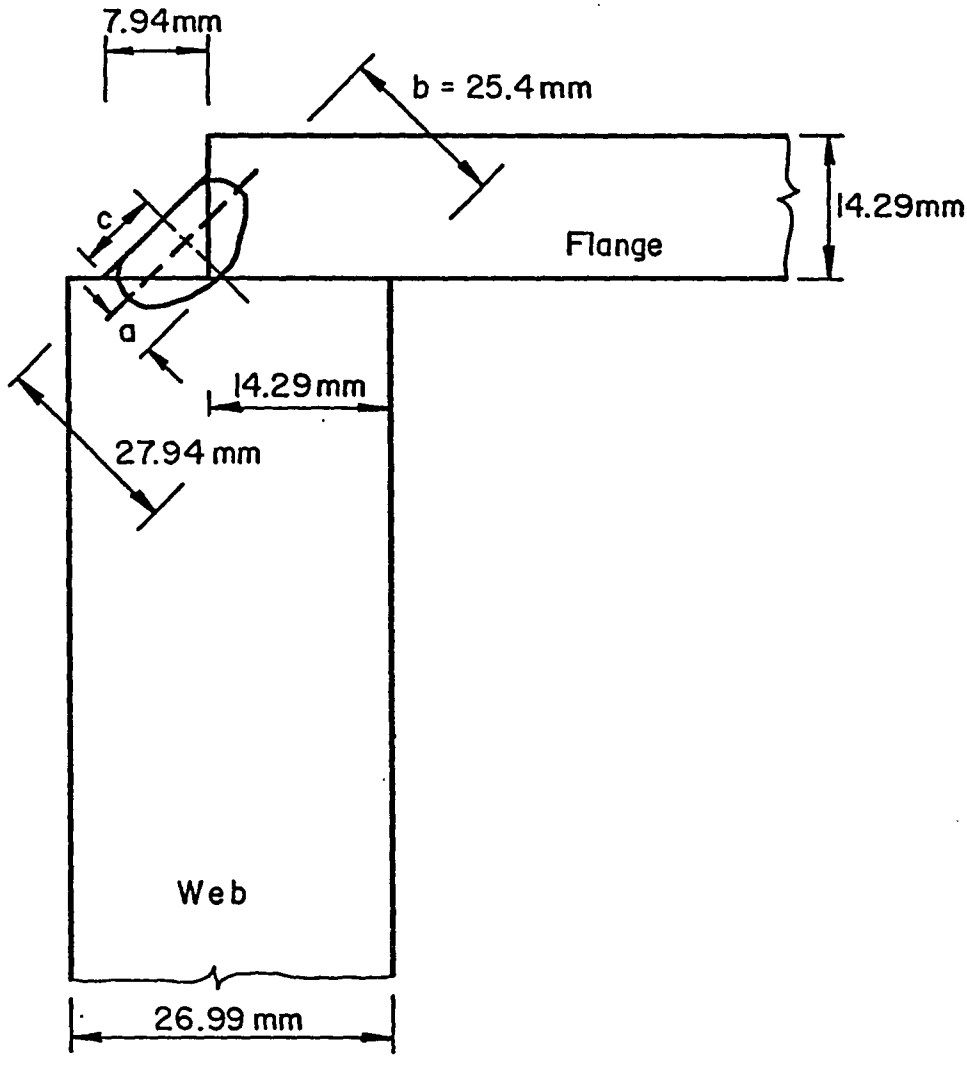

Fig. 5.1 Idealized Box Corner Crack

REFERENCES

1. Jacobson, F.
   Private Communication to J. W. Fisher, Stress Measurements on the I24 Tie Girders, 1981.

2. Bathe, K. J., Wilson, E. L., and Peterson, F. E.
   SAP IV - A STRUCTURAL ANALYSIS PROGRAM FOR STATIC AND DYNAMIC RESPONSE OF LINEAR SYSTEMS, EERC Report 73-11, University of California, Berkeley, CA, April 1974.

3. Fisher, J. W. and Pense, A. W.
   EVALUATION OF THE CRACKING OF THE I24 BRIDGE OVER THE OHIO RIVER NEAR PADUCAH, KENTUCKY AND RECOMMENDATIONS FOR ITS RETORFIT, for Illinois Department of Transportation, November 1980.

4. "Welding Flaws Close Interstate Tied-Arch Bridge," Engineering News Record, August 16, 1979.

5. Fisher, J. W.
   BRIDGE FATIGUE GUIDE, Design and Details, American Institute of Steel Constuction, 1977.

6. American Association of State Highway and Transportation Officials
   AASHTO, STANDARD SPECIFICATION FOR HIGHWAY BRIDGES, Washington, D.C., 12th Edition, 1977.

7. Fisher, J. W.
   CLASSIFICATION OF WELDED BRIDGE DETAILS FOR FATIGUE LOADING, Research Result Digest 59, NCHRP, Transportation Research Board, March 1974.

8. Fisher, J. W.
   INSPECTING STEEL BRIDGES FOR FATIGUE DAMAGE, Fritz Engineering Laboratory Report No. 386-15(81), Lehigh University, March 1981.

9. Schilling, C. G., Klippstein, K. H., Barson, J. M., and Blake, G. T.
   FATIGUE OF WELDED STEEL BRIDGE MEMBERS UNDER VARIABLE AMPLITUDE LOADINGS, NCHRP Report 188, Transportation Research Board, 1978.

10. Miner, M. A.
CUMULATIVE DAMAGE IN FATIGUE, Journal of Applied Mechanics, September 1945.

11. Paris, P. C.
THE GROWTH OF FATIGUE CRACKS DUE TO VARIATIONS IN LOAD, Ph.D. Dissertation, Lehigh University, 1962.

12. Paris, P. C. and Erdogan, F.
A CRITICAL ANALYSIS OF CRACK PROPAGATION LAWS, Transactions, ASME, Series D, Vol. 85, No. 4, December 1963, pp. 528-434.

13. Tuma, Jan J.
ENGINEERING MATHEMATICS HANDBOOK, Second Edition, McGraw Hill Book Co., 1979.

14. Fisher, J. W., Albrecht, P. A., Yen, B. T., Klingerman, D. J., and McNamee, B. M.
FATIGUE STRENGTH OF STEEL BEAMS WITH WELDED STIFFENERS AND ATTACHMENTS, NCHRP Report No. 147, Transportation Research Board, National Research Council, Washington, D.C., 1974.

VITA

The author was born on July 19, 1958 in Madras, India. He is the last of five offspring of Mr. and Mrs. Bhanduvula Venkatachalam.

The author attended the "KENDRIYA VIDYALAYA" in Secunderabad and graduated in 1975. He graduated with distinction from the Indian Institute of Technology, Madras, in May 1980.

In September 1980 the author began his graduate program at Lehigh University and served as a half-time research assistant in the fatigue and fracture division at Fritz Engineering Research Laboratory. Since that time he has worked on several projects which include the "Cracking in Electroslag Welds of Meadville," "Steel Bridge Members Under Variable Amplitude Long Life Loading," and "Blue Route Bridge Defects and Structural Response."